

Topical Review

Magnetically insulated baffled probe (MIBP) for low-temperature and fusion-boundary plasma studies

C Yuan¹ , I P Kurlyandskaya^{1,2} , V I Demidov^{2,*} , M Gryaznevich³ , M E Koepke²  and Y Raitsev⁴ 

¹ School of Physics, Harbin Institute of Technology, Harbin, Heilongjiang 150001, People's Republic of China

² Department of Physics and Astronomy, West Virginia University, Morgantown, WV 26506, United States of America

³ Tokamak Energy Ltd, 173 Brook Drive, Milton Park OX14 4SD, United Kingdom

⁴ Princeton Plasma Physics Laboratory, Princeton, NJ 08540, United States of America

E-mail: vldemidov@mail.wvu.edu

Received 9 April 2021, revised 21 June 2021

Accepted for publication 27 July 2021

Published 13 August 2021



Abstract

The application of the magnetically insulated baffled probe (MIBP) and MIBP cluster for studying properties of low-temperature and peripheral fusion plasmas is reviewed. MIBP operation principles, MIBP design strategy, and MIBP examples of measurement, data analysis, and interpretation are discussed. The implementation convenience and diagnostic usefulness, as well as the inconvenience and drawbacks, for studying plasma equilibrium and dynamics properties, are demonstrated. MIBP determination of oscillations of fluid observables, such as electron and ion temperatures, electrostatic plasma potential, and electron and ion density reveal plasma instabilities and waves. Ion and electron distribution functions, and the transport of charged-particle number, momentum, and energy can also be measured.

Keywords: electric probe, magnetically insulated baffled probe, magnetized-plasma dynamics, diagnostic techniques, plasma dynamics and transport

(Some figures may appear in colour only in the online journal)

Nomenclature

B	magnetic field magnitude	D_{ip}	ion diffusion coefficient perpendicular to magnetic field
D_e	electron diffusion coefficient along magnetic field	e	electron charge ($e = -1.6 \times 10^{-19}$ C)
D_{ep}	electron diffusion coefficient perpendicular to magnetic field	E_s	electric field magnitude
D_i	ion diffusion coefficient along the magnetic field	\tilde{E}_s	electric field fluctuations
		F_e	electron distribution function (EDF)
		F_i	ion distribution function (IDF)
		h	near-probe sheath thickness
		I_e	collected-electron probe current
		I_e^{sat}	collected-electron saturation probe current
		\tilde{I}_e^{sat}	collected-electron saturation probe current fluctuations
		I_i	collected-ion probe current
		I_i^{sat}	collected-ion saturation probe current

* Author to whom any correspondence should be addressed.

\tilde{j}_i^{sat}	collected-ion saturation probe current fluctuations
j_e	collected-electron probe current per collection area
j_i	collected-ion probe current per collection area
L	probe length
m	electron mass
M	ion mass
n_e	electron number per volume
\tilde{n}_e	electron density fluctuations
n_i	ion number per volume
\tilde{n}_i	ion density fluctuations
R	probe radius
T	charged-particle temperature magnitude (in units of energy)
T_e	electron temperature magnitude (in units of energy)
\tilde{T}_e	electron temperature fluctuations
T_i	ion temperature magnitude (in units of energy)
\tilde{T}_i	ion temperature fluctuations
v	charged particle velocity
V	probe voltage relative to the plasma (space) potential
V_0	floating probe voltage offset in equation (17)
V_f	potential of the floating probe
V_S	plasma (space) potential
\tilde{V}_S	plasma (space) potential oscillations
W	electron kinetic energy
x_e	ratio of electron mean-free path to gyro radius
x_i	ratio of ion mean-free path to gyro radius

Greek symbols

α	normalized electron to electron-saturation probe current
$\alpha_{n_e E}$	cross-phase between n_e and E_θ
β	normalized ion to ion-saturation probe current
γ	geometrical factor in equation (10)
γ_e	$L/2Rx_e$
γ_i	$L/\left[2R\sqrt{1+x_i^2}\right]$
$\gamma_{n_e E}$	cross coherence between n_e and E_θ
ν_e	electron collision rate with electrons and neutrals
$\bar{\nu}_e$	average electron collision rate
ν_i	ion collision rate with ions and neutrals
$\bar{\nu}_i$	average ion collision rate
ν_{ei}	electron-ion collision rate
λ_e	mean free path of electrons
λ_i	mean free path of ions
λ	electron energy relaxation length
μ_e	coefficient in equations (17) and (18)
μ_i	coefficient in equations (17) and (18)
ρ_L^e	electron gyro radius
$\bar{\rho}_L^e$	average electron gyro radius
ρ_L^i	ion gyro radius
$\bar{\rho}_L^i$	average ion gyro radius
Ψ	diffusion parameter
ω	frequency

Abbreviations

ac	alternative current
dc	direct current
EDF	electron distribution function
IDF	ion distribution function
<i>IV</i> trace	current–voltage trace
MIBP	magnetically insulated baffled probe

1. Introduction

An electric probe is a current-collecting sensor, in contact with the plasma, that serves as a discrete conductive element in an electric circuit. The probe, whether mounted onto a probe positioner, or a plasma-facing wall is capable of diagnosing plasma conditions by interpreting the characteristic trace relating the current collected and bias voltage applied to the sensing-electrode [1]. Probes can be adapted for diagnosing low-temperature and peripheral fusion plasmas [2–13] and typically can measure a current–voltage trace or floating probe potential from which a wide variety of plasma parameters can be determined, ranging from fluid observables, such as electron temperature T_e , plasma potential V_S , and electron n_e and ion n_i densities, to electron $F_e(v)$ and ion $F_i(v)$ distribution functions (EDF and IDF, respectively), where v is the charged particle velocity. To minimize probe-tip damage from extended contact with fusion-grade plasma, the sensor may be mounted flush with the plasma-facing surface or used in reciprocated regime.

In the majority of previous studies, unbaffled (cylindrical and spherical) probes have been applied for measuring [3–5, 8, 10, 12, 13] T_e , n_e , V_S and $F_e(v)$ in stationary low-pressure (usually less than several Torr) plasma [4, 5, 8, 10, 12]. Probe theories have since been expanded to higher pressures, up to and beyond atmospheric pressure [10, 12–15]. Fast sweeping probes [16–18] can respond to plasma evolution and oscillation in time-varying plasmas, allowing measurement time resolution on the order of a fraction of one microsecond. However, it may be impossible this way to measure fluctuations in a magnetized plasma due to diffusion of electrons to the probe hindered by the magnetic field [10].

In application to magnetized and flowing plasmas, a floating emissive probe could measure fluctuations of the plasma potential [19–22]. Depending on the plasma conditions, the hot emissive probe can float very close to the plasma potential or a few electron temperatures below the plasma potential [23]. There are several limitations to application of this probe which are considered in detail elsewhere. However, the most critical issue of this probe is its limited lifetime due to either evaporation or sputtering of the probe wire.

In the case of anisotropic volumetric transport of the charged particles, the relative and absolute magnitudes of electron and ion collected currents depend on the relative orientation between the collecting sensor access and the transport flux. Measuring this transport anisotropy can be exploited for

diagnostic advantage. For example, in the low-pressure gas-discharge having anisotropic near-cathode plasma, a rotatable unbaffled cylinder or a rotatable single-sided planar probe can quantitatively analyze the angular anisotropy of electrons and measure anisotropic EDF [10, 12, 24].

This report is devoted to reviewing, discussing, and implementing the specialized magnetically-insulated-baffled probe (MIBP) and MIBP-cluster design for diagnosing low-temperature and peripheral fusion (anisotropic) magnetized plasmas. Operating principles, effective designs, methods of measurements, and some important results of representative experiments that employ MIBP comprise the scope of this review.

Transport of charged particles toward the probe depends on the sensor-local direction and magnitude of the magnetic field relative to the collecting sensor access and the transport flux. While an unbaffled probe is useful for magnetized plasma measurements [7, 9, 10, 12, 25–28], temperature fluctuations complicate the interpretation of unbaffled-probe data to the extent that floating and plasma potential can appear anti-correlated. The presence of strategically placed particle-trajectory-blocking obstacles in the probe construction can simplify and improve measurement and interpretation fidelity. Accordingly, such a probe featuring obstacles (or baffles) could be referred to as a baffled probe, as proposed by Demidov *et al* [29] and promoted by Chen [11]. Later, considering the importance of using magnetic field in combination with baffles for separating electron and ion fluxes to the probe, a more descriptive generic name, ‘magnetically insulated baffled probe’ or MIBP, was adopted [30].

At the dawn of the MIB probe development, the diagnostic was used to measure the characteristic ion temperature and the IDF by suppressing the electron current collected at positive probe potentials with respect to the plasma potential and by measuring the ion probe *IV*-trace or its derivatives for those potentials [31, 32]. At that time, the functional label ‘ion-sensitive probe’ was given to the technique. Correspondingly, the specific probe construction from [31] has been frequently referred to as the Katsumata probe (see, for example, [10]). Although the ion-sensitive probe benefits potential measurements, the design and operation are too complex for measurement results of IDF and ion temperature to be fully simulated and interpreted in detail [10].

While ‘ion-sensitive probe’, as a generic name, reflects the intended diagnosis for a specific case, the label may be misleading, to some extent, as the collection of mostly electron current is a consequence of the positive potential applied to this probe and application of negative potential to a probe generally leads to the collection of net-ion current. When measuring other quantities, not directly connected to the IDF, expanding the capability, beyond ion sensitivity, benefits the specific diagnosis. To minimize ambiguity, the generic label ‘ion-sensitive probe’ is not used in subsequent sections of this review. When contrasting performance limitations, we have kept names for specific MIBP construction, like the plug [10], the baffled [29], the Katsumata [31, 32] and the ball-pen (developed by Stöckel *et al*) designs [33]. See section 2.2 for details of the probe designs.

Because the MIBP diagnostic is designed for use in a partially and fully magnetized plasma, for its use in unmagnetized plasma it is necessary to create a local magnetic field near the probe. As noted in [10], in a plasma without magnetic field or with sub-optimal magnetic field strength, the local magnetic field can be artificially created or augmented to support the magnetic field for MIBP-optimal conditions. In this case, it is necessary to select the local magnetic field so that it does not significantly affect the properties of the plasma and their measurements [34].

To the best of our knowledge, the concept of real-time measurement of plasma-parameter oscillation using MIBP (first realized with a plug probe) while electrically floating was proposed, developed and experimentally implemented in works [29, 35–38]. This method was extended to the MIBP (first labeled the ion-sensitive probe) of any design in [10]. MIBP, with its instantaneous signal, dramatically increases temporal resolution relative to measuring full or partial *IV*-traces with any and all designs, including MIBP, of fast-sweep-repetition probes in magnetized plasmas. Typically, the fast sweeping probe in sufficiently magnetized plasmas can resolve the evolution of average V_S and other plasma parameters, but not V_S oscillations (ac-only signals are denoted later with tilde, say, \tilde{V}_S for V_S), because of the limited temporal resolution due to reduced diffusion rates of the charged particles to the probe in the magnetic field (see [10] for more details).

In order to better understand the advantages of the MIB probe in relation to a conventional (unbaffled) probe, we note here that a change in the orientation of a conventional probe also may lead to a change in the ratio of the electron and ion saturation currents in the *IV* probe traces [27, 28]. Without dwelling here on the comprehensive theory of an ordinary probe, which is described in more details, for example, in reviews [4, 8, 10, 12, 13], we note that the presence of obstacles (baffles) leads to a dramatic increase in the difference between the electron and ion saturation currents of the MIB probe, as compared to the conventional probe. For a MIB probe, it is possible to obtain a regime when the electron saturation current is much less than the ion saturation current, which is problematic to obtain for a conventional probe. As a result, while a conventional probe or their combinations can provide some, if not all, of the results obtained by MIB probes, their accuracy drops sharply in comparison with the same results obtained by MIB probes.

Section 2 discusses the MIBP principles of operation and design distinctions of typical practical realizations while also summarizing the operation-oriented, analytical theory of the MIBP approaches. So far, three MIBP designs have been used in practice with more or less applicability, model accuracy, prediction reliability, and control convenience for specific plasma types and conditions. In order of development and implementation to the practical applications, they are the Katsumata probe, the plug probe and the baffled probe. The Katsumata probe modifications (the ball-pen probe, and the divertor-located flush-mounted probe) have also been used in real measurements. The latter two modifications serve as examples of simply adapting the geometry of the Katsumata probe’s conducting surface to improve a specific probe

property. A third example of modifying the Katsumata probe design is also demonstrated in section 2. The pros and cons for different probe constructions are discussed.

One of the main advantages of the plug and baffle probes, relative to the other MIBP, is the experimentally confirmed ability to use the simple analytical formulas described in section 2.3 to quantitatively simulate their acquired signal during operation and directly infer the plasma parameters of interest. This simplifies parameter profiling for plasma studies compared to the more complex, and assumption-heavy, numerical modeling required for some of the other MIBP designs.

Section 3 briefly discusses three distinctly different plasma conditions, and the respective chamber configurations, that have been the subjects of detailed MIBP investigations. They are (a) the ‘ $T_e/T_i = 5 \text{ eV}/0.5 \text{ eV}$ ’ low-temperature plasma, sometimes referred to as fusion-related plasma, found in the toroidal magnetically confined dc discharge device, (b) the ‘ $T_e/T_i = 0.2 \text{ eV}/0.2 \text{ eV}$ ’ thermally produced, fully-ionized Q-machine plasma, and (c) the ‘ $T_e/T_i = 50 \text{ eV}/25 \text{ eV}$ ’ hot fusion-boundary plasma in stellarators and tokamaks. The described devices have been carefully selected to convey the reliable demonstration of the main features, methodologies, and results of MIBP measurements in different applications, main properties and to convey the benefits of single-tip and tip-cluster MIBP designs.

The impact of MIBP is most unique when documenting plasma fluctuations and is most conveniently illustrated when MIBP electrostatically floats for various ratios of the electron and ion saturation currents. Sections 4 through 7 are devoted to describing uncontaminated local measurements and sequential raw-data processing of various plasma oscillating parameters. As the study of each plasma parameter is discussed in turn, the range of diagnostic capabilities is appreciated by analyzing the cross-parameter cross-correlation.

Although these sections do not discuss the dc measurement, and absolute calibration, of specific parameter values of interest (time-averaged V_s , T_e and T_i , except for demonstrating the method with T in section 6.2), experience with MIBP dc-measurements is documented in the literature. Note that the possible presence of an apparent plasma-potential shift, as discussed in section 2.4, risks the introduction of non-negligible dc errors (in contrast to ac errors). Therefore, referring to the MIBP as potential-specific probes (see [39]) might be misleading.

Section 4 discusses direct MIBP measurements of plasma potential fluctuations \tilde{V}_s . Plug-probe measurement of \tilde{V}_s was conducted in simple-magnetized-torus plasma [35–37]. Apparently, the first direct MIBP measurement in fusion-boundary plasma was carried out and presented in [40], which employed a baffled probe, translating in and out of the HSX stellarator plasma, in reciprocal fashion, to avoid heat damage. Flush-mounted, divertor-located, MIBP were later developed and installed in the spherical tokamak NSTX (see, figure 18, top, right). Baffled and plug probe measurements of \tilde{V}_s in a zero-plasma-beta Q-machine (electron and ion temperatures are below 0.2 eV) were first performed and partially published in [29]. Katsumata probe measurements of \tilde{V}_s in

the TEDDI plasma device (Kiel, Germany) [41] and, subsequently, ball-pen probe measurements of \tilde{V}_s in the CASTOR tokamak (Prague, Czechia) [33, 39] followed. This section gives examples of measuring the amplitude of potential oscillations in plasma of various types. Section 4 also outlines how fluctuations in charged-particle temperature contaminate the measurement of \tilde{V}_s .

Section 5 describes how two proximity MIBP, both measuring local \tilde{V}_s , are combined to determine the local electric field oscillations \tilde{E}_s . First-time measurement of \tilde{E}_s was performed with a two-plug-probe cluster [42] in the simple magnetized torus. Subsequently, a compact baffled-probe cluster, featuring open (unbaffled) and closed (baffled) probes, was exploited for highly localized \tilde{E}_s and \tilde{T}_e measurements in Q-machine plasma [30]. Measurements with two ordinary probes have been qualitatively compared with the measurements of MIBP to distinguish different fluctuation modes.

Section 6 outlines MIBP measurement of electron and ion temperatures. Electron temperature oscillation \tilde{T}_e has been measured and reported in several devices [10, 35, 36, 42–44], made possible by the natural dominance of electron-current collection over ion-current collection. Ion temperature T_i has been measured and reported in a few devices [31, 32, 45]. Ion temperature oscillation \tilde{T}_i , on the other hand, requires regime of the almost complete suppression of electron-current collection, which has been experimentally demonstrated, for example, in [46]. It has also been demonstrated that measuring the temperatures of charged particles makes it possible to correct the results of measurements of potentials and electric fields in plasma, for example, using iteration schemes.

Section 7 demonstrates measurements of anomalous energy and particle fluxes, arising from low-frequency oscillations in a magnetized plasma [10, 44]. Those measurements have been performed in simple-magnetized-torus plasma. In different plasma parts of the same simple-magnetized-torus plasma volume, the charged-particle flow and energy flow have been shown to have different characters and oscillation natures. Plasma density oscillations, yet to be mentioned, are discussed briefly in section 7 because these measurements do not require the use of MIBPs, but are necessary to quantify anomalous transport of particles and energy.

Section 8 discusses the extraction of the time-integrated IDF and EDF, and time-averaged temperature determination, from MIBP-acquired IV -traces. Non-instantaneous measurement of the IDF is possible in sufficiently magnetized plasma. EDF measurement is generally complementary and could substitute as a technique should a standard cylindrical probe be impractical. For calculations of IDFs and/or EDFs, refer to formulas from section 2.3 [4, 5, 8, 10, 12, 13].

Section 9 provides some afterword which puts the subject of the review in a wider context.

Finally, a major achievement of the MIBP methodology is that the probe can be operated in two modes. First, ‘optimal’ or ‘equalized’ suppression (when electron saturation current is approximately equal to the ion saturation current) of the electron-current collection, while electrostatically floating, enables the ac or dc value of a plasma potential to be documented. Second, ‘maximal’ suppression (when electron

saturation current is as small as possible compared to the ion saturation current) of the electron-current collection, while electrostatically floating, enables the ac or dc value of an ion temperature to be documented. Along with these two modes, the MIB probe in many cases can work as a standard probe, that is, as a probe with removed obstacles (baffles), enables the ac or dc value of an electron temperature to be documented. Over the applicable range of plasma conditions, some uniformity exists in extracting useful information from strategically acquired probe measurements.

2. MIB probe: principles of operation, constructions and simple analytical theories

Principles of the MIB probe operations are based on independently controlled, direction-specific, probe collection of electrons and ions. The tested designs, presented here, have proven operationally reliable and convenient to interpret. Compared to the open (unbaffled) probe, MIBP's baffling introduces negligible effects on unbaffled ion-current collection, while negligibly distorting the unbaffled shape of electron-current collection in the *IV*-trace.

MIBP may be a useful tool for fusion-boundary plasma studies [47–50]. Simple analytical probe theories, that can describe the plug and baffled probe designs are presented at the section 2.3. The Katsumata-style and divertor-located, flush-mounted style of the MIBP family can probably be described using the formulas for a wall probe [7, 51–54]. So far, this has not been accomplished and, therefore, the pertinent detailed formulas are neither discussed nor presented. For the more-complicated MIBP designs, appropriately complicated numerical simulations are needed, which are more difficult to perform and use. These issues are also not discussed in this review. Complicated probe constructions, for example, like bunker-type probes [39], can hardly be referred to, and used, as MIBP surrogates.

2.1. Principle of operation

In a magnetized-orbit plasma, probe collection of electron and ion currents depends on direction with respect to the magnetic field (charged particle diffusion is different along and perpendicular to the magnetic lines) [10, 55–57]. An example of these distinct collection areas for a cylindrical probe, which is situated parallel to the magnetic lines (heretofore referred to as a parallel probe), is shown in figure 1(a) (top). In that figure, the distinct areas are denoted as the electron and ion ellipsoids (of revolution). In this geometrically simple case, analytical calculations of the parameters of the electron and ion ellipsoids are possible [55, 56]. For a parallel probe, electron and ion ellipsoids will be 3D and extended along the probe. Figure 1(b) shows electron and ion collection areas for a flat disc probe at a wall. In the left pictures, the magnetic field is parallel to the wall surface, and in the right picture it is perpendicular.

For other probe designs and orientations analogous collecting areas, in principle, could be calculated numerically. Obviously, they must have a complex shape (although

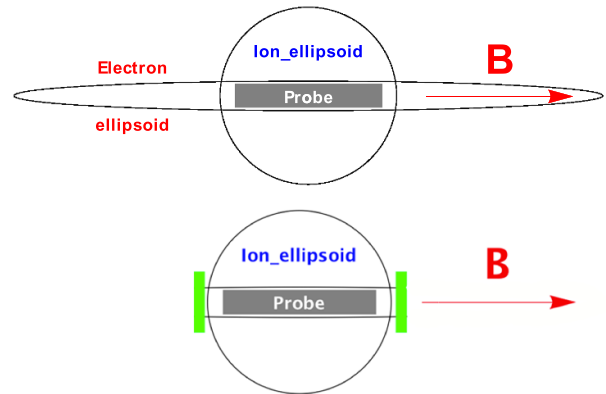


Figure 1(a). Plasma regions from which electrons (electron ellipsoid) and ions (ion ellipsoid) are drawn to the parallel cylindrical probe. The same probe with insulating obstacles (in this case plugs, shown in green) to cut off a part of the electron ellipsoid and therefore reduce the electron probe current (bottom). Red arrow shows the direction of the magnetic field *B* (top).

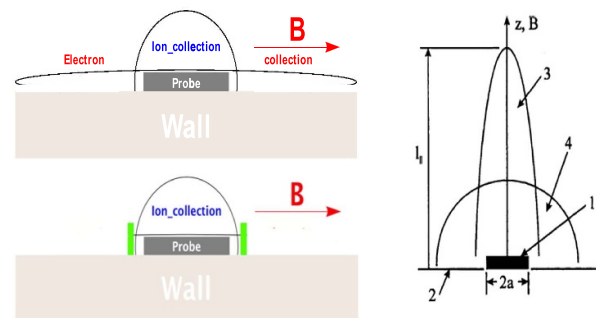


Figure 1(b). Plasma regions from which electrons and ions are drawn to the flat disc probe (left, top). The same probe with insulating obstacles (in this case plugs, shown in green) to reduce electron probe current (left, bottom). Red arrows show the direction of the magnetic field *B*. Similar probe, but magnetic field lines are perpendicular to the wall (right): electron (3) and ion (4) current collection regions; (1) probe, (2) wall, right figure taken from [51]. Reprinted by permission from Springer Nature Customer Service Centre GmbH: Springer Nature, Technical Physics Letters [51], Copyright (1998).

the volume from which the electrons are collected must be extended along the magnetic field much larger than the volume from which the ions are collected) and can only be calculated numerically. We are currently not aware of such calculations.

Placing obstacles (for example, baffles or plugs) near the probe (examples are shown in green in figures 1(a) (a plug probe) and 1(b) (a Katsumata-type probe; in this case the obstacle is a piece of a cylindrical tube), cut off a portion of the electron collecting area, as shown in figures 1(a) (bottom) and 1(b) (left, bottom). Although such an obstacle is not shown in the right figure 1(b), it is easy to see that a part of the electron collecting space can also be cut off by a plug placed parallel to the wall at some distance from the probe surface. Such obstacles reduce the electron current to the probe. Depending

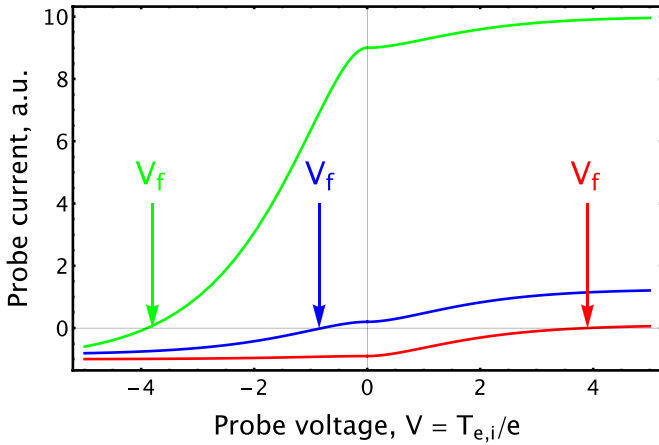


Figure 2. *IV*-traces for different ratios of electron and ion saturation currents in the magnetized plasma; case $I_e^{\text{sat}} \gg |I_i^{\text{sat}}|$ (green), case $I_e^{\text{sat}} = |I_i^{\text{sat}}|$ (blue) and case $I_e^{\text{sat}} \ll |I_i^{\text{sat}}|$ (red). Floating probe potentials, V_f , shown with arrows of the appropriate color.

on the situation, this decrease may be small or very large. Moving the obstacles with respect to the probe or changing the probe and obstacles orientation together with respect to the magnetic field, serve to regulate electron-current collection, leaving ion-current collection relatively unchanged. It is also possible to substantially reduce or eliminate the ion-current collection by recessing the probe tip into the insulating tube, beyond a few electron gyro-radii [27].

As a result, it is possible to have electron saturation current, I_e^{sat} much higher than absolute value of ion saturation current $|I_i^{\text{sat}}|$ (as it is for an ordinary electric probe) for measurement of EDF, T_e , or electron temperature oscillations \tilde{T}_e , or to have vice versa, $I_e^{\text{sat}} \ll |I_i^{\text{sat}}|$, for measurements of IDF, T_i , or ion temperature oscillations \tilde{T}_i (note, that a possibility of such measurements may depend on the applicable probe theory [10]). It is also possible to adjust the ratio of electron to ion saturation current between both limiting cases.

Sometimes (but not always, compare, for example, figures 11–13) the decrease in electron (or ion) current can be described using the shading coefficient (see also section 2.3). This can be done when the change in the electron current from the probe potential with a change in its orientation does not depend essentially on the probe potential (the shape of the *IV* trace for the electron current does not depend essentially on the probe orientation). Since the computational simulation of the current in these cases can be too complicated, the verification of the possibility of using the shading coefficient can be carried out experimentally, as shown below in the experiments (see section 3).

Figure 2 shows examples of *IV*-traces for different ratios of electron and ion saturation currents in the magnetized plasma, $I_e^{\text{sat}} \gg |I_i^{\text{sat}}|$ (hereafter referred to as ‘open MIBP’), $I_e^{\text{sat}} = |I_i^{\text{sat}}|$ (later referred to as ‘equalized MIBP’) and $I_e^{\text{sat}} \ll |I_i^{\text{sat}}|$ (hereafter referred to as ‘closed MIBP’). Corresponding floating probe potentials are shown with arrows of the appropriate color.

Assuming that electron and ion temperatures are comparable in the shown cases, the floating potential is negative and

equal to several electron temperatures for the first case (green curve), positive and equal to several ion temperatures in the last case (red curve), but can also include some influence of electron temperature (see section 2.4 for more explanations). For the middle case of equal electron and ion saturation currents (blue curve), the floating probe potential may more accurately represent the plasma potential, without necessarily being equal to it.

Connecting V_f to electron and ion temperatures is done more precisely using corresponding probe theory. More details of interpreting *IV*-traces with analytical theories can be found, below, in section 2.3, along with an explanation of why floating MIBP probe potential is generally different from plasma potential, even for the case $T_e = T_i$ and $I_e^{\text{sat}} = |I_i^{\text{sat}}|$.

2.2. Actual MIBP constructions

So far, three distinct MIBP constructions have been developed and used in experiments. They are shown in table 1. Pros and cons are also given in table 1 for each MIBP design and modification.

Table 2 shows two additional Katsumata-type probe modifications used in experiments as well as with one more Katsumata-type design, which could be useful in the future research. Pros and cons are also provided for each Katsumata-type probe modification.

2.3. Theories for the probe currents in a magnetized plasma

For the simple determination of plasma parameters from *IV*-traces and/or floating probe potentials, an applicable probe theory could be used if possible [10, 12, 55–57]. Corresponding theories have been developed for ordinary cylindrical and spherical probes for some (not for all) regimes of the probe operations (for regimes of the probe operations see, for example, table I from [10], which should be supplemented by corresponding gyro radii). There are also analytical theories (see, for example, [51–54]) for a flat wall probe, which, probably, could be used for description of the simple Katsumata and/or flush-mounted MIBPs, but this proposition has not been checked experimentally yet.

Generally, the theories should be corrected on the presence of the baffles, which in the simplest case may be performed by introducing corresponding shading coefficients, as it was mentioned above, but possibility to use this proposition should be checked experimentally in any particular case. It is possible to expect, that due to a simple construction, the plug probe is the best for similar modeling. The possibility of such modeling and demonstration of applicability of the shading coefficient for the plug probe have been shown experimentally, for example, in [36]. In this case, plugs have practically no effect on the ion current and reduce the electron current by a certain permanent factor without changing its shape. Obviously, if the baffles are too large, this approach may not be correct. In each specific case, for a certain plasma and the sizes of the probe and plugs, the analytical theory formulas should be verified experimentally, as demonstrated, for example, in section 3.

Table 1. Various MIBP designs: schematic of the Katsumata probe (top); schematic of the plug probe (middle): (1) ceramic probe holder, (2) tungsten wire tip, (3) ceramic plugs [36, 45] (middle); schematic of the baffled probe (bottom): (1) tungsten wire tip, (2) ceramic baffles, (3) ceramic probe holder [40, 46] (left). Arrows B show the direction of the magnetic field. Brown tube is the insulated probe holder. White arrow shows directions of the collector move for the Katsumata probe regulation.

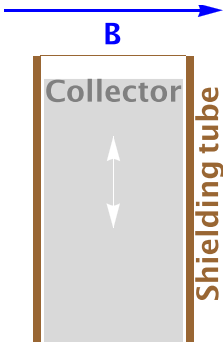
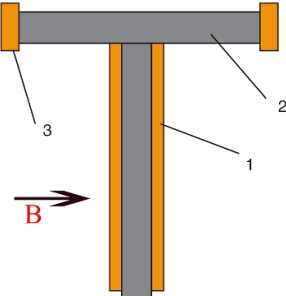
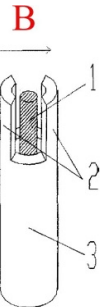
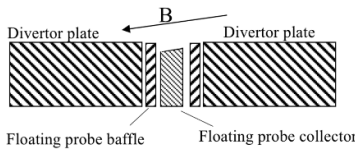
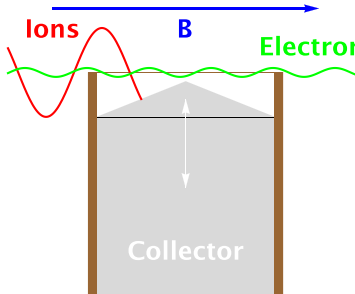
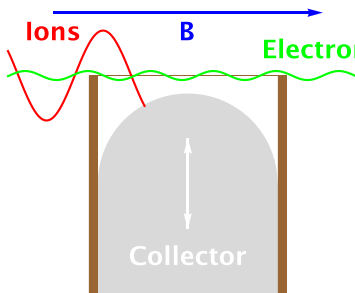
MIBP constructions	Description	Pros and Cons
 <p>Figure 3(a). Katsumata probe schematic [31, 32].</p>	<p>Schematic of the Katsumata probe is shown in figure 3(a). Several more complicated modifications of this probe, including additional conducting screens and grids, have been used in various measurements [10]. The widespread use of this type of probe for measuring IDF was, probably, hampered by a design that is notoriously difficult to model and to substantiate its reliable operation. The floating potential of the probe design may strongly depend on the probe design [10]. Attempts to model Katsumata probe (occasionally referred to as a ball-pen probe) were published [59, 60]. The accuracy of that model is unknown, especially for the case of anomalous charged particle fluxes to the probe immersed in a plasma.</p>	<p>Pros: robust design allows measurements in fusion plasma; smooth adjustability in the ratio of the electron and ion saturation currents; numerical/modeling of classic and anomalous regimes simplified due to flat conductor surface.</p> <p>Cons: yet-to-implement simple probe theory and formulae for analyzing the operation of the probe because numerical methods for analyzing probe operation are required; the accuracy of numerical methods is unknown, so it may be difficult to account for various distorting factors, including conditions on the probe and probe holder surfaces after interaction with plasmas.</p>
 <p>Figure 3(b). A plug probe or T-probe with two plugs [35, 36, 43].</p>	<p>Schematic of the plug probe is shown in figure 3(b). It looks that this probe has higher space resolution and lower probe-holder-induced plasma distortion than other MIBP. The plug probe allows measurements of IDF and/or ion temperature [45]. In the electrostatically floating mode, this probe has measured plasma-potential oscillation in a low-temperature, fusion-relevant, magnetized plasma [42]. Such a probe requires precise alignment with respect to the magnetic field lines (with an accuracy of several angular degrees). Note, that plug probes are typically compatible in low-temperature plasma only due to the delicate design, while other probe constructions might be suitable for fusion-boundary temperature plasma with standard limitations (e.g. reciprocated probes in the vicinity of walls and divertor-located, flush-mounted probes).</p>	<p>Pros: design simplicity enabling comparison with ordinary probes; cluster-configuration suitability; compatibility with standard-probe theory if shading coefficients are incorporated; tolerance for a probe holder because of lower plasma distortion even with increased spatial resolution.</p> <p>Cons: delicate design is too fragile to serve as a reciprocating probe in the fusion-grade plasma; the need for precise angular installation with precision better than a few (several) angular degrees; the design makes it difficult to smoothly adjust the ratio of the electron and ion saturation currents.</p>
 <p>Figure 3(c). The baffled probe schematic [40, 46].</p>	<p>Schematic of the baffled probe is shown in figure 3(c). In contrast to the plug probe, the baffled probe design is more robust and is usable in fusion-relevant plasma [40]. Compared to a plug probe, major advantages of the baffled probe are reduced sensitivity to the probe's alignment with respect to the magnetic lines and the continuous adjustability in electron- and ion-current-collection ratio.</p>	<p>Pros: design simplicity enabling comparison with ordinary probes; Design robustness, allowing reciprocating probe movement when required; tolerant about angular installation; the design makes it easy to smoothly adjust the ratio of the electron and ion saturation currents; cluster-configuration suitability; compatibility with standard-probe theory, if shading coefficients are incorporated (with some restrictions), providing simple modeling and description of the probe.</p> <p>Cons: design may be prone to errors associated with complicated numerical modelling when simple analytical theory is not possible; incompatibility with standard-probe theory even with shading coefficients.</p>

Table 2. Various Katsumata-type probe modifications: schematics of the flush-mounted NSTX MIB probe [61–63] (top), the ball-pen probe [1, 33, 39] (bottom, left) and alternative Katsumata-type probe [1, 31, 32] (bottom, right). Arrows B show the direction of the magnetic field. Brown tubes are the insulated probe holders. White arrows show directions of the collector move for the probe regulation. Trajectories of electrons (green) and ions (red) are also shown for bottom designs.

Katsumata-type probe modifications	Description	Pros and Cons
	<p>A divertor-located, flush-mounted MIBP is shown in figure 3(d). This probe has been developed and installed in the spherical tokamak NSTX [61–63] and latter in stellarator TJ-II. Unlike the original Katsumata probe, this design has a probe surface inclined towards the device wall. This is due to the fact that the magnetic lines in the place where the probe was installed was also inclined towards the wall.</p>	<p>Pros: robust design allowing measurements in fusion-boundary plasma; possibility of smooth change in the ratio of the electron and ion saturation currents; flat conductor surface could make it simpler for numerical and maybe even for analytical modeling. Cons: ordinary probe theories and formulas have not been developed yet for analyzing the operation of the probe; at present the need to use numerical methods for analyzing the operation of the probe, the accuracy of which is not known; it is difficult to consider various distorting factors, including conditions of the probe and probe holder surfaces after interaction with plasmas.</p>
	<p>The schematic of the ball-pen probe [33, 39] is shown in figure 3(e). This probe is a modification of the Katsumata probe. According to the developers of this probe, the conical collector improves the control of the transition between full electron collection and zero electron collection, in contrast to the original Katsumata probe. However, the geometry of the cone complicates both the analytical description and the numerical model of the operation of the probe for obtaining plasma parameters from the measurements [59, 60]. The influence of various distorting factors, such as probe-surface conditioning [64] and the electrostatic perturbation due to the probe holder for non-flush-mounted probes [10, 12], is also not known.</p>	<p>Pros: according to the developers, magnetic insulation is highly controllable. Cons: uncertainty in model-based predictions of IV-traces. McCarrick <i>et al</i> [1] used a flat-collector Katsumata probe to document the IDF of collected ion collection in ‘$T_e/T_i = 10$ eV/100 eV’ fully-ionized magnetized-orbit mirror-machine plasma supplied by a gas-injected washer gun. Pros: magnetic insulation is highly controllable by adjustment of uniform, adjustable baffle-to-collector gap; numerical calculation of IV traces is possible.</p>
	<p>The schematic of one more possible modification of the Katsumata probe is shown in figure 3(f). That modification has a spherical probe surface and could provide a smoother IV-trace than the ball-pen probes because it rounds the sharp end of the cone and removes possible increased electric fields near it, while providing better simulation capabilities. However, the accuracy of that proposition requires experimental and modeling verifications.</p>	<p>Cons: space-charge limit plasma penetration to a density-dependent thickness of the plasma’s radial profile. Pros: the collector as a spherical tip can make the transition between full electron collection and no electron collection smoother; robust design allowing measurements in fusion plasma; possibility of smooth change in the ratio of the electron and ion saturation currents; spherical conductor surface could make it simpler for numerical and maybe even for analytical modeling. Cons: difficult or impossible to make a simple analytical model for the probe operation description; in numerical modeling it is difficult to consider various distorting factors, including conditions of the probe and insulated probe holder surfaces.</p>

The similar proposition looks to be true for the baffled probe also [46, 58]. In this case, the baffles can also somewhat reduce the ion current, which does not depend on the angle of its rotation and does not change ion current shape. This can be verified experimentally by rotating the probe or by comparing the measurements of the ion part of the trace with a conventional probe of the same size. However, in this case, the theories may be invalid for some angles of rotation. That is, the applicability of the theory may be somewhat (but not essentially for correctly designed baffles) limited. Experiments with baffled probes allow to check the applicability of the analytical theories and to identify those problems that exist. This comparison of the theory and experiments is discussed in the next section. Possible deviations of experiments from the results of theory for certain rotation angles are also demonstrated (see, for example, figure 13).

As it is mentioned above, the application of this approach to the Katsumata and/or flush-mounted MIBPs has not been checked yet. The ball-pen and other Katsumata-type probes with non-flat conducting surfaces may not have the straightforward simple analytical theory descriptions. In those cases, existing theories, probably, could provide only some qualitative insights into the general behavior of the MIBPs and only numerical simulations would be more useful. However, the complex shapes of the ball-pin probe and the flush-mounted MIBP make this task not easy. As far as we know, the problem of numerical modeling has not yet been fully solved, although some useful attempts have been made [59, 60].

The main plasma/probe characteristic lengths (in an unmagnetized plasma), defining applicability of certain probe theories, are mean free paths of electrons, λ_e , and ions, λ_i , probe radius, R , and length, L , sheath thickness (connected to the Debye length and electron energy), h , and electron energy-relaxation length, λ [10]. In the magnetized plasma, gyro radii of electrons, ρ_L^e and ions, ρ_L^i , as well as the probe orientation with respect to the magnetic lines are also important.

Two probe orientations, when the probe is parallel to the magnetic lines and the probe is perpendicular to the magnetic lines (further perpendicular probe), are most important in practice. Below we will discuss the most interesting modes and related theories that can be applied to calculate electron and ion currents to MIBPs. In practice, the most interesting for the purposes of this review and widely applicable for probes in magnetized plasma is the classic diffusion regime. Therefore, the discussion begins with this mode. This mode can exist in a wide range of plasmas, from fusion to cold plasma.

Anomalous diffusion-to-probe mode is also possible for fusion-boundary plasma, but probably in large machines with higher magnetic fields only. It may be more likely for the Katsumata-type probes which normally have greater dimension perpendicular to magnetic lines, than for baffled probes.

After anomalous diffusion case, we also recall the collisionless and nonlocal (the last one only exists for electrons) regimes. These modes are apparently less interesting and less applicable for the strong suppression of the electron current. The latter mode partially overlaps with the classical diffusion mode. Note, that regimes for ions and electrons can be simultaneously in different domains.

Classic diffusion probe theory is valid for weakly ionized plasma for the case of $\rho_L^e < R$ (for electrons) and $\rho_L^i < R$ (for ions) [10, 55–57, 65]. For the parallel probe, a reliable separation of the electron and ion currents may be obtained in the conditions $L < 2x_e R$ and $L > 2R\sqrt{1+x_i^2}$, where $x_e = \lambda_e/\rho_L^e$ and $x_i = \lambda_i/\rho_L^i$. In this case, the electron current flows mainly to the ends of the probe, while the ion current flows to the lateral surface. In this case, the density of plasma is disturbed near the probe in the electron ellipsoid (see, figure 1(a)) with semi-axes R and Rx_e for electron saturation current and the ion ellipsoid with semi-axes $L/(2\sqrt{1+x_i^2})$ and $L/2$ for ion saturation current.

The ion saturation current for a parallel probe may be found as [55, 66]

$$I_i^{\text{sat}} = \frac{8\pi e R n_e (1 + T_e/T_i) D_i \sqrt{\gamma_i^2 - 1}}{(1 + x_i^2) \times \ln \left[\frac{\left(1 + \sqrt{1 - \gamma_i^{-2}}\right)}{\left(1 - \sqrt{1 - \gamma_i^{-2}}\right)} \right]}, \quad (1)$$

where $D_i = T_i/(M\nu_i)$ is the ion diffusion coefficient along the magnetic field, ν_i ion collision rate with ions and neutrals and $\gamma_i = L/[2R\sqrt{1+x_i^2}]$. The electron current is [65, 66]

$$I_e^{\text{sat}} = -\frac{4\pi e n_e (1 + T_i/T_e) D_{\text{ep}} x_e R (1 - \gamma_e^2)^{1/2}}{\tan^{-1} \sqrt{(1 - \gamma_e^2)/\gamma_e^2}}, \quad (2)$$

where e is the electron charge ($-1.6 \times 10^{-19}\text{C}$), $D_{\text{ep}} = T_e/(m\nu_e(1+x_e^2))$ is the electron diffusion coefficient perpendicular to the magnetic lines, ν_e electron collision rate with electrons and neutrals and $\gamma_e = L/(2Rx_e)$. Note that in equations (1) and (2) I_e^{sat} is positive and I_i^{sat} is negative, that corresponds to currents shown in figure 2. If the probe is short enough (which is typically correct for experiments considered in this review), that is, $L \ll Rx_e$, the last equation may be rewritten as [26]

$$I_e^{\text{sat}} = \frac{8n_e R (T_e + T_i)}{B}. \quad (3)$$

For the case of $L < 2R\sqrt{1+x_i^2}$, the ion density is perturbed inside the electron ellipsoid. This case may be not very interesting to MIBPs, as it is difficult to regulate electron current with respect to ion current. If needed, the solution for this case may be found in [10, 55, 66].

The above equations can be rewritten for any angle between probe axis and magnetic line. Corresponding equations can be found in [66]. For a perpendicular probe, the electron saturation current in strongly magnetized (electron gyro radius is small in comparison with probe radius [10]) plasma may be written as [27]

$$I_e^{\text{sat}} = \frac{2\pi L n_e (T_e + T_i)}{B \ln[\pi L/(4R)]}. \quad (4)$$

The transitional part of the IV -trace may be obtained by the standard way [7, 26, 55, 67] by relating the potential overshoot

in the sheath (see [68]) to the particle fluxes to the probe from the plasma. If β is the ion current, normalized by the ion saturation current, as $I_i = \beta I_i^{\text{sat}}$, it is possible to find β for the thin sheath as a function of probe voltage V for parallel probe from expression

$$eV = -T_i \ln \left[\frac{2\pi n_e R L \bar{\rho}_L^i \bar{v}_i (1 - \beta)}{\beta I_i^{\text{sat}}} \right] - T_e \ln [1 - \beta], \quad (5)$$

where $\bar{\rho}_L^i$ is the average ion gyro radius and \bar{v}_i is the average ion collision rate, $\bar{\rho}_L^i \bar{v}_i \approx \sqrt{T_i/(2m_i)}$ for $x_i < 1$ and $\bar{\rho}_L^i \bar{v}_i \approx \sqrt{T_i/(2m_i)}/x_i$ for $x_i > 1$ [65].

Similarly, α defined by equation $I_e = \alpha I_e^{\text{sat}}$ for parallel probe can be found from

$$eV = T_e \ln \left[\frac{\pi n_e R^2 \bar{\rho}_L^e \bar{v}_e (\alpha - 1)}{\alpha I_e^{\text{sat}}} \right] + T_i \ln [(1 - \alpha)], \quad (6)$$

where $\bar{\rho}_L^e \bar{v}_e \approx \sqrt{T_i/(2m_i)}$. Note, that equation (19) in [1] contains a misprint (electron gyro radius is omitted). Similar equations for the diffusion (thick) sheath can be found, for example, in [69]. For perpendicular probe equation (6) may be rewritten as

$$eV = T_e \ln \left[\frac{\pi n_e R L \bar{\rho}_L^e \bar{v}_e (\alpha - 1)}{2\alpha I_e^{\text{sat}}} \right] + T_i \ln [(1 - \alpha)]. \quad (7)$$

Since the ions are weakly magnetized, equation (5) can be used to calculate the intermediate part of the probe characteristic for the ion current.

In the strongly ionized (electron-ion collision rate is comparable or higher than electron-atom collision rate) plasma, the electron current to a small probe can be obtained by the same way as for weakly ionized plasma [51, 55–57]. In this case collisions of electrons and ions with charged particles play main role in the diffusion. The small probe means that its perpendicular (to the magnetic lines) size is somewhat less than the ion gyro radius. In the opposite case anomalous charged particle transport will be the main process (see below).

The above classic diffusion probe mode assumes that electrons and ions are in the diffusion mode and have Maxwellian distributions with temperatures T_e and T_i . In the event that the nonlocality condition is satisfied for electrons, then the corresponding equations (see below) can be included in the above theory for calculating the electron current. This may be important, provided that the EDF is not Maxwellian. We note that the nonlocal theory for electrons considered below also includes the collisionless regime. If necessary, the collisionless theory for ions can also be used to analyze the movement of ions. The collisionless regime for electrons and ions is also discussed below.

The theory of classical diffusion onto the wall probes was also developed in [7, 26, 51]. Apparently, that theory could be, probably, used to describe the operation of the Katsumata probe and flush-mounted MIB probe for the case of classic diffusion regime.

Collisionless theory for electrons is valid for the case when there are no electron collisions with any particles (including electrons) in the area of plasma distorted by the probe. For

the case $\lambda_e \gg \rho_L^e$ and the thin sheath ($h \ll R$), the criteria for validity of the theory are $\rho_L^e \gg L$ for parallel probe and $\rho_L^e \gg R \ln(L/R)$, for perpendicular probe (for thick sheath, h should be inserted into the criteria) [10, 12]. In collisionless case, the density of electron current to the negatively charged probe can be calculated as [3, 10, 12]

$$j_e(V) = -\frac{2\pi n_e}{m^2} \int_{eV}^{\infty} (W - eV) F_e(W) dW, \quad (8)$$

where F_e is the EDF in the undisturbed plasma, W is the electron kinetic energy, m is the electron mass, V is a (negative) probe voltage and n_e is the electron density. The EDF can be found from electron probe current density, using the Druyvesteyn formula [10, 12, 70]

$$F_e(\varepsilon) = -\frac{m^2}{2\pi n_e e^3} \frac{d^2 j_e}{dV^2}. \quad (9)$$

Collisionless theory for ions is valid for the case when there are no ion collisions with any particles in the area of plasma distorted by the probe. For ions and positively charged probe in the above formulas λ_e , ρ_L^e , j_e and m should be replaced by λ_i , ρ_L^i , j_i and the ion mass M , correspondingly.

For electrons with positively charged probe (electron saturation current), ions with negatively charged probe (ion saturation current) and very weak magnetic fields, the collisionless theories for unmagnetized plasma could be used. For the very thick sheath, the orbital limited motion theory may be valid [3, 10]. The domain of validity of the orbital motion limit regime for cylindrical probes in more details has been investigated in [71, 72]. Thin sheath and transition to the thick sheath have been considered in [4, 5, 73–77].

Laframboise performed extensive numerical computations of ion and electron currents for the collisionless regime [78]. There are several approximations, that fits to his results [79–82]. A cross-check of the models and comparison with results from alternative diagnostics allow us to find the limits of theories validity [83–86].

Collisionless regime for electrons may not be good for obtaining cases of $I_e^{\text{sat}} = |I_i^{\text{sat}}|$ and $I_e^{\text{sat}} \ll |I_i^{\text{sat}}|$ (blue and red lines in figure 2), as difference in the electron and ion shading by the baffles may not be sufficient. Regime $I_e^{\text{sat}} \gg |I_i^{\text{sat}}|$ may easily be obtained. This regime could be used for measurements of the EDF, electron temperature and its oscillations.

Electron nonlocal probe theory for weakly-ionized magnetized plasma is valid for the case when there is no loss of the kinetic electron energy during elastic electron collisions with any particles in the area of plasma distorted by the probe (plasma with nonlocal EDF [87]). In the plasma, for the case $\lambda_e \gg \rho_L^e$ and $h \ll R$, this theory is valid for $2m\rho_L^e/M \gg L$ (for parallel probe) and $2m\rho_L^e/M \gg R \ln(L/R)$ (for perpendicular probe) [10, 12]. It was shown [10, 12, 88–90], that the probe electric current for negative probe potentials may be calculated as

$$j_e = -\frac{8\pi n_e}{3m^2} \int_{eV}^{\infty} \frac{(W - eV) F_e(W) dW}{\gamma(W) \left(1 + \frac{W - eV}{W} \Psi(W)\right)}, \quad (10)$$

where Ψ is the diffusion parameter. The previous collisionless case is a part of this regime. The diffusion parameter Ψ depends on the plasma parameters, and the shape, size and orientation of the probe [10, 12]. If the cylindrical probe is oriented perpendicular to the magnetic field, then

$$\Psi(W) = \frac{R \ln \pi L / 4R}{\gamma \rho_L^e} \quad (11)$$

If the probe is oriented parallel to the magnetic line then

$$\Psi(W) = \frac{\pi L}{4\gamma \rho_L^e}. \quad (12)$$

Equations (5) and (6) are valid for $h \ll R$ (thin sheath). Otherwise Ψ will depend on electric field distribution in the sheath [10].

In the strong magnetic field ($\Psi \gg 1$) (this case excludes collisionless regime), we can neglect unity in the denominator of equation (10). Then we obtain for the perpendicular probe

$$j_e(V) = -\frac{8\pi en_e}{3m^2 R \ln \pi L / 4R} \int_{eV}^{\infty} \rho_L^e W F_e(W) dW, \quad (13)$$

and

$$F_e(eV) = -\frac{3m^2 R \ln \pi L / 4R}{8\pi e^3 \rho_L^e V} \frac{dj_e}{dV}. \quad (14)$$

For parallel probe

$$j_e(V) = -\frac{32\pi en_e}{3m^2 L} \int_{eV}^{\infty} \rho_L^e W F_e(W) dW, \quad (15)$$

and

$$F_e(eV) = -\frac{3m^2 L}{32e^3 \rho_L^e V} \frac{dj_e}{dV}. \quad (16)$$

The nonlocal regime does not exist for electrons in strongly ionized plasma and for ions, since the mean free path for them coincides with the energy relaxation length.

Anomalous diffusion probe regime may exist in the case of strongly ionized plasma and a small ion gyro radius with respect to the transversal characteristic probe size [52–55]. If the diffusion to the probe is classical, then a situation is possible when diffusion in the plasma volume is anomalous at the same time [10, 42, 44]. While a complete theory of anomalous transport to probes has not yet been formulated, developments permit a quantitative interpretation of probe characteristics when analyzing MIBP behavior in some cases, for example, Katsumata and wall probes (see below).

When the transverse scale of the probe is larger than the ion gyro radius, the distribution of potential is in large extent determined by the across magnetic field conductivity [52]. Effect of the transverse conductivity caused by the ion-neutral collisions was considered, for example, in [91, 92] (ion viscosity and inertia were neglected). The conclusion has been made

Table 3. The main regimes for electrons and ions in magnetized plasma for parallel or perpendicular probe. For each regime (for exception anomalous transport), upper cells are for electrons and lower cell are for ions.

		Conditions of applicability	
Regime		Perpendicular probe	Parallel probe
1	Classic diffusion	$\rho_L^e < R$ $\rho_L^i < R$	$L < 2x_e R$ $L < 2R \sqrt{1 + x_i^2}$
2	Collisionless	$\rho_L^e \gg R \ln(\frac{L}{R})$ $\rho_L^i \gg R \ln(\frac{L}{R})$	$\rho_L^e \gg L$ $\rho_L^i \gg L$
3	Nonlocal	$2m\rho_L^e/M \gg R \ln(L/R)$ Absent	$2m\rho_L^e/M \gg L$ Absent
4	Anomalous transport	May exist in the case of strongly ionized plasma and a small ion gyro radius with respect to the transversal characteristic probe size	

that the transverse conductivity is very important and should never be ignored [91].

For the case of anomalous diffusion, see [48, 93–95] for calculations of the wall MIBP traces. Apparently, if necessary, they could be used to analytically studying wall MIBPs, for example, such as shown in the figures 3(a) (left) and (b) (top). The equations from [52] are not presented in this review, since they were not used to analyze the operation of MIBPs in the literature known to us and were not needed to analyze the operation of the probes used in the measurements under consideration below. Apparently, this theory could be used to describe the operation of the Katsumata probe and flush-mounted MIBP for the case of anomalous diffusion regime.

Conditions of applicability of the above theories are summarized in table 3. Electrons and ions may be in the same or different regimes at the same time.

With the practical use of probe theories in the next sections of this review, it was found that in sections 4–7, the theory of classical diffusion works well in all devices with the used magnetic fields. This makes it possible to calculate total probe IV traces; to compare experimental and calculated IV traces and find probe configurations for which the theory does not work; to determine the temperatures of electrons and ions (this was done in section 8 as well); to find the coefficients μ_e and μ_i , by varying within small limits temperatures of electrons and ions in calculations; to determine the value of V_0 and to determine the shading coefficients of the probes for electrons and possibly ions. To measure EDF or IDF in section 8, much weaker magnetic fields were used. In this case, the nonlocal theory worked for electrons, and the collisionless theory worked for ions. Anomalous transport to probes apparently may exist in large fusion devices at higher magnetic fields and is beyond the scope of this review.

2.4. Floating regime of the MIB probe operation

Floating regime of the MIBPs is the most important for studying oscillations in plasma. It can be modeled with application

of the above theories. In a general case the potential of a floating ordinary or MIBP V_f can be approximated as

$$V_f = V_S + V_0 - \mu_e T_e / e + \mu_i T_i / e, \quad (17)$$

where voltage offset $V_0 \approx 0$ in an unmagnetized plasma and V_0 in a magnetized plasma may be of the order of electron and/or ion temperatures (or a combination of electron and ion temperatures). Dimensionless coefficients μ_e and μ_i could be substantially greater or lower than the unity [43, 46]. For a MIBP probe, coefficients μ_e and sometime μ_i may include obstacle shading. The voltage offset V_0 , μ_e and μ_i may depend on the probe construction, magnitude of the magnetic field and some plasma parameters. Values of μ_e , μ_i and V_0 may be calculated by application of the corresponding theory, for example, from this subsection [10, 46] and/or measured in experiments [42]. Note, that the sometime-used (see, for example, [33, 39]) formula $\mu_e = \ln[I_e^{\text{sat}} / |I_i^{\text{sat}}|]$ for plasma in a magnetic field may give a large error.

The voltage offset is arising as a result of the complicity of the probe IV -trace, which can even have ‘plateaus’ and linear parts in the magnetized plasma [10, 55–57]. Note, that the floating MIBP potential is generally different from plasma potential even for the case $I_e^{\text{sat}} = |I_i^{\text{sat}}|$ not only due to existence of the voltage offset, but also the fact that $\mu_e T_e$ and $\mu_i T_i$ maybe not equal.

It may also be important, that in the plasma there is a possibility in some cases that both electron and ion saturation currents can flow to the probe simultaneously [55–57]. That may not be the case in an unmagnetized plasma, but this case is, probably, not suitable for direct V_S measurements due to absent of shading the electrons by the baffles. Therefore, for practically important plasma, V_0 may be up to the order of a few $T_{e,i}/e$.

That may substantially influence the possible direct measurement of the dc plasma potential from V_f . At the same time the presence of V_0 does not affect the direct measurements of plasma potential oscillations. In this case

$$\tilde{V}_f \approx \tilde{V}_S - \mu_e \tilde{T}_e / e + \mu_i \tilde{T}_i / e, \quad (18)$$

Equation (18) provides a possibility to measure fluctuations of V_S (see the next section) and T_e , or T_i (see section 6) by measuring V_f . Remind here, that floating MIBPs potentially can provide study of plasma oscillations, while, for example, fast swiping probes in the magnetized plasma can allow us to study the plasma evolution only, but not oscillations [10].

In the following sections, examples of measurements of plasma potentials and analytical modeling in different types of magnetized plasma are demonstrated. So far, those measurements and corresponding calculations are performed mainly for plug and baffled probes.

3. Experimental devices and MIBP systems

To date, the MIBPs have been used to analyze the properties of several types of magnetized plasma in different devices.

Table 4. Different devices and used MIBP-types.

Device	MIB probe type	References
Simple Magnetized Torus Blaamann	Plug probes, their clusters	[36]
Simple Magnetized Torus TEDDI	Katsumata probes	[41]
WVU Q-machine	Baffled/Plug probes	[29]
Texas Helimak	Baffled probes	[96–98]
Stellarator TJ-II	Katsumata-type, baffled probes	[99]
Stellarator HSX	Baffled probes	[40]
Stellarator W-7X	Katsumata-type probes	[100, 101]
Tokamak NSTX	Katsumata-type probes	[61–63]
Tokamak EAST	Katsumata-type probes	[102]
Tokamak ASDEX Upgrade	Katsumata-type (ball-pen) probes	[39, 103, 104]
Tokamak MST	Katsumata-type (ball-pen) probes	[39]
Tokamak ALCATOR C-Mod	Katsumata-type probes	[105, 106]
Tokamak CASTOR	Katsumata-type (ball-pen) probes	[107]
Tokamak ST40	Katsumata-type probes	[108]
Tokamak COMPASS	Katsumata-type (ball-pen) probes	[103, 109]
Tokamak START	Katsumata-type probes	[110]
Tokamak ISSTOK	Katsumata-type (ball-pen) probes	[104]

As examples (the list may be not complete), the MIBPs, their clusters and analogs have been installed and used in devices shown in table 4. To demonstrate the capabilities of the MIBPs, typical measurement methods and some significant results in various plasma types, three devices with very different kinds of plasma have been selected and briefly described in this section to show the use of such probes in a variety of different plasmas. These devices, as well as the subsequent studies in the following sections, are described in the order of their practical use in experiments with MIBPs. They are (a) a magnetized torus with low-temperature plasma, (b) Q-machine, which can create cold low-temperature strongly-ionized plasma and (c) a stellarator with hot fusion-boundary plasma.

All those types of plasmas may be unstable and contain substantial/strong oscillations, waves, and global anomalous charged-particle and energy transport, allowing corresponding studies of plasma oscillation properties. This section also demonstrates the real MIBPs and MIBP clusters, which have been used in experiments. Typical experimental probe characteristics and results of their modeling are also provided. The relationships between floating probe potentials and plasma parameters for various probes are shown. Thus, the following sections demonstrate the real MIB probes experiments in the devices as well as their results from those three devices.

3.1. Toroidal low-temperature plasma

A low-temperature toroidal magnetized plasma has various types of oscillations and waves, as well global turbulent

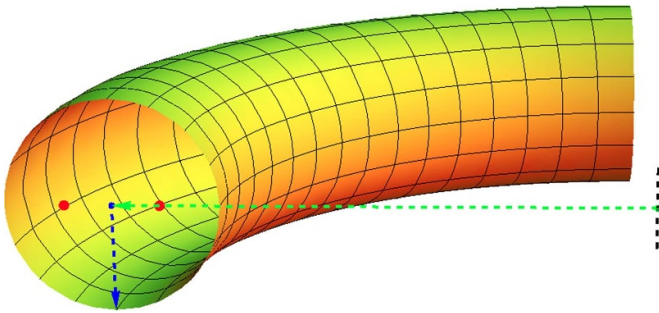


Figure 4. Sketch of a cut of a quarter of the Blaamann torus are to scale. The major, green arrow, 67 cm and minor, blue arrow, 13.5 cm radii are shown. The red dots show probe positions, +6, left (outer plasma) and -6 cm, right (inner plasma). Vertical black dashed line at very right shows axis of symmetry of the torus.

(anomalous) particle and energy transport. In such plasma, oscillation and abnormal transport research can be performed to support basic studies. In the plasma, rather detailed experiments with MIBPs have been conducted, for example, in the magnetized torus ‘Blaamann’ [111] with pure toroidal magnetic field with no rotational transform. A cut of a quarter of the Blaamann torus is shown in figure 4. Basically, this is a dc (although other types of excitation are possible) gas discharged plasma, which is produced by electron emission from a hot, negatively biased cathode, located near the center of the plasma column.

Typical plasma and discharge parameters in the device are the following. Gas pressure is in the range from 0.1 to 0.5 Pa, magnetic field is varied up to 0.5 T, discharge currents are from a fraction of one Amp to several Amps, electron temperatures are from 1 to 20 electron-volt and ion temperature is a fraction of one electron-volt. For those conditions, the typical plasma density may be of order of 10^{11} cm^{-3} . The plasma is turbulent, with relative fluctuation levels of electron temperature and density, as well as plasma potential, of 10% or more.

For measurements of plasma potentials and electric fields, two molybdenum probes with wire radius ranging from 0.125 to 0.5 mm and length varied from 5 to 20 mm have been used (see figure 5, left) [42]. The probes were situated along the magnetic field lines at the distance between them of 6 mm. The probes were short enough and their length practically does not influence the spatial resolution of the measurements. Each probe has insulating plugs at the ends of each rod which has radius from 0.2 to 0.8 mm and made from ceramic.

In order to prevent the most of electrons from reaching the side surface of the probe, the radius of the plugs supposed to be larger than the average electron gyro radius. With larger plugs, making the correct alignment of the probe is easier. Within the above limits on the probe and plug sizes, experiments yield consistent results.

This robustness of the results indicates that the basic idea of plug probe operation works, i.e. the influence of the electron temperature may be effectively eliminated by the plugs and the parallel probe orientation. Along with plug-probes, a system of two standard probes (without plugs), which had the same

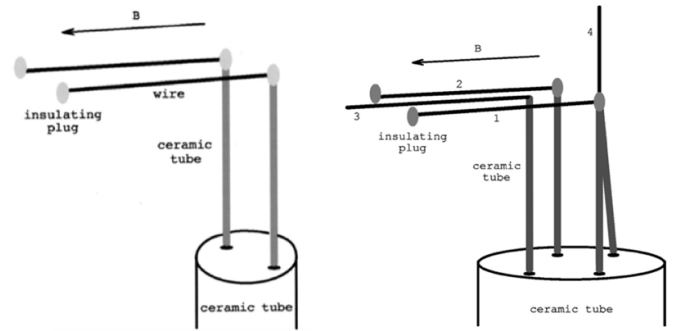


Figure 5. Sketch of the plug probe system for plasma potential measurements (left) [42]. Sketch of the probe cluster for flux measurements (right) [44]. (1) and (2) are plug probes parallel to the magnetic field, (3) and (4) are conventional probes parallel and perpendicular to the magnetic field, respectively. Reprinted left figure with permission from [42], Copyright (2002) by AIP Publishing. Reprinted right figure with permission from [44], Copyright (2002) by the American Physical Society

dimensions as the previous plug-system, was used to measure fluctuations which include the electron temperature.

Figure 5 (right) shows a probe cluster for measurements of anomalous charged particle transport [44]. The cluster contains two parallel plug probes (1) and (2), similar to shown in figure 5 (left). Compared to the cluster shown in the left figure, it also contains an ordinary cylindrical parallel probe (3) and a perpendicular cylindrical probe (4). In this cluster, the plug probes have been used for plasma potential and electric field measurements. The parallel cylindrical probe allows to obtain electron temperature measurements, while the perpendicular probe could measure plasma density oscillations.

As an example, figure 6 shows an experimental plug probe IV -trace [42] in the plasma with following conditions: helium gas pressure is 0.35 Pa, $B = 0.15 \text{ T}$, $n_e = 2 \times 10^{11} \text{ cm}^{-3}$, $T_e = 2.5 \text{ eV}$ and $T_i = 0.22 \text{ eV}$. The probe had $R = 0.125 \text{ mm}$, $L = 18 \text{ mm}$ and plug radius was 0.5 mm. In the described experiments, both ion and electron currents may be described as governed by classical diffusion for a small probe in a weakly ionized, magnetized plasma and probe IV -trace can be simulated by equations (1), (2), (5) and (6) [42, 44].

The result of the calculations is shown in figure 6 by the full curve. In this calculation, to include the influence of baffles, electron current, given by the theory, was reduced to fit the experimental value. A comparison of the experimental results from the plug and conventional parallel probes demonstrates that the plugs could lead to the observed reduction of the electron current.

Figure 7 shows the measured shift of the floating potential from the plasma potential as a function of the electron temperature (dots). This dependence is well approximated by a linear function (solid line)

$$V_f = V_S + 1.1 - 0.4T_e/e \text{ [in Volts]}. \quad (19)$$

The relation yields $\mu_e = 0.4$ and $V_0 = 1.1 \text{ V}$. It is seen that nonlinearity is weak and taking μ_e as a constant is a very good approximation.

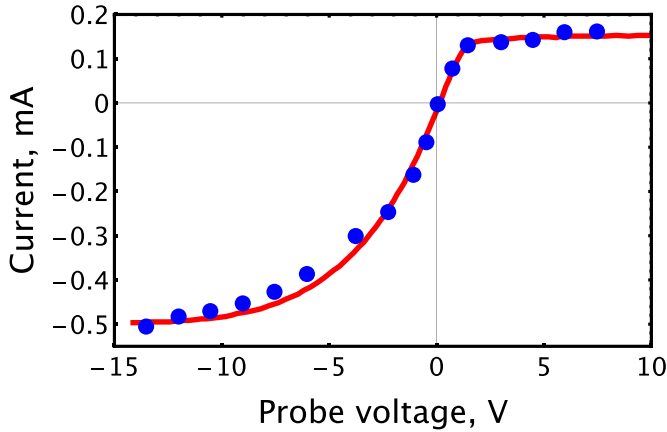


Figure 6. Typical experimental plug probe IV -trace (dots) in helium with pressure of 0.35 Pa and magnetic field $B = 0.15$ T. Calculated IV -trace (full line). V_f is taken as zero. Electron saturation current is positive and ion saturation current is negative [42]. Adapted from [42], with the permission of AIP Publishing.

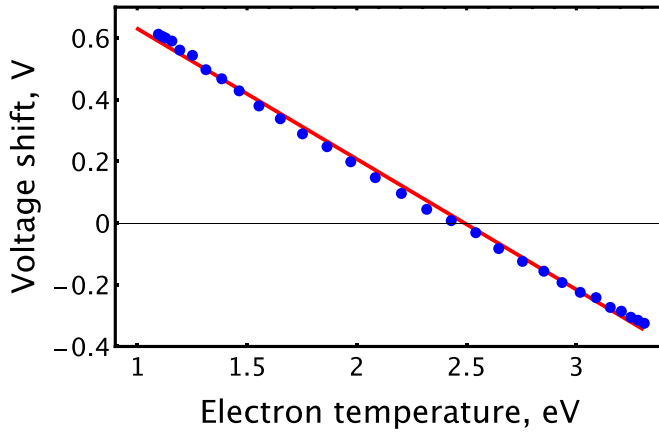


Figure 7. Measured voltage shift of the plug probe as a function of T_e (dots). Approximation of V_f by a linear function (solid line). $B = 0.15$ T [42]. Adapted from [42], with the permission of AIP Publishing.

It was demonstrated that, as ion temperature is much lower than electron temperature and the influences of T_i on the measurements is negligible, ion temperature should not be considered for modeling and experiments. In this situation it may be convenient for measurements of plasma potential oscillations to choose regime $I_e^{\text{sat}} \ll |I_i^{\text{sat}}|$ (about five times in figure 6), which lead to reduction of μ_e considerably lower than unity.

For an ordinary cylindrical probe formula, similar to equation (19), is also valid [10]. To demonstrate that, for perpendicular probe and plasma parameters are: helium pressure $p = 0.3$ Pa, plasma density $n_e = 3 \times 10^{17} \text{ m}^{-3}$ and the ion temperature $T_i = 0.2$ eV, in the same torus it was obtained experimentally that

$$V_f = V_S + 2.2 - 4.6T_e/e \text{ [in Volts]}. \quad (20)$$

So, there is a large difference with formula (17) in μ_e and V_0 . Corresponding measurements are shown in figure 8.

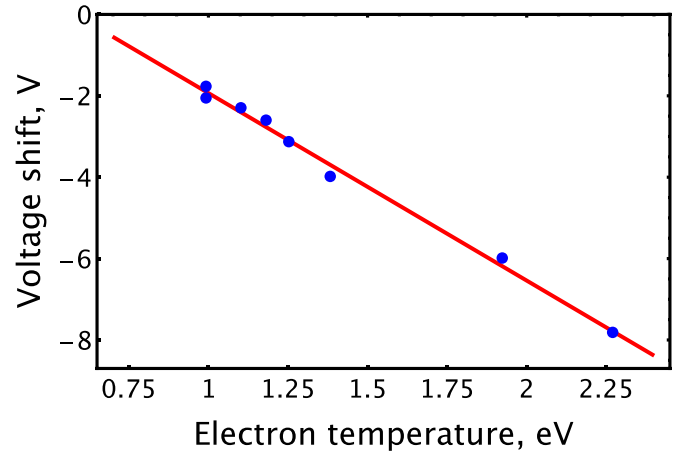


Figure 8. Experimental measurements of V_f for perpendicular cylindrical probe with $R = 0.25$ mm and $L = 5$ mm in magnetic field $B = 0.15$ T (dots). Approximation of V_f by a linear function (solid line) [10]. Adapted from [10], with the permission of AIP Publishing.

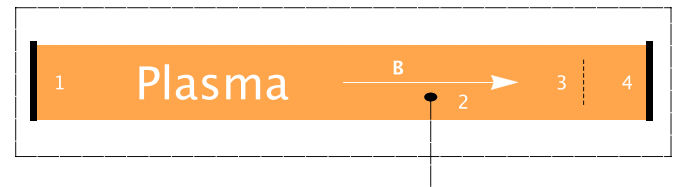


Figure 9. Schematic diagram of WVU Q-machine [30]: the grounded hot plate (1), the four-probe cluster (2), the mesh-electrode (3), and a solid terminating electrode, which can also work as the second hot plate (4).

Below in the following sections related to the Blaamann device, we refer to the probe positions along the diameter of the cross section of the torus r from 0 (center of the cross section) to $+13.5$ cm as outer plasma positions and from 0 to -13.5 cm as inner plasma positions, respectively.

Thus, the simple magnetized torus Blaamann creates a low-temperature plasma with electron temperature of several electron-volts and ion temperature of several tenths of one electron-volt. The degree of ionization in such a plasma is of the order of magnitude of a fraction of 1% or less. The operation of the plug probes and their clusters is well described by the theory for classical diffusion of charged particles for a small probe in a weakly ionized, magnetized plasma, which makes it possible to calculate the probe IV -traces, the floating probe potentials and to estimate the influence of the temperatures of charged particles on measurements.

3.2. Strongly ionized cold low-temperature plasma

The measurements of plasma oscillations in strongly ionized magnetized plasma has been conducted in WVU Q-machine [30]. The Q-machine has the steady-state barium plasma column of 3 m length. The schematic of the experimental device is presented in figure 9.

Plasma is produced by surface ionization on a grounded, hot, rhenium-coated tungsten 10 cm diameter plate (1). At the opposite end of the device, at the distance of 10 cm before the terminating electrode (4), which can also work as the second hot plate, and a 2.5 cm diameter bias-able mesh-electrode (3) is placed perpendicular to the axis of the tube. Typical electron and ion temperatures are $T_e \approx T_i \approx 0.15 - 0.20$ eV and magnetic fields $B = 0.05 - 0.3$ T. Average gyro radius for electrons $\rho_L^e = 0.005$ mm and for ions $\rho_L^i = 2.8$ mm (for $B = 0.3$ T).

The measurements have been conducted with a baffled probe and a baffled probe cluster, shown in figure 10. The baffled probe holder had outer diameter of 7.9 mm and inner diameter of 4.8 mm. The width and length of each gap in the probe holder were 3.8 mm and 7 mm, correspondingly. The probe rode had diameter of 2.4 mm and protruding length of 5 mm. The probe axis was oriented perpendicular to magnetic field. The probe was rotated at different baffle rotation angles φ so that $\varphi = 0$ corresponds situation shown in figure 3(c). Accordingly, if two diametrically opposite probe holder gaps intersected the same magnetic line, the angle was 90° or 270° .

The probe cluster had the following dimensions. Outer diameter of the four-bore tube (C) was 2.8 mm and diameter of each bore was 0.5 mm. The four-bore tube has length of 10 mm. The outer diameter of the single bore tube was 6.4 mm and its inner diameter was 3.2 mm. The width and length of each gap in the outer tube were 2 mm and 5 mm, correspondingly. Malleable 0.050 mm radius gold wire was tightly wound (no gaps between turns) over the ceramic tube corners to form a flat, plasma-facing, current-collection sensor. Four turns of the gold wire served as each baffled probe tip.

The cluster axis was oriented perpendicular to magnetic field. The cluster was rotated so that two diametrically opposite probe tips intersected the same magnetic line. For this cluster orientation, these two baffled probes are open since electrons had full access to the probe from one direction. One open probe faces the plasma source (1) and the other open probe faces the mesh (3). The other two baffled probes in the cluster are closed since electron access to the probe was minimal.

The cluster axis was oriented perpendicular to magnetic field. The cluster was rotated so that two diametrically opposite probe tips intersected the same magnetic line. For this cluster orientation, these two baffled probes are open since electrons had full access to the probe from one direction. One open probe faces the plasma source (1) and the other open probe faces the mesh (3). The other two baffled probes in the cluster are closed since electron access to the probe was minimal. More details about the probe cluster can be found in [30].

Typical experimental IV -traces for MIB probe shown in figure 10 (left) for magnetic field $B = 0.3$ T and different baffle rotation angles φ are shown in figures 11–13. It is seen that for angles between about 0° and 35° and between about 55° and 90° probe IV -traces have well pronounced saturation. For angles in the vicinity of 45° , a maximum appears in the region of the beginning electron saturation current (see, figure 13).

Due to symmetry the same is valid for corresponding angles in the range $90^\circ - 360^\circ$. The nature of the maximum is unclear

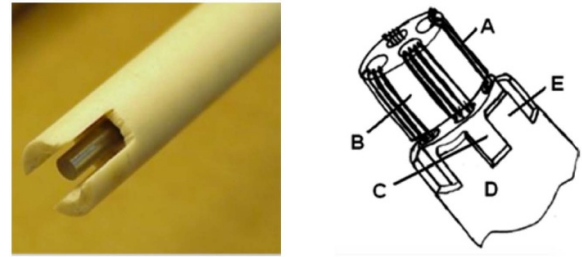


Figure 10. Photograph of a baffled probe [46] (left). Sketch of the baffled probe cluster [30]: collection wire (A), short four-bore ceramic tube (B), four-bore ceramic tube (C), outer single-bore ceramic tube (D) and baffles (E). In the sketch, the four-bore tubes of the cluster shifted out of outer tube to demonstrate the probe construction. Reprinted from [30], with the permission of AIP Publishing.

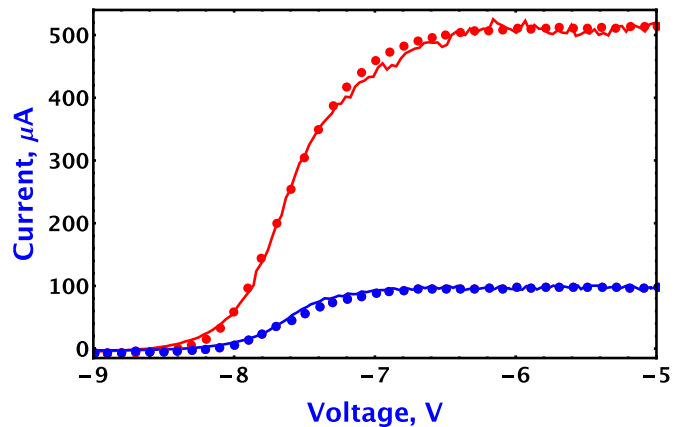


Figure 11. Measured baffled probe IV -trace for $\varphi = 90^\circ$ (upper solid curve) and $\varphi = 60^\circ$ (lower solid curve). Modeled IV -trace (dots). $B = 0.3$ T [46]. [46] John Wiley & Sons. © 2004 WILEY-VCH Verlag GmbH & Co. KGaA, Weinheim.

and requires further investigation. Note, that for ordinary cylindrical probes in magnetized plasma, there are also IV -traces with maxima at certain conditions [46]. Thus, from figures it is seen that by rotation, the probe allows us to obtain various ratio between electron and ion saturation current. In the investigated cases the change of current ratio may be different by factor of 2200 due to rotation.

Modeling the probe current has been performed with the classic diffusion probe theory (see, section 2.3). Results of the modeling are shown in figures 11 and 12 by dots. When calculating the IV -traces, the electron and ion saturation currents were adjusted to match the experimental currents. It is seen, that the theory and experiments give very consistent results. There are no calculations for figure 13, In this case the simple theory cannot describe maximum on the electron saturation current. Such phenomena occur when the edge of the baffle crosses the magnetic line passing through the probe. In this case, the flow of electrons begins to overlap with the baffle, and there is a redistribution of currents between the baffle and the probe.

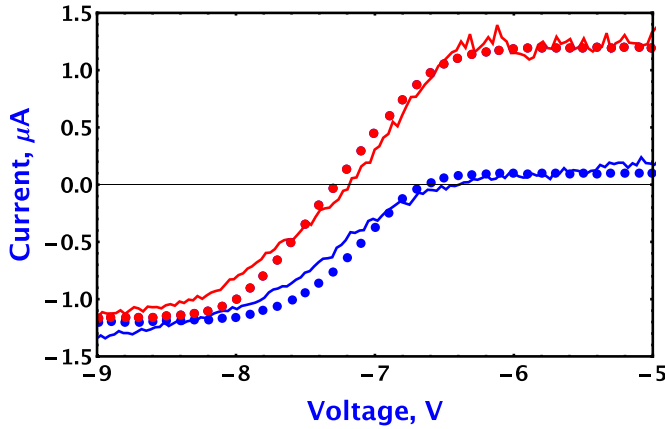


Figure 12. Measured baffled probe IV-trace for $\varphi = 30^\circ$ (upper solid curve) and $\varphi = 0^\circ$ (lower solid curve). Modeled IV-trace (dots). $B = 0.3$ T [46]. [46] John Wiley & Sons. © 2004 WILEY-VCH Verlag GmbH & Co. KGaA, Weinheim.

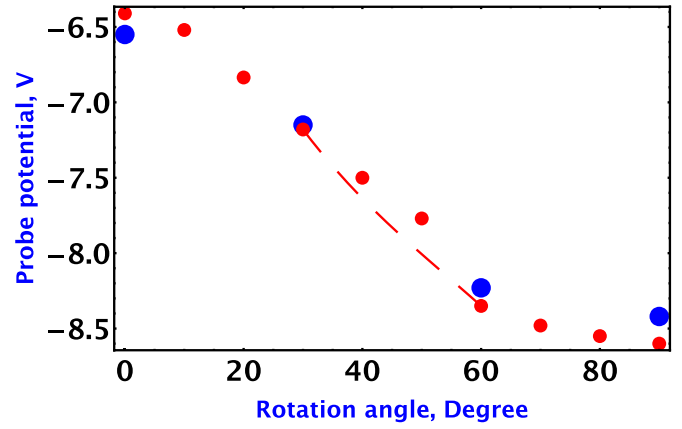


Figure 14. Experimental (small red dots) and calculated (big blue dots) floating probe potential V_f with respect to the rotation angle for $B = 0.3$ T [46]. [46] John Wiley & Sons. © 2004 WILEY-VCH Verlag GmbH & Co. KGaA, Weinheim.

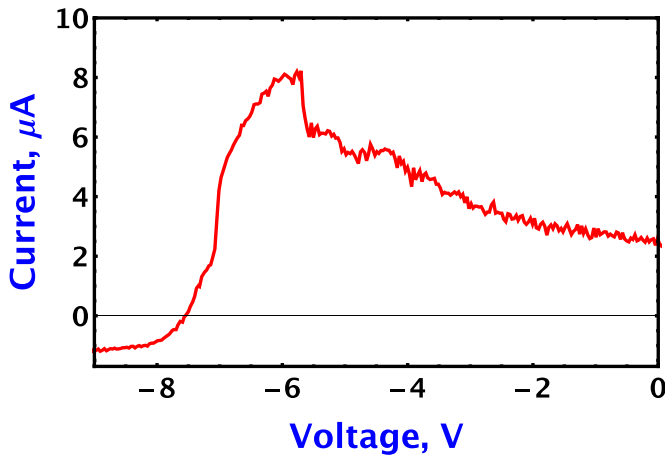


Figure 13. Measured baffled probe IV-trace for $\varphi = 40^\circ$ (upper solid curve). $B = 0.3$ T [46]. [46] John Wiley & Sons. © 2004 WILEY-VCH Verlag GmbH & Co. KGaA, Weinheim.

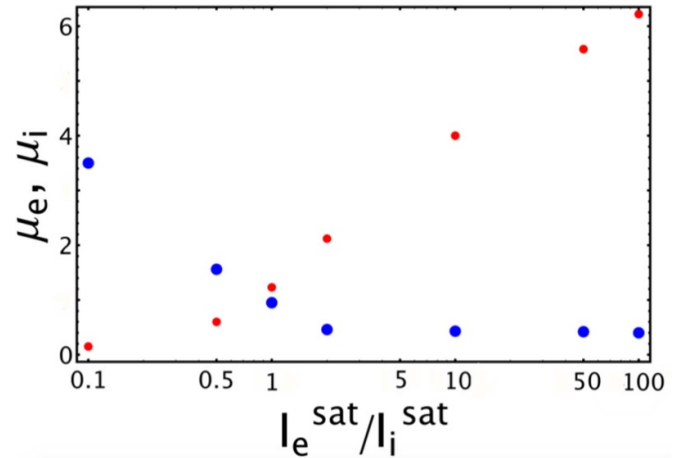


Figure 15. Coefficients μ_e (small red dots) and μ_i (large blue dots), calculated for the baffled probe with diffusion theory. $B = 0.3$ T [46]. Note, that for $I_e^{\text{sat}} = I_i^{\text{sat}}$, $\mu_e \neq \mu_i$.

A change in the probe potential leads to a different degree of current overdistribution and cannot be described by a simplified theory that considers only the shading effect of the partition. Therefore, angles between 35° and 55° cannot be used for measurements and should be excluded from consideration, as they give large and uncontrollable errors.

Figure 14 shows examples of experimental and calculated floating probe potential for the magnetic field of 0.3 T. It is seen that the floating probe potential behavior is rather well reproduced by the model, for exception of angles between 35° and 55° , where the floating potentials for these angles, indicated by red dots, fall out of the smooth manners for the potentials, shown by red dashed curve (best visible for angle of 50°). That is, for those angles, where the simple probe theory is not valid, as discussed above.

The theory also allows calculation of coefficients from equations (17) and (18). That provides a possibility to analyze results of measurements of floating probe potentials and subtract information about plasma potential and electron and ion

temperature oscillations as described in the following sections. The results of modeling are shown in figures 15 and 16.

Figure 16 shows examples of calculations of the floating probe potential with respect to the electron temperature for $T_i = 0.16$ eV for $I_e^{\text{sat}} = 100I_i^{\text{sat}}$ and with respect to the ion temperature for $T_e = 0.16$ eV for $I_i^{\text{sat}} = 10I_e^{\text{sat}}$. It is demonstrated, that for lower curve $\mu_e = 6.2$ and for upper curve $\mu_i = 3.4$. Comparison the calculated probe potentials and corresponding linear dependences shown in figure 16 shows that the variation of V_f is practically linear for changing temperature within 75% of the real temperature value.

Thus, the Q-machine creates a rather cold low-temperature plasma with electron and ion temperatures of the order of a small fraction of one electron-volt. This plasma is strongly ionized. The operation of the proposed MIB probes and their clusters is well described by the theory for classical diffusion of charged particles, which makes it possible to calculate the probe characteristics, the potentials of the floating probes

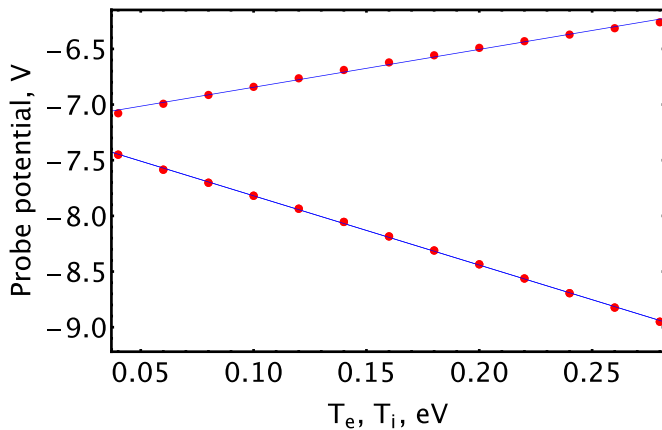


Figure 16. Model floating probe potential with respect to T_e for $T_i = 0.16$ eV (lower curve) and with respect to T_i for $T_e = 0.16$ eV (upper curve). For lower curve $\mu_e = 6.2$ and $I_e^{\text{sat}}/|I_i^{\text{sat}}| = 100$; for upper curve $\mu_i = 3.4$ and $I_e^{\text{sat}}/|I_i^{\text{sat}}| = 0.1$ [46]. [46] John Wiley & Sons. © 2004 WILEY-VCH Verlag GmbH & Co. KGaA, Weinheim.

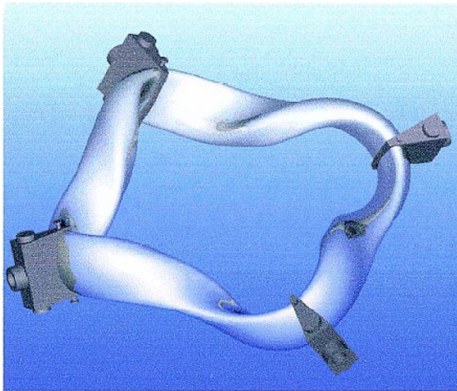


Figure 17. The stellarator vacuum chamber. The four field-period shape is readily apparent [112]. Reprinted with permission from [113], Copyright (1999) by IEEE.

and to estimate the influence of the temperatures of charged particles on measurements.

3.3. Hot fusion-boundary plasma

MIB probes have been used in a variety of fusion-boundary plasmas. The measurements of plasma oscillations in a hot fusion-boundary strongly-ionized magnetized plasma has been conducted in a plasma of the stellarator HSX [40, 112]. The vacuum chamber of the stellarator is shown in figure 17. It has a very complicated shape. The dimensions and other technical data for HSX can be found in [112].

Some probe designs with baffles used in various fusion-related devices are shown in figure 18. For contrast, because it is not technically a MIBP, a Mach probe with a baffle, widely used in the fusion research [10], is also shown (bottom, right). This probe, along with other probes, was used for plasma studies in the START spherical tokamak. Detailed probe studies in that tokamak have not been comprehensively published yet and the authors of this review plan to do this in a future article.

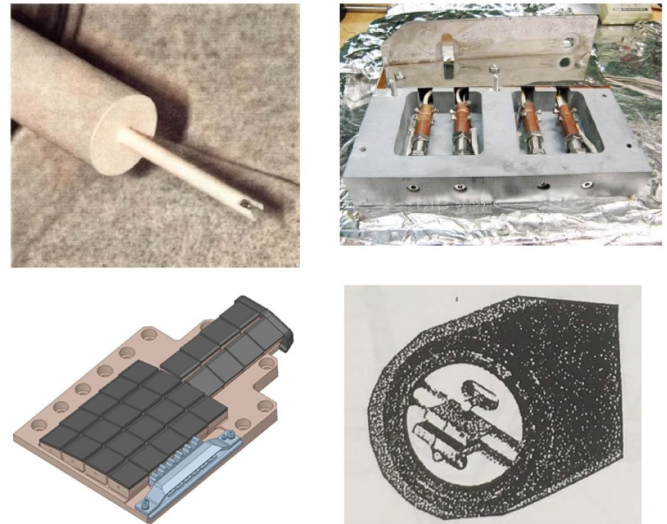


Figure 18. Photographs of the reciprocated baffled probe for fusion-boundary plasma of HSX stellarator [40] (top, left); four wall baffled probes (their schematic is in figure 3(d)), at divertor plate of spherical tokamak NSTX [61–63] (top, right); a probe cluster for tokamak ST40 [106] (bottom, left). A Mach probe with a baffle, used in the START spherical tokamak [110], is also shown (bottom, right). Adapted from [40], with the permission of AIP Publishing.

The baffled probe used in the stellarator HSX is shown in figure 18 (top, left). In the figure the boron nitride probe holder has outer diameter of 2 mm. The slot width and depth are 1 mm and 2 mm, correspondingly. The tungsten probe tip has the diameter of 0.75 mm and is recessed back for 1 mm from the far end of the boron nitride baffles. The probe holder has length of 2 cm and connected to a piece with the diameter of 1.26 cm. The total length of the exposed boron nitride part is 6 cm and that part is held by a stainless-steel tube.

This tube runs inside a bellows assembly and is held by a vacuum rotary feedthrough, which is attached to a translation stage outside the vacuum vessel. The discharges produced by HSX in hydrogen are heated by 50 kW of second harmonic (28 GHz at $B = 0.5$ T) electron cyclotron resonance heating power using a gyrotron. The typical central averaged electron densities are in range from 0.5 to $2 \times 10^{12} \text{ cm}^{-3}$. Typical central electron temperature is of the order of 500 eV. The electron temperature could be measured by Thomson scattering method.

From the standard Langmuir probe measurement, it was found that the edge densities are less than 50% of the central averaged densities, $T_e \leq 40$ eV and $T_i \leq 25$ eV. For those parameters, ion and electron gyro radii are estimated as $\rho_L^i < 1.4$ mm and $\rho_L^e < 40$ μm , respectively. To make radial scans with the Langmuir probe or one orientation of the baffled probes many discharges are required. Each discharge lasts about 50 ms [40].

Typical probe IV -trace for the equalized baffled probe is shown in figure 19 [40]. As usually for the equalized probe $I_e^{\text{sat}} \approx I_i^{\text{sat}}$. In figure 19 floating probe potential is taken as zero. In the regime shown in figure 19, there is a classical diffusion of charged particles to the tip of the probe [46]

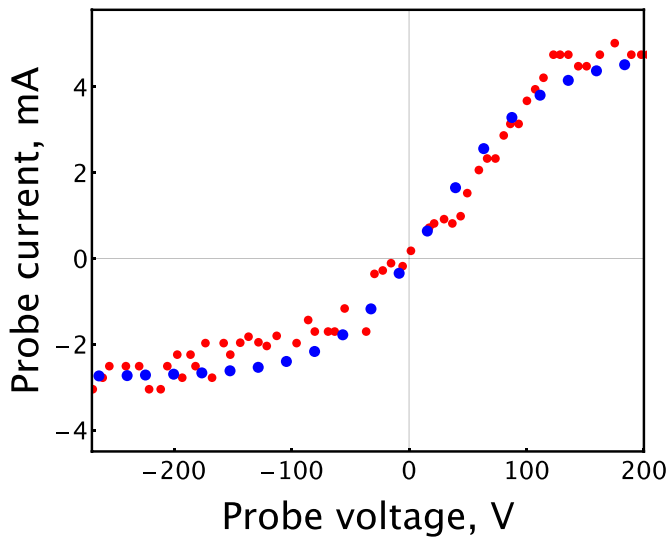


Figure 19. Smoothed IV-traces for equalized baffled probe. V_f is taken as zero [40]. Experimental curve (red small dots) and modeled curve (blue large dots). For the calculations the following plasma parameters were taken: $T_e = 31$ eV, $T_i = 22$ eV and $n_e = 6 \times 10^{11} \text{ cm}^{-3}$.

(see section 2.3). In similar regimes, the voltage shift V_0 can be a certain combination of electron and ion temperatures. In this work, this issue has not been studied in detail, although it is clear that the equalizing probe can hardly be used for direct measurements of plasma potentials.

Calculations, using the formulas of classical diffusion, makes it possible to determine the dependence of fluctuations in the potential of a floating probe on the plasma potential and fluctuations in the temperatures of electrons and ions. Under the investigated conditions for an open probe, this formula has the form

$$\tilde{V}_f = \tilde{V}_S - 3.3 \times \tilde{T}_e + 0.7 \times \tilde{T}_i. \quad (21)$$

For an equalized probe, the formula is given as

$$\tilde{V}_f = \tilde{V}_S - 0.9 \times \tilde{T}_e + 1.2 \times \tilde{T}_i. \quad (22)$$

For the case shown in figure 19, measured $T_e = 31$ eV, $T_i = 22$ eV and $n_e = 6 \times 10^{11} \text{ cm}^{-3}$.

Thus, the stellarator has near-wall hot plasma with an electron temperature equal to or below 40 eV and an ion temperature of no more than 25 eV. Plasma is substantially ionized. Due to the high plasma temperature, a reciprocating probe design should be used in experiments with measurement time of 50 ms. The operation of the proposed MIBP is described by the theory of classic diffusion of charged particles, which allows us to calculate the characteristics of the probe, the potentials of the floating probe, and also to evaluate the influence of the temperature of charged particles on measurements.

4. Measurements of electric potential oscillations

Measurement of space potential oscillations is a priority task for studying various types of instabilities, waves and the associated transport of particles and energy in the magnetized plasma. Sometimes, for measurements of the plasma potential oscillations, direct measurements of the floating conventional probe potentials are used [10]. Generally speaking, from equations (17) and (18), it follows that such measurements are possible and reliable in the case of absence or a very small value of the charged particle temperature fluctuations only. Note, that in some plasmas $T_e \gg T_i$ and it is possible mainly consider the electron temperature fluctuations, since their influence is much greater than the effect of the ion temperature. Then, in the case of application of ordinary probes for measuring the amplitude of plasma potential oscillations with an expected accuracy of, for example, 10%, the amplitude of the oscillations of the electron temperature should not exceed about a few (two or three) percent of the amplitude of the plasma potential oscillations, since equation (18) includes term with $\mu_e \tilde{T}_e / e$. In a general case, the term $\mu_i \tilde{T}_i / e$ should also be considered.

If for the direct measurements of the plasma potential oscillations, the closed or the equalized MIBPs are used, the measurement errors (with respect to ordinary probes) can be decreased by a factor of between 5 and 10 (or sometimes even more), as can be seen, for example, from equations (19), (20) and figure 15. Therefore, for a direct measurement of the plasma potential oscillations, the use of MIBP is always much more reliable and preferable than using conventional probes. Note, that equation (17) also includes a term with a constant offset voltage V_0 , which is absent in equation (18). Since the voltage shift V_0 can be equal to several sum of electron and ion temperatures, direct measurement of the absolute value of probe potentials by this method may be not always practical.

So, it can be expected that the accuracy of measuring the plasma potential oscillations with a MIBP can be significantly higher than the accuracy of measuring the absolute value of the plasma potential and, in this section below, we will discuss mainly the measurement of plasma potential oscillations. In some cases, the error in measuring the plasma potential oscillations by the MIBP becomes acceptable and does not require further correction. To estimate the measurement accuracy, one may use the calculations using the probe theories from section 2.3 (not for all MIB probe designs). That is, in order to study the error in measuring the oscillations of the plasma potential, it is necessary to measure other plasma parameters, which are considered in the following sections. Thus, the estimations of the errors in measuring the plasma potentials are carried also over to the subsequent sections.

We only point out here that in the simplest case to know how much the fluctuations in the temperature of electrons or ions affect direct measurements of the plasma potential fluctuations, it is possible to compare measurements with a closed or equalized probe and an open probe, with different ratios of electron and ion saturation currents. For exact isolation of the component of the oscillations of the plasma potential, generally it may be necessary to analyze the oscillations of

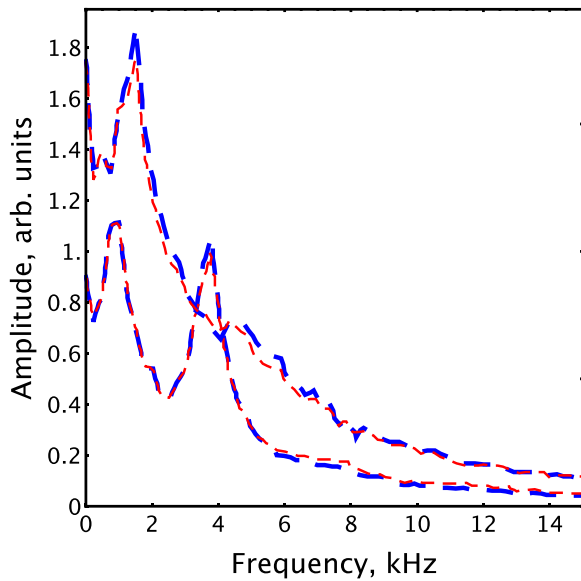


Figure 20. Amplitude spectra of potential oscillations V_S obtained from two closed plug probes. The probe position $r = +6$ cm (bottom pair of lines) and $r = -6$ cm (top pair of lines) [42]. Adapted from [42], with the permission of AIP Publishing.

the temperature of electrons and ions. To do that, the measuring cross-phases and coherencies between MIBP and standard probe oscillations may be necessary (see also some more details in sections 5 and 6).

Thus, this section briefly describes direct measurements of plasma potential fluctuations in the plasma devices depicted in section 3. For this, plug-probes, baffled probes and associated probe clusters have been used. This section provides examples of measurements of the potential oscillation amplitude in various plasmas. At the same time, this section does not provide specific errors in measuring oscillations of the plasma potential as a result of oscillations of the temperature of charged particles, while formulas relating these errors to fluctuations of the electron and ion temperatures are discussed.

4.1. Toroidal low-temperature plasma

Measurements of plasma potentials in toroidal low-temperature plasma have been conducted and published, for example, in [10, 36, 42, 44]. Figure 20 shows typical experimental amplitude spectra of the plasma potential oscillations V_S , obtained from the cluster with two-closed-plug probe, shown in figure 5 on the left, at positions $+6$ cm (outer plasma) and -6 cm (inner plasma). Of course, in reality these are measurements of the potential of a floating closed plug probe under the assumption that fluctuations in the temperature of charged particles do not play a significant role. The figures show two curves obtained from different probes, which makes it possible to evaluate the errors arising from imperfect manufacturing of the probes and cluster itself. It allows to make sure that the measurements are carried out with sufficient quality and convincingness.

Both probes were used in a mode when the ion saturation current is about five times greater than the electron saturation

current, that is, in a mode similar to that shown in figure 6. Since the electron temperature under experimental conditions was much higher than the ion temperature, in equations (17) and (18), the ion temperature or its fluctuations could be neglected and equation (19) and (20) have to be used. The last equation shows how temperature fluctuations affect measurements of the plasma potential fluctuations.

It is seen, that in this case, the effect of the electron temperature on plasma potential oscillation measurements with a closed probe decreases by factor of 11.5 of magnitude in comparison with the open probe. If both probes are well aligned, the signals from the two probes are very similar in magnitude, as shown by curves 1 and 2 in figure 20. Note also, that it is demonstrated experimentally that acceptable misalignment depends on the probe length and plug sizes. For probes used in presented measurements, misalignment up to three angular degrees in any angular direction is acceptable for reliable measurements. At the same time, the angular deviation of the probe from the magnetic line by an angle of six angular degrees could lead to a discrepancy between the signals measured by the well aligned probe and by different probes in the used cluster by 20%–40% [42].

For the measured conditions, the plasma potential oscillation spectra of have two peaks at about 1.5 and 4 kHz for the position $+6$ cm and the only one peak at 1.5 kHz (the peak at 4 kHz is hardly visible) for the position -6 cm. That allows us to assume the simultaneous presence of different oscillation modes in the outer and inner parts of the plasma torus. To obtain more detailed information on the oscillations present in the plasma and their modes, detailed measurements of temperature fluctuations and phase relations between the oscillations of various plasma parameters are needed. This will be done in sections 5 and 6. This will also allow correcting the measured fluctuations in the plasma potential and making the measurements more accurate by using, for example, an iterative method.

4.2. Strongly ionized cold low-temperature plasma

The measurements of the plasma potential fluctuations in cold low-temperature strongly ionized plasma have been carried out in the WVU Q-machine [29, 30, 46]. For the measurements, single baffled probes and baffled probe clusters have been used. Figures 21 and 22 shows the results of such measurements with the single baffled probe, shown in figure 10 (left).

Since the temperatures of ions and electrons in this plasma are approximately the same, it is optimal to choose a regime of the equalized probe for the measurements. This is done to reduce the possible influence of the ion temperature on the measurements since here, in contrast to the toroidal plasma, fluctuations in the ion temperature can affect the measurements of the plasma potential even with a small increase in the ion saturation current. So, under investigated conditions for the equalized baffled probe, \tilde{V}_f is equal to

$$\tilde{V}_f \approx \tilde{V}_S - 1.1 \times \tilde{T}_e + 0.9 \times \tilde{T}_i. \quad (23)$$

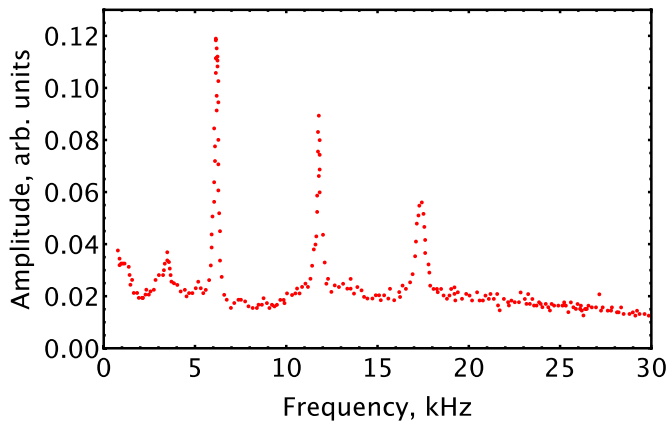


Figure 21. Amplitude spectra of the plasma potential fluctuations for equalized baffled probe, $B = 0.1$ T [46]. [46] John Wiley & Sons. © 2004 WILEY-VCH Verlag GmbH & Co. KGaA, Weinheim.

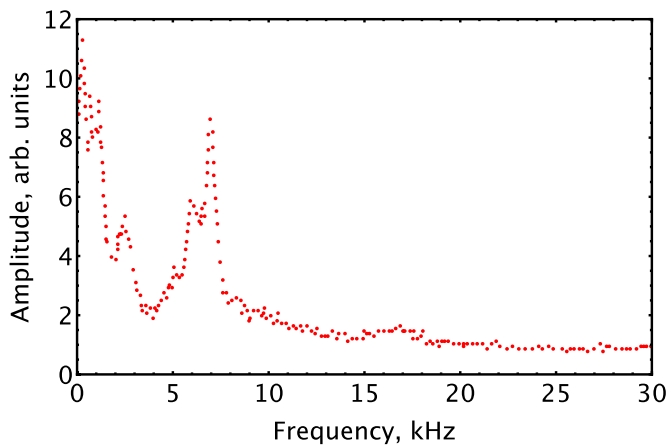


Figure 22. Amplitude spectra of the plasma potential fluctuations for equalized baffled probe, $B = 0.3$ T [46]. [46] John Wiley & Sons. © 2004 WILEY-VCH Verlag GmbH & Co. KGaA, Weinheim.

This equation shows how the electron and ion temperature fluctuations affect measurements of plasma potential fluctuations.

Thus, figures 21 and 22 show amplitude spectra of the floating baffled probe potentials for case $I_e^{\text{sat}} \approx I_i^{\text{sat}}$ and different magnetic fields. It can be seen from the figures that the nature of the spectra and, therefore, the type of oscillations strongly depends on the magnitude of the magnetic field. With an increase in the magnetic field from 0.1 T to 0.3 T, the amplitude of the spectral oscillations significantly increases, which can be seen from the figures, since they have the same arbitrary units are used.

The spectrum for a magnetic field $B = 0.1$ T contains a narrow-band peak at about 6 kHz and at least two rather intense narrow-band harmonics. For a stronger magnetic field, the oscillations of the plasma potential are concentrated mainly in somewhat wider-band region from 5 to 8 kHz and they are much more intensive. To assess the effect of the electron temperature, it is necessary to carry out additional measurements with ordinary or open baffled probes, which will be reported in section 6.

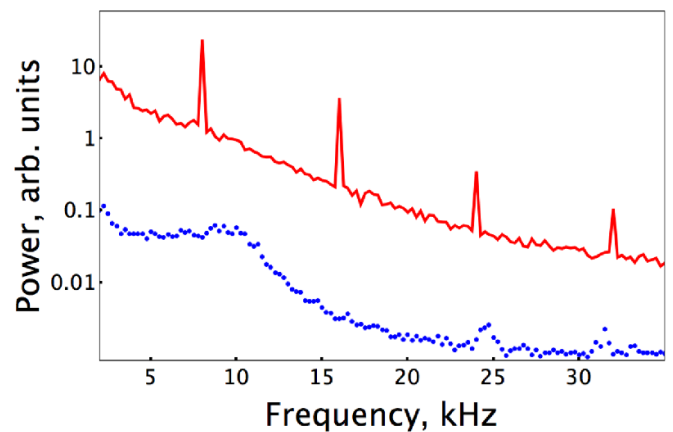


Figure 23. Power spectra of the plasma potential fluctuations for equalized baffled probe (red curve). Power spectrum of the plasma potential fluctuations in the plasma without modulation of the mesh bias (blue dots) [30], $B = 0.3$ T. Adapted from [30], with the permission of AIP Publishing.

For a more detailed study of the oscillations, it is also important to measure the phase difference of the spectra which have not been done in [46]. At this time, it can be assumed that at a lower magnetic field, there could be ion-acoustic oscillations, and at a higher magnetic field, oscillations could be related to drift waves. However, those propositions have to be got confirmation.

A more detailed study of fluctuations in plasma potentials requires the use of two or more MIBPs or a combination of MIBP and conventional probe. This makes it possible to obtain phase shifts and coherencies between different types of oscillations and to better separate them. Such measurements were also carried out in the Q-machine plasma.

Figure 23 shows the results of the measurements with a cluster shown in figure 10 (right) [30]. For the measurements, a mode was selected in the Q-machine in which there were no significant fluctuations and waves in the plasma. Such a regime can be obtained without changing the magnetic field, for example, by small changes in the temperature of the hot plate (1) (see figure 9). Therefore, the nature of the oscillations in figures 22 and 23 is completely different, despite the same magnetic field. Further, the mesh-electrode (3) in figure 9 was supplied with a sinusoidal voltage with a frequency of 8 kHz and amplitude of 70 V.

The applied voltage causes an alternating current to flow to the mesh. In this case, most of the voltage (>99%) falls on the near-mesh sheath. A small part of the voltage is applied to the plasma and should cause oscillations of the plasma potential at a frequency of 8 kHz and its harmonics. In this case, measurements with four probes are needed simultaneously and allow us to distinguish oscillations of different natures.

Figure 23 shows power spectra of plasma potential oscillations measured by the closed equalized probe (red curve) [30]. Power spectrum of plasma potential oscillations in the plasma without modulation of the mesh bias is also shown (blue dots). Figure 24 shows the result of measurements of cross coherence of the signals from the two probes [30]. It is seen, that

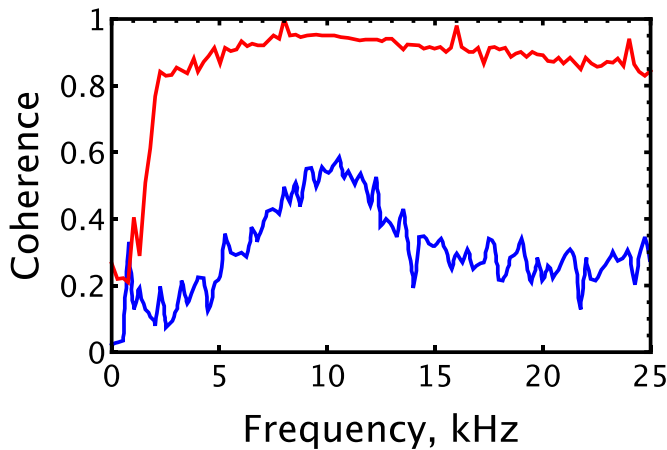


Figure 24. Cross coherence between two closed-probe potential oscillations with application of ac voltage to the mesh (top red curve) and without this bias modulation (bottom blue curve) [30]. Adapted from [30], with the permission of AIP Publishing.

for the regime without oscillation (no ac signal on the mesh), there may be weak waves near 10 kHz (cross coherence is a bit greater than 0.5). The rest of the curve is just a kind of noise.

In figure 23 in the power spectrum of the plasma potential oscillations there are narrow-band peaks at 8 kHz and its harmonics [30]. They may be connected as predicted above due to the penetration of weak oscillations of the plasma potential, creating an alternating current on the mesh. Since most of the alternating voltage applied to the mesh falls in the mesh sheath of the space charge, only small fluctuations of the potential penetrate into the plasma (a small fraction of 1 V), which are recorded by the baffled probes. The nature of the remaining oscillations of the plasma potential, which create a continuous spectrum, will be discussed in the following sections as additional information is obtained on the oscillations of various plasma parameters. In this regime cross coherence is higher than 0.8 for frequencies greater than 2 kHz and higher than 0.95 for frequencies of mesh-electrode voltage oscillations and their harmonics.

4.3. Hot fusion-boundary plasma

The measurements have been conducted in the near wall region of plasma in the stellarator HSX with a reciprocated baffled probe which is shown in figure 18 (top, left) [40]. Tests of a baffled probe in plasma having T_e about or less than 40 eV, T_i about or less than 25 eV and n_e about 10^{12} cm^{-3} show that the probe, as built, survives many 50 ms long discharges.

A typical result of the measurements of amplitude spectrum of plasma potential oscillations is shown in figure 25 [40]. The spectrum is obtained with balanced baffled probe for IV -trace shown in figure 19. For this case equation (22) is valid. This equation shows how temperature fluctuations affect measurements of plasma potential fluctuations. The influence of fluctuations in the temperature of charged particles on the measurement of the plasma potential is discussed in section 6.

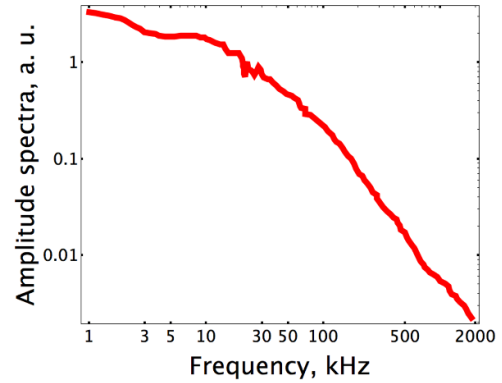


Figure 25. Smoothed amplitude plasma potential oscillation spectrum obtained by the equalized baffled probe orientations for $n_e = 6 \times 10^{12} \text{ cm}^{-3}$ [40]. Adapted from [40], with the permission of AIP Publishing.

5. Measurements of electric fields

Measurements of fluctuations of electric fields in a magnetized plasma are necessary for investigating various properties of plasma, including the study of instabilities and anomalous transport of charged particles and energy. Anomalous transport can be caused by turbulent convection arising during the development of instabilities in the plasma. Particle and energy transport increase and decrease by controlling plasma instability. The component of the electric field perpendicular to the magnetic lines can provide information about the $E \times B$ drift velocity. Such data can identify azimuthally symmetric bands of flow-shear structure, known as zonal flow, that regulate turbulence-induced transport and that quench the underlying micro instability.

The study of oscillations of electric fields can be carried out using MIB probes. To measure the electric field oscillations, it is necessary to determine the electric potential oscillations with MIB probes at least in two points of the plasma simultaneously. Since measurements of fluctuations in electric potentials have already been discussed in the previous section, this information can be used to measure fluctuations of the electric fields. Such measurements make it possible to obtain the magnitude of the electric field component in the direction from one probe to another. The minimum resolved wavelength determined in this way will be equal to the half of the distance between the probes. This means that during the measurements, the characteristic wavelength of the oscillations should be significantly greater than the distance between the probes. On the other hand, the distance between the probes should not be too small, as this leads to a decrease in the measured signal and an increase in the measurement error.

Thus, in this section the measurements of the electric field oscillations with two MIB probes are demonstrated. The system is shown to provide results consistent with theoretical understanding of the fluctuations in the studied plasma configuration. This section discusses measurements made in toroidal and strongly ionized cold low-temperature plasmas. It has been also shown that studies with two conventional probes provide a qualitative comparison with measurements with

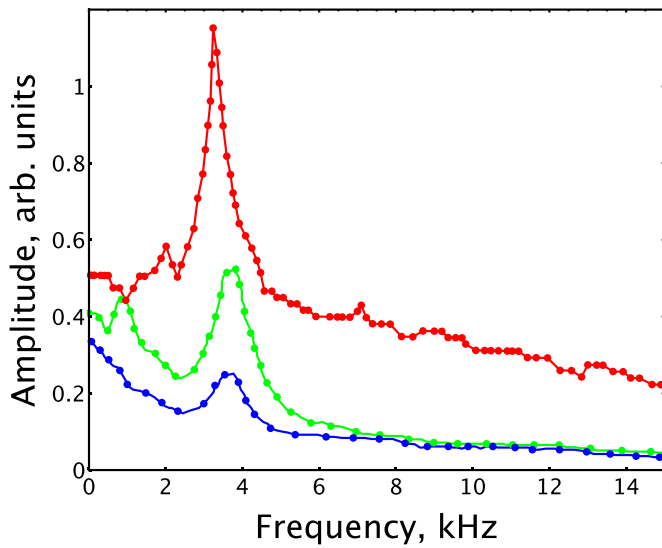


Figure 26. Amplitude spectra of poloidal electric field (lower blue curve) measured by two plug probes, conditional poloidal electric field measured by two conventional probes (upper red curve) and distorted electric field, measured by two misaligned plug probes (middle green curve). The plasma conditions are: $B = 0.154$ T, helium pressure $p = 0.35$ Pa, $n_e = 2 \times 10^{11}$ cm $^{-3}$, and $T_e = 1$ eV. The probe position $r = +6$ cm [42]. Adapted from [42], with the permission of AIP Publishing.

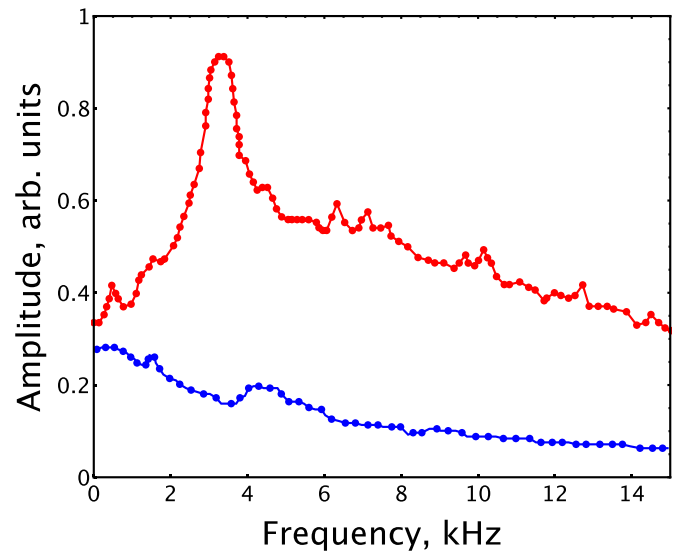


Figure 27. Amplitude spectra of electric field (lower curve) measured by two plug probes and conditional electric field measured by two conventional probes (upper curve). The same plasma conditions as in figure 26. The probe position $r = -6$ cm [42]. Adapted from [42], with the permission of AIP Publishing.

MIB probes and allow to distinguish between different oscillation modes.

5.1. Toroidal low-temperature plasma

Oscillations of electric fields in toroidal plasma of a Blaamann toroidal device have been studied in [10, 33, 37, 42, 44]. In the previous section, measurements of electric potential oscillations using clusters consisting of two plug-probes in the Blaamann device were discussed. There, two probes were used to confirm the correctness of measurements of fluctuations in plasma potentials. Typical measurement results are shown in figure 20. Obviously, the same measurements can be used to determine the electric fields in plasma. In this case, it is sufficient to measure the difference between the signals from the two plug-probes by momentarily subtracting the signal from one plug-probe from the signal of the other plug-probe.

Thus, the oscillations of the electric field will be measured as

$$\tilde{E} = \tilde{V}_{f2} - \tilde{V}_{f1}, \quad (24)$$

where the various probes are marked with indices ‘1’ and ‘2’. Figures 26 and 27 show the typical amplitude spectra for poloidal electric field oscillations, obtaining from measurements shown in figure 20 (blue bottom curves). Figure 26 shows results of measurements for outer plasma (position $r = +6$ cm) and figure 27 is for inner plasma (position $r = -6$ cm). In the present case, the same probe clusters have been used that have been used to measure the electric potentials.

It is seen from figure 26 that in outer plasma probe position the amplitude spectrum of the poloidal electric field has

only one well-pronounced peak at 4 kHz in contrast to spectrum for the plasma potential oscillation which has peaks at 1.5 and 4 kHz (bottom pair of lines in figure 20). It means that potential oscillations at 1.5 kHz do not create poloidal electric field and may have been just global oscillations of electric potentials or create oscillations of electric field along the magnetic lines only. The cross-phase between the probe potentials for this position is presented in figure 28 by blue top curve. It is practically proportional to the oscillation frequency (wave speed does not depend on frequency), except for small frequency values, where the measurement error is large.

Figure 27 shows the measured amplitude of the electric field obtained from two plug-probes (bottom blue curve) for the inner probe position ($r = -6$ cm) with using equation (23). For this probe cluster position, the amplitude of spectrum of the potential (top pair of curves in figure 20) have only one peak at 1.5 kHz. The spectrum of the electric field has smooth behavior with almost invisible peak at 4 kHz. It means that similar to the outer position, potential oscillations at 1.5 kHz do not create poloidal electric field and may be global oscillations of electric potentials or create oscillations of electric field along the magnetic lines only. The cross-phase for two plug-probes in this case shown in figure 28 (red middle curve). It is also practically proportional to the oscillation frequency as for outer position (and also wave speed does not depend on frequency) It has opposite sign, compared to the position at $r = +6$ cm, because the flow velocity and the wave vector has the opposite direction.

Comparison of the cross-phases for the inner and outer positions of the probes shows that wave numbers are different and the propagation speed of electric field waves in the outer position is approximately half that in the inner position. That may mean that electric field oscillations belong to the different

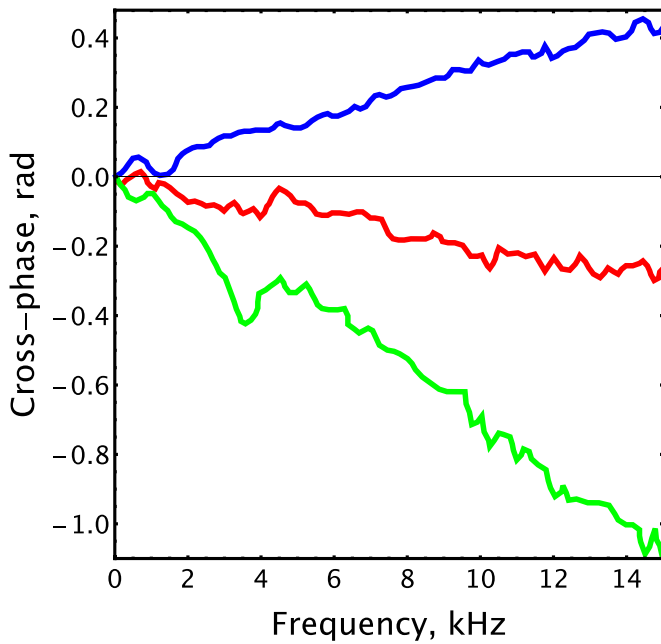


Figure 28. Cross-phase between two plug probes for $r = +6$ cm (blue top curve) and $r = -6$ cm (red middle curve) probe position. Cross-phase between two conventional probes for $r = -6$ cm probe position (green bottom curve). Similar cross-phase for $r = +6$ cm coincide with the blue top curve [42]. Adapted from [42], with the permission of AIP Publishing.

oscillation modes. Remind, that for the plasma potentials, it was found in the previous subsection that there are different types of oscillations inside and outside the center of the toroidal section. Thus, the study of the cross-phases of electrical potentials confirms the statement about the existence of various oscillation modes.

In addition to measuring the electric field fluctuations with two plug-probes, similar measurements were performed using a cluster of the conventional probes having the same dimensions (but of course without plugs) as in the cluster of the plug-probes. Of course, in this case, the values obtained is not strictly speaking an electric field (or it can be called an ‘electric field’ purely conditionally, for exception, the case of plasma without noticeable temperature oscillations), since there may be contamination by fluctuations of the electron temperatures. However, comparing such conditional electric fields with the electric fields obtained with the MIB-probes provides additional useful insight to the problem, as discussed below. To estimate the errors in measuring the oscillations of the electric field in plasma, equation (24) can be rewritten as follows

$$\tilde{E} = (\tilde{V}_{S2} - \tilde{V}_{S1}) - \mu_e/e (\tilde{T}_{e2} - \tilde{T}_{e1}). \quad (25)$$

where as before, the various probes are marked with indices ‘1’ and ‘2’. Since μ_e for a conventional probe in the case under consideration is about 4.6, and for a plug-probe it about 0.4, it can be seen that when measuring oscillations of the electric field, the measurement error of the plug-probes is more than

an order of magnitude smaller than when measuring with the conventional probes.

The conditional electric field in the outer plasma probe position is shown in figure 26 as a top red curve. It can be seen, that it is strongly distorted by the influence of electron temperature oscillations, although it basically repeats the behavior of a real electric field. That is, it is overestimated by up to four times (so the error in measuring the electric field with a conventional probe exceeds the field itself by several times). A cross-phase for conventional probes for outer position (it is not shown in the figure) practically coincides with that obtained for plug-probes [42]. This may indicate that the oscillations of the plasma potential, poloidal electric field and electron temperature belong to the same oscillation mode.

Figure 27 presents amplitude spectrum of the conditional electric field (top red curve) The conditional electric field has a few times higher amplitude than the real one and a strongly pronounced peak at the frequency about 4 kHz. Figure 28 shows that the cross-phases between two plug probes (red middle curve) and two conventional probes (green bottom curve) are very different from each other, both in magnitude (the cross-phase between conventional probes is more than five times larger than that between plug probes) and in the presence of a maximum on curve 2 at a frequency of about 4 kHz. The cross-phases shown by red and green curves in figure 28 yield different wave numbers and hence different propagation velocities. This suggests that there are at least two oscillation modes in the internal plasma, and oscillations of the plasma potential and electron temperature belong to the different modes, since the curve associated with ordinary probes can be heavily contaminated by oscillations of the electron temperature. This example shows that measurements of the plasma potentials and electric fields with ordinary probes can contain significant quantitative and qualitative errors due to spurious effects from temperature fluctuations that appear in the cross-phases.

In order to demonstrate the importance of accurate angular alignment of the plug probes, figure 26 also shows the electric field measurements with plug probes tilted to the magnetic lines at an angle of six angular degrees. As one can see, the measured amplitude of the electric field (middle green curve) is very different from the field measured with well-aligned plug-probes. This curve clearly shows a peak at a frequency of about 4 kHz, which is about two times higher than that measured by plug probes. In addition, the peak at a frequency of about 1.5 kHz is quite noticeable, which is practically absent in other measurements and is obviously a fake structure. As a result, even a small deviation of the probes from the direction of the magnetic line can distort the result of measurements of the electric field, both quantitatively and qualitatively.

Thus, measurements by the clusters of plug and conventional probes make it possible to compare the measured values and obtain additional information that is not possible or difficult to obtain from measurements with a single MIB or conventional probes. This makes it possible to carry out significantly more detailed studies of oscillations and waves in a magnetized plasma.

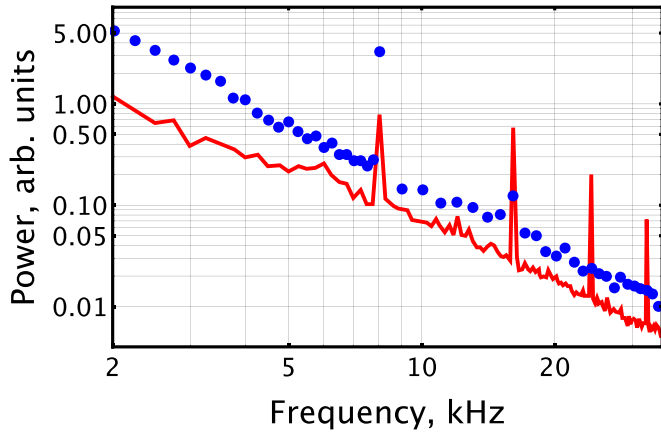


Figure 29. Power spectrum of electric field component E_y perpendicular to the magnetic field in azimuthal direction (blue dots). Power spectrum of electric field component E_z along the magnetic field (red curve) [30]. Adapted from [30], with the permission of AIP Publishing.

5.2. Strongly ionized cold low-temperature plasma

The measurement of electric field fluctuations [30] in cold low-temperature plasma was carried out in the VVU Q-machine, shown in figure 9. For the measurements, a baffled probe cluster, shown in figure 10 (right) has been used. The measurements were carried out under the conditions in which the measurements of the oscillations of the plasma potential shown in figure 23 were carried out. As in the previous section, the oscillations were excited by applying an alternating voltage to the mesh (3) shown in figure 9. Figure 29 shows the results of measurements of power spectrum of electric field component E_y perpendicular to the magnetic field in azimuthal direction (blue dots) and power spectrum of electric field component E_z along the magnetic field (red curve). Frequency of 8 kHz and amplitude of 70 V has been applied to the mesh.

The azimuthal component of the electric field, perpendicular to the magnetic lines E_y , was measured as the difference between the signals from two floating equalized baffled probes from the cluster. As can be seen from the power spectrum in figure 29, this component of the electric field is broadband. The narrow maximum in the spectrum corresponds to the frequency applied to the mesh (8 kHz). An insignificant first harmonic is somewhat visible on the spectrum. Higher harmonics are practically invisible. The spectrum-line area at this maximum at 8 kHz corresponds to an electric field amplitude of 0.2 V m^{-1} .

The cross-phase between signals from the balanced baffled probes, shown in figure 30, is typical for drift waves [113]. The cross-phase at 8 kHz frequency is coincide with cross-phase of the power spectrum. At the same time, at the harmonic frequencies (16, 24 and 32 kHz) the cross-phase sharply decreases to about zero. This means that axial global oscillations dominate at these harmonic frequencies do not belong to the azimuthal wave, but the main 8 kHz frequency belongs to the azimuthal wave.

Cross-phase between floating probe oscillations in the direction parallel to the magnetic field (open probes, red curve) is

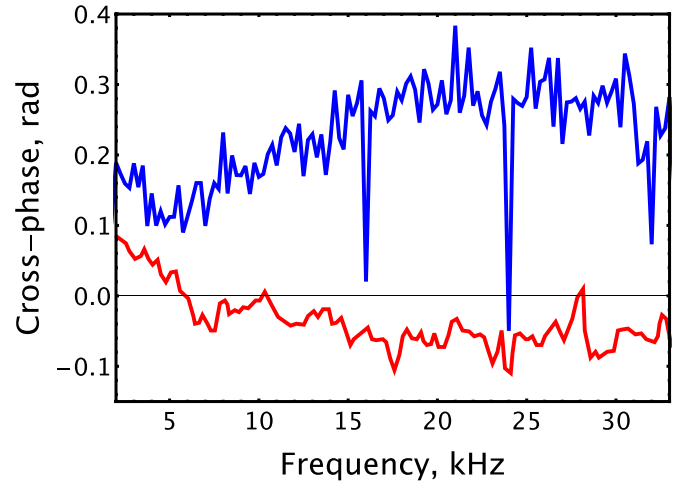


Figure 30. Cross-phase between space potential oscillations perpendicular to the magnetic field in azimuthal direction (equalized probes, top blue curve). Phase between floating probe oscillations in the direction parallel to the magnetic field (open probes, bottom red curve) [30]. Adapted from [30], with the permission of AIP Publishing.

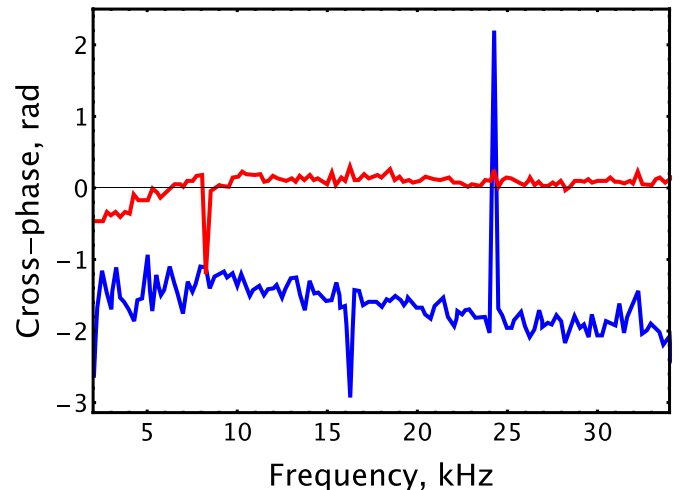


Figure 31. Cross-phase between space potential oscillations and E_z (top red curve). Cross-phase between space potential oscillations and E_y (bottom blue curve B) [30]. Adapted from [30], with the permission of AIP Publishing.

close to zero. This means that no wave propagates in the axial direction (the velocity of its propagation in the axial direction is practically zero). That is, the oscillations at the frequency of harmonics are practically immobile. Electric fields at different frequencies in the axial direction give rise to an electric current along the plasma and heat the plasma.

The study of the cross-phases shown in figure 31 confirms our findings. Indeed, between the oscillations of the electric field and the potential along the axis, the phase shift is about zero, with the exception of the frequency of 8 kHz, for which it is equal to $-\pi/2$. At the same time, the phase shift between oscillations of the azimuthal electric field and potential is equal to $-\pi/2$ for all frequencies except 16 and 24 kHz, for which it is equal to π or $-\pi$, which is the same.

In this section, our study confirms that there are two oscillations of interest in the scenario discussed in the previous section. First, there are oscillations at 8 kHz and their harmonics that are associated with the electron heating in the plasma. They do not propagate in the space and have the same phase at all points in the plasma. Secondly, apparently, there are drift-acoustic waves propagating in the azimuthal direction. In this case, temperature fluctuations at a frequency of 8 kHz belong mainly to azimuthal oscillations, but there are practically no such azimuthal oscillations of the electron temperature at harmonic frequencies of 8 kHz, i.e. at 16, 24 and 32 kHz.

6. Measurements of charged particle temperature oscillations

Measurements of fluctuations of the charged particle temperatures, as well as fluctuations of plasma potentials and electric fields, considered in the previous sections, are of great interest for studying various aspects of physics of the magnetized plasma. Such measurements are important, for example, for studying anomalous fluxes of energy and charged particles [10], which will be discussed in more detail in the next section. Although the absolute values of the electron and ion temperatures (not temperature fluctuations) can also be obtained from the floating potentials of the probes, for such measurements it is better, more reliable and more convenient to study the current–voltage characteristics or *IV*-traces of the ordinary and MIBPs, which will be discussed in more detail in section 8. Therefore, this section mainly deals with measurements of charged particle temperature fluctuations, although measurements of absolute values of temperatures are also demonstrated.

If only one MIBP is available for research, a simple way to find out how much electron and/or ion temperature fluctuations affect direct measurements of plasma potential fluctuations is to compare successive measurements with a closed/equalized and open MIBP. Any difference in the measured floating-potential oscillation amplitudes of respective probes may indicate an influence of charged-particle (usually electron) temperature on measurements.

Even more informative could be a sequential measurement of the oscillations of the probe potential at various ratios of the electron and ion saturation currents. A change in the measured amplitude of fluctuations of the floating probe potential with a change in the ratio of electron and ion saturation currents indicates that temperature fluctuations are important and, conversely, insignificant changes in fluctuations in the floating probe potential with a change of the ratio may indicate the absence of significant temperature fluctuations. Since the coefficients μ_e and μ_i can be calculated theoretically or determined experimentally, it may be possible to calculate or quantify the effect of temperature fluctuations on plasma potential measurements using equations (17) and (18). To do this in detail, information is needed on whether the oscillations of the plasma potential are coherent and, if coherent, then what is the phase shift between them. If there is no such information, then from measurements by an isolated MIBP it is still

possible to estimate the minimum and maximum possible values of the amplitude of oscillations of the electron temperature in the plasma.

For exact isolation of the component of the oscillations of the plasma potential, generally it is necessary to analyze the oscillations of the temperature of electrons and ions and their relationship, phase shifts and cross coherence, with oscillations of other parameters. To do that, a probe cluster should be used. The probe cluster must have at least two probes. Of these, at least one of the probes must be a MIBP, and as the other, it is better to use a conventional probe with a large μ_e coefficient. In this case, the probe sensitivity to temperature measurement is increased (multiplied by the μ_e factor). As can be seen from section 3, an increase in the ratio of the electron saturation current to the ion saturation current leads to an increase in the μ_e coefficient and a decrease in the μ_i coefficient, and vice versa. Then, by measuring oscillation at different ratios of saturation currents, one can distinguish fluctuations in the temperatures of electrons and ions. The absence of a significant difference between open and closed/equalized probes may be as due to the fact that the temperature fluctuations are insignificant or the temperature fluctuations are shifted in phase so that the difference would not be noticeable. The last possibility can be checked by measuring cross-phase between MIBP and standard probe oscillations. This situation may require a more detailed analysis, for example make measurements of the probe floating potentials for several ratios of electron to ion saturation currents (see also some more details below).

Thus, this section demonstrates that in addition to measurements with MIBPs, it may be useful to make measurements with conventional cylindrical probes and the presence of a significant difference in the measured amplitudes is a possible indication of the presence of substantial charged particle temperature fluctuations. Probe clusters allow distinguish different types of oscillations and their modes. Note, that after measuring the temperature fluctuations, as discussed below, various iteration schemes can be used to refine the measured plasma potential fluctuations. It is shown that measuring the charged particle temperatures makes it possible to correct the results of measuring potential and electric field oscillation in plasma, for instance, using iterative schemes.

6.1. Toroidal low-temperature plasma

In toroidal plasma, to determine the fluctuations of the electron temperature in the Blaumann torus, measurements of ordinary and plug probes floating potential oscillations with cluster shown in figure 5 (right) have been carried out [42, 44]. As can be seen from formula (18), the instantaneous difference between the signals from those probes gives

$$\tilde{V}_{f2} - \tilde{V}_{f1} = \tilde{V}_{S2} - \tilde{V}_{S1} - \mu_{e2} \tilde{T}_e/e + \mu_{e1} \tilde{T}_e/e, \quad (26)$$

which is $4.2 \times \tilde{T}_e/e$ for the case of using equations (19) and (20).

Figure 32 shows the results of measurements of the amplitude of floating potential oscillations of the ordinary probe (blue upper curve) in the outer plasma at the +6 cm position

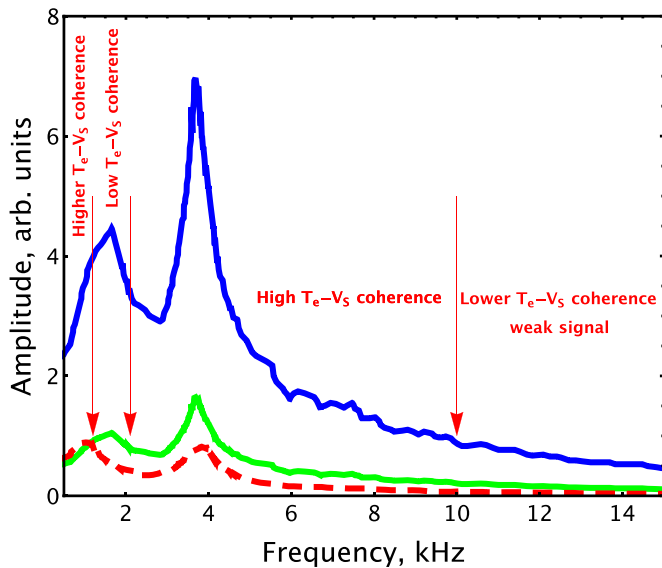


Figure 32. Amplitude spectra of the V_f oscillations of an ordinary probe (top blue curve). Amplitude spectra of electron temperature oscillations (middle green curve). Amplitude spectra of plasma potential oscillations (red dashed curve). Probe position $r = +6$ cm.

for the same conditions as shown in figures 20 and 26. It is possible to see, that the amplitude spectrum obtained with the ordinary probe is several times greater than similar amplitude spectrum obtained with the plug probe (compare figures 20 and 32), which indicates the presence of intense fluctuations of the electron temperature. The spectrum from the ordinary probe contains two maxima at frequencies about 1.5 kHz and 4 kHz, that is, at the same frequencies as the result of measurements with the plug-probe (see figure 20, bottom line), which is considered as fluctuations in the plasma potentials in section 4.

The electron temperature may be obtained using equation (26) and its amplitude spectrum is also shown in figure 32 (middle green curve). The same figure shows the results of refining the amplitude of oscillations of the plasma potential, shown by the lower pair of lines in figure 20 (red dashed curve in figure 32). The difference in the measured amplitude of potential fluctuations without considering temperature fluctuations does not exceed 20% for frequencies below 5 kHz. Thus, even though the amplitude of temperature fluctuations exceeds the amplitude of fluctuations in the plasma potential, the plug probe allows to obtain satisfactory measurement results, which of course can be refined if necessary. We also note that the presence of electron temperature fluctuations practically does not affect the behavior of the phase shift between fluctuations in the floating potentials of ordinary probes as compared to plug probes [44].

Thus, it can be seen that the spectra of the amplitude of the plasma potential oscillations at the outer plasma (+6 cm) position are similar to spectra obtained with the plug probes, but have a much larger amplitude. The spectrum of oscillations

of the electron temperature is somewhat higher in magnitude than the spectrum of oscillations of the plasma potentials. Since the spectrum of oscillations of the electron temperature when measured with a conventional probe is multiplied by a factor much greater than unity, such a spectrum contains mainly oscillations of the electron temperature and can hardly be used to estimate oscillations of the plasma potential without using plug-probes.

Figure 32 also shows a frequency displacement between high and low cross coherence between fluctuations in the measured electron temperature and plasma potential. It is seen that, at frequencies of about 1.5 kHz, the oscillations of the electron temperature and plasma potential are not related to each other. At the same time, the oscillations of the electron temperature and potential at a frequency of about 4 kHz belong to the same mode.

This example demonstrates that measurements of the plasma potential by the conventional probe might contain significant qualitative errors due to spurious effects from temperature fluctuations. These errors come in addition to errors arising from enhanced floating potential amplitudes caused by temperature fluctuations.

For the -6 cm position, the \tilde{V}_f amplitude spectrum of ordinary probe (top blue curve shown in figure 33) does not differ much in amplitude from that measured with the plug-probes (dashed magenta curve, which is also shown in figure 20, top curves), but has a number of small peaks caused by the contribution of \tilde{T}_e and its harmonics. Amplitude of electron temperature oscillations (bottom red curve) is substantially smaller than amplitude of potential oscillations. At the same time amplitude of $\mu_e \tilde{T}_e$ oscillations for ordinary probe (green curve) is generally greater than amplitude of potential oscillations (dashed black curve). As a result, in this situation, while estimation of electron potential oscillations with ordinary probe does not provide catastrophic errors, the cross-phase between two ordinary probes and two plug probes are very different (up to five times), as shown in figure 28.

It was seen from the previous section (figure 28) that oscillations of the plasma potential and electron temperature belong to the different modes, since the curve associated with ordinary probes can be heavily contaminated by oscillations of the electron temperature. Analysis of the cross coherence of electron temperature and plasma potential oscillations shows that it is low and that confirms that those oscillations in the internal plasma belong to different oscillation modes. In this case, the amplitude of oscillations of the electron temperature is substantially lower than the oscillations of the plasma potential.

Thus, the presence of large oscillations of the electron temperature gives large errors in the amplitude of oscillations when trying to measure oscillations of the plasma potential with ordinary probes. At the same time, even if the amplitude of oscillations of the electron temperature is much less than the amplitude of oscillations of the plasma potential, this can lead to errors in the study of the oscillation phases with ordinary probes. The use of clusters of conventional and MIBPs allows obtaining reliable results.

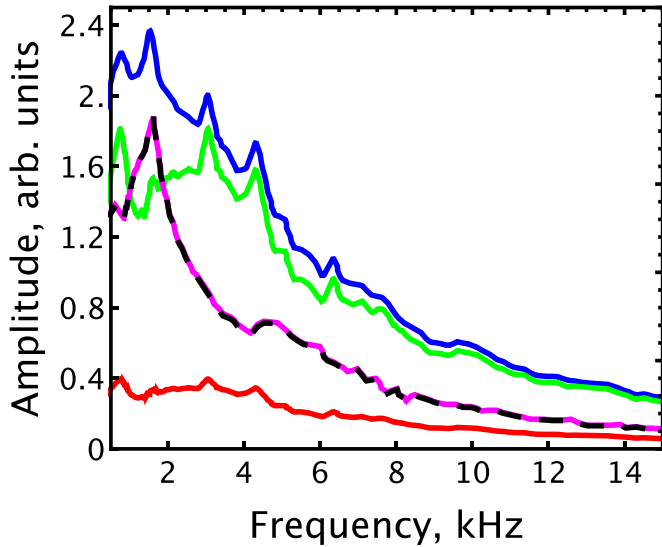


Figure 33. Amplitude spectra of floating potential oscillations of ordinary probe (top blue curve), electron temperature oscillations (bottom red curve), contribution of the electron temperature oscillations to the ordinary probe oscillations (second from top green curve), floating potential oscillations of plug probe (magenta curve) and plasma potential oscillations obtained from plug probe (dashed black curve). The probe position $r = -6$ cm.

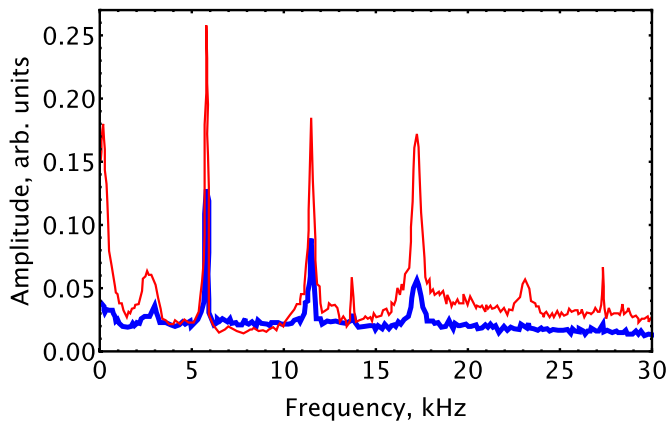


Figure 34. Amplitude spectra of the floating baffled probe potentials for cases $I_e^{\text{sat}} \gg I_i^{\text{sat}}$ (upper red curve) and $I_e^{\text{sat}} \approx I_i^{\text{sat}}$ (lower blue curve), $B = 0.1$ T [46]. [46] John Wiley & Sons. © 2004 WILEY-VCH Verlag GmbH & Co. KGaA, Weinheim.

6.2. Strongly ionized cold low-temperature plasma

To demonstrate the operation of the baffled probe in a plasma with electron temperature fluctuations of different relative magnitude in the barium plasma of the WVU Q-machine, measurements were carried out with a single baffle probe at different magnetic fields. Figures 34 and 35 show the results of such measurements for open and equalized baffles probes. It can be seen from the figures that the nature of the spectrum changes greatly with a change in the magnetic field.

That was discussed briefly in section 5. As can be seen from figure 34, for the magnetic field of 0.1 T, the amplitude spectrum of oscillations contains several narrow harmonics. The

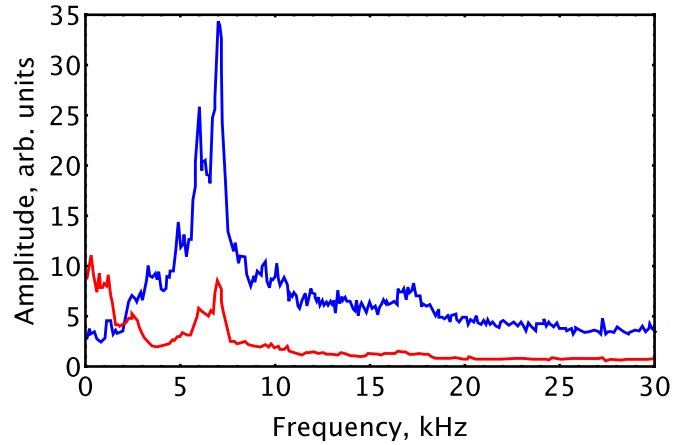


Figure 35. Amplitude spectra of the floating baffled probe potentials for cases $I_e^{\text{sat}} \gg I_i^{\text{sat}}$ (upper curve) and $I_e^{\text{sat}} \approx I_i^{\text{sat}}$ (lower curve), $B = 0.3$ T [46]. [46] John Wiley & Sons. © 2004 WILEY-VCH Verlag GmbH & Co. KGaA, Weinheim.

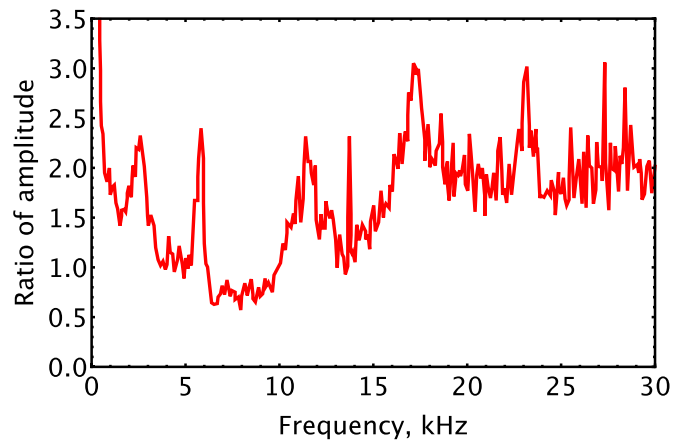


Figure 36. Ratio of amplitude spectra from figure 34 [46]. [46] John Wiley & Sons. © 2004 WILEY-VCH Verlag GmbH & Co. KGaA, Weinheim.

ratio of signals from the open to equalized probe is highly frequency dependent. At some frequencies it is less than one, at other frequencies it is more than one and reaches three. This may indicate that for those frequencies the fluctuations of the electron temperature are significant. There are areas where it is almost equal to one. This may indicate that for those frequencies the fluctuations of the electron temperature are not significant. In addition, the cross-phase of temperature and plasma potential fluctuations can vary. The cross coherence of these oscillations can also depend on frequency. For example, for those frequency ranges in which the ratio is less than unity, the oscillations of the electron temperature and potential can be in phase, and for the ion temperature they can be in antiphase. For a more detailed analysis of this situation, measurements with probe clusters are required.

Amplitude spectra shown in figure 35 for magnetic field of 0.3 T demonstrates a narrow spectrum band in the range from 4 to 8 kHz. There are practically no harmonics in this

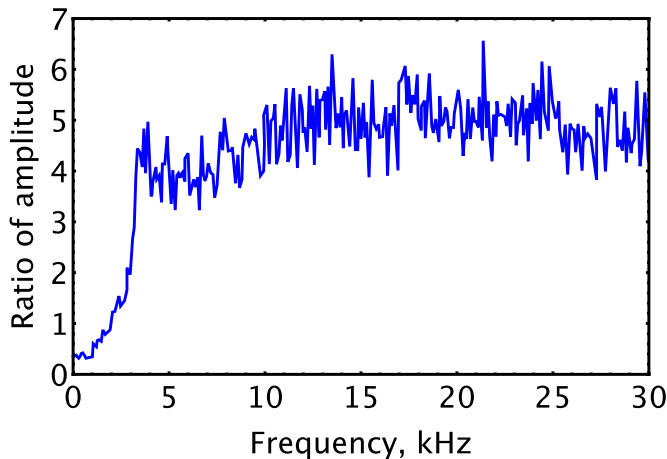


Figure 37. Ratio of amplitude spectra from figure 35 [46]. [46] John Wiley & Sons. © 2004 WILEY-VCH Verlag GmbH & Co. KGaA, Weinheim.

spectrum. As can be seen from figure 37, for such magnetic field, the role of electron temperature oscillations is high and weakly depends on the frequency, for a frequency above 4 kHz. The ratio of the open to equalized probe signals is close to 4.5. This behavior may be typical for drift waves, for which the potential and temperature fluctuations are significantly related [114]. At $B = 0.1$ T, the amplitude of the spectra is much smaller than for the case of a stronger magnetic field (in figures 34 and 35, the same arbitrary units are used).

A more detailed study of fluctuations in plasma potentials and the effect of fluctuations in the temperature of charged particles on them requires the use of two or more MIBPs or a combination of MIBP and conventional probes. This will allow obtaining phase shifts and cross coherence between different types of oscillations and better separating them. Such measurements were also carried out in a WVU Q-machine and are discussed below.

The measurements under the conditions in which the study of oscillations of the plasma potential and electric fields shown in figures 23 and 29 with a baffled probe cluster, shown in figure 10 (right), were carried out. As in the previous sections, the oscillations were excited by applying an alternating voltage to the mesh electrode (3) shown in figure 9. Figure 38 shows the results of measurements of power spectrum of V_f for open (top red curve), equalized (blue dots) probes and power spectrum of electron temperature oscillations (bottom green curve).

For a more convenient analysis of figures 38 and 39 shows the cross coherence between fluctuations of the plasma potential and electron temperature. As can be seen from figure 38, electron temperature oscillation amplitude and power is significantly smaller than that of the plasma potential. At a frequency of 8 kHz, the oscillation power of the open probe is less than that of the equalized probe. This suggests that the plasma potential oscillations at this frequency are in phase with temperature oscillations. For harmonics 16, 24 and 32 kHz, the ratio is reversed, that is, in these harmonics, the oscillations of

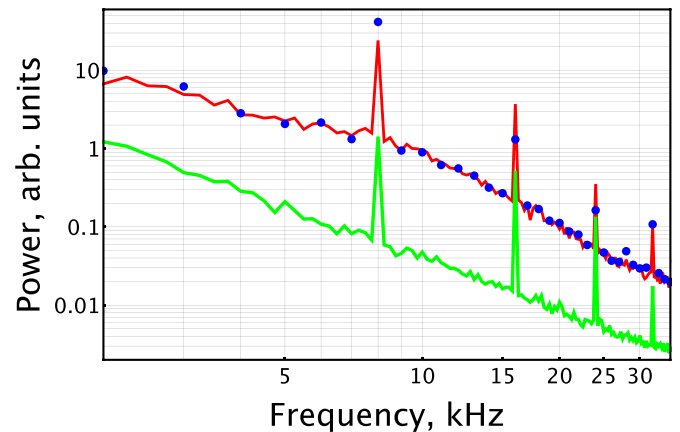


Figure 38. Power spectra of V_f for open (top red curve) and equalized (blue dots) probes. Power spectrum of \tilde{T}_e (bottom green curve) [30]. Adapted from [30], with the permission of AIP Publishing.

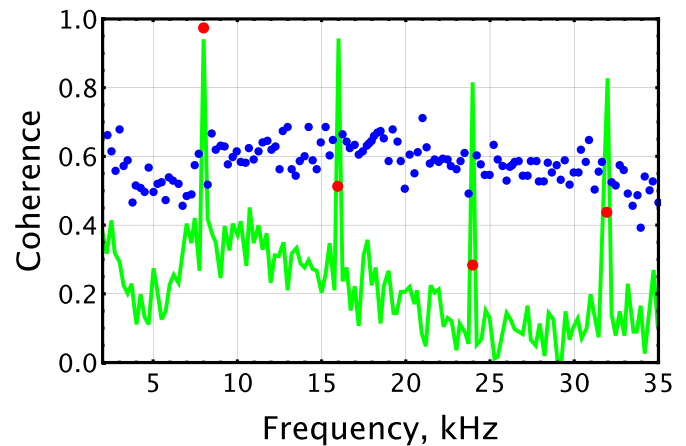


Figure 39. Cross coherence between plasma potential oscillation and \tilde{E}_y (small blue dots); the same for frequency of 8 kHz and its harmonics (large red dots); cross coherence between electron temperature and plasma potential oscillations (bottom green curve) [30]. Adapted from [30], with the permission of AIP Publishing.

the potential and electron temperature are in antiphase. Note that the cross coherence between the oscillations of the electric field component perpendicular to the magnetic field in azimuthal direction and the exciting oscillations at a frequency of 8 kHz is high, and at harmonic frequencies the cross coherence is low, which means that the main contribution to oscillations at a frequency of 8 kHz is made by oscillations that are not associated with the heating mode.

The cross coherence of the oscillations of the potential and the electron temperature is high only at an exciting frequency of 8 kHz and its harmonics. Cross coherence is low between these frequencies (see green curve in figure 39). That is, the oscillations of the electron temperature belong to the oscillation mode of the plasma potential only for the exciting frequency and its harmonics. Cross coherence between plasma potential oscillation and \tilde{E}_y is high at frequency of 8 kHz, but low at its harmonics (large red dots). It means that frequency

of 8 kHz belongs mainly to the wave, associated with the electric field component perpendicular to the magnetic field in azimuthal direction, but not its harmonics, which associated with electric field component along the magnetic field. Now, after the relationship between temperature and potential fluctuations has been sorted out, and considering the results of measurements in the two previous sections for the same mode, the complete oscillation pattern can be described.

So, the changing potential of the grid creates a sinusoidally varying potential that penetrates into the plasma. This potential has the same oscillation phase for all points of the plasma, but the oscillation amplitude is different and decreases with distance from the grid (that is, these oscillations are not a wave). The amplitude of oscillations at the boundary of the layer near the grid is comparable to or less than 0.02 V, which is much less than one percent of the amplitude of the potential supplied to the grid. Since the amplitude of oscillations in the plasma is different, an electric current is created that passes through the plasma (and goes to the grid) and heats it at a frequency of 8 kHz.

The current flowing to the grid depends nonlinearly on the potential applied to it, and therefore current harmonics exist in the plasma at frequencies 16, 24, 32, etc. A wave is also excited in the plasma, perpendicular to the magnetic lines at a frequency of 8 kHz. This wave has no harmonics but spectrally broadens, apparently as a drift wave propagating perpendicular to the magnetic lines. Absolute values of amplitudes for frequency of 8 kHz and its three harmonics correspond to temperature of 2.3, 1.4, 0.7, and 0.2 K, respectively. The rms amplitude of the perpendicular-to-B component of the 8 kHz-wave's electric field is substantially greater than the rms amplitude of the parallel-to-B component of the 8 kHz-wave's electric field.

As is clear from section 3, the measurements carried out in the plasma of Q-machine plasma make it possible the determination of the absolute values of electron and ion temperatures from the shifting of the potential of the floating MIB probe with variation of ratio of electron and ion saturation currents. For this, formula (17) and the measurement data shown in figures 11, 12 and 15 can be used. As a result of measurements, it was obtained that $T_e \approx T_i \approx 0.2$ eV. Obviously, such a methodology of dc measurements is neither highly precise ($\pm 20\%$) nor highly accurate ($\pm 20\%$) but it demonstrates how temperature shifts the floating potential toward or away from the plasma potential. Measurements can be performed for a scan of baffling levels, i.e. at several ratios of electron and ion saturation currents. Then, we can solve systems of equations for different ratios and thus improve the measurement accuracy.

6.3. Hot fusion-boundary plasma

In the near-wall plasma of the stellarator HSX, the floating potential oscillations of an open and equalized single MIBP have been measured. A typical example of such measurements is shown in figure 40. In this work, measurements with a probe cluster were not carried out; therefore, it is not possible to establish an exact relationship between the oscillations of

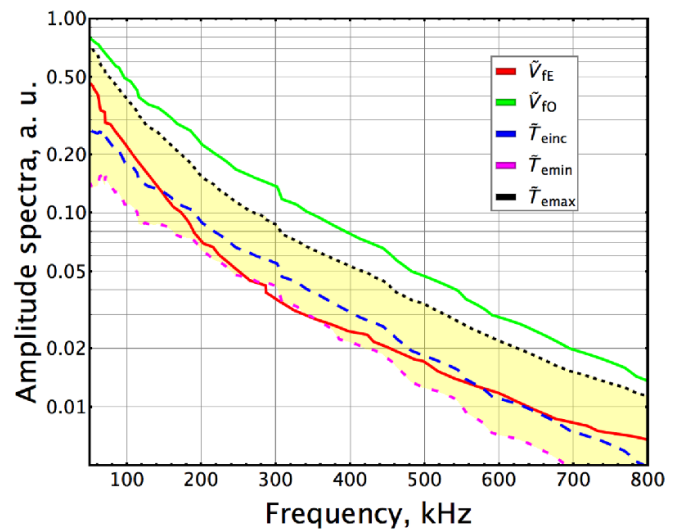


Figure 40. Amplitude spectra of electron temperature and plasma potential oscillations: V_{FE} is floating potential amplitude, measured by the equalized baffled probe, V_{F0} is the potential amplitude of the floating open baffled probe, T_{einc} is calculated amplitude of the electron temperature oscillations with assumption of incoherent potential and temperature oscillations, $T_{eincmin}$ and $T_{eincmax}$ are minimal and maximal possible amplitudes of electron temperature oscillations, calculated from experiment. The area marked in yellow shows where the experimental amplitudes of temperature fluctuations are located.

the plasma potential and temperature, considering the phase shifts and cross coherence between different oscillations. Nevertheless, the evidence indicates that the open probe, the floating potential of which monitors space potential and temperature fluctuations combined, has a floating-potential oscillation approximately twice that of the equalized probe, the floating potential of which monitors only the space potential.

To find the amplitude of the electron temperature oscillations, it is necessary to know whether the temperature and potential oscillations are coherent and, if so, what is the phase shift between these oscillations. Since the measurements were carried out with a single MIB probe, such information is not available at the moment. In figure 40 the plasma potential oscillation amplitude, measured by the equalized baffled probe, is shown as a red curve (marked as V_{FE}). The green curve, marked as V_{F0} , shows the amplitude of the open baffled probe. If we assume that the oscillations of the plasma potential and temperature are incoherent, then the calculated amplitude of the electron temperature oscillations (T_{einc}) is shown by a blue dotted line. The calculated maximum and minimum amplitudes of temperature oscillations under the condition of high cross coherence of oscillations of the plasma potential and temperature are shown by magenta and black dashed lines. The true amplitude of oscillations may lie somewhere between them in the shaded yellow area.

When calculating the amplitude of the electron temperature oscillations, it was taken into account that formulas (21) and (22) contain the temperature multiplication factors during measurement. Therefore, the temperature calculation result was divided by the corresponding coefficient. Thus, it can

be seen from figure 40 that the amplitude of the plasma potential oscillations is close (or the same order as) to the amplitude of the temperature oscillations in the corresponding units. It can also be seen that in the range from 50 to 800 kHz, this dependence is adequately described by an exponential.

7. Measurements of anomalous particle and energy fluxes

As demonstrated above, MIBPs can greatly simplify measurements of charged particle fluxes and energy, since they can provide direct measurements of fluctuations in plasma potentials, electric field and electron temperature. This section provides demonstration of the flux measurements.

7.1. Low-frequency turbulence and transport

There are a number of publications devoted to measurements with different techniques of particle and energy fluxes in magnetized plasma (see, for example, [115–117]). To the best of our knowledge, such measurements using the MIBPs were first carried out in [44]. Review [10] is also describes the measurements of anomalous fluxes using probes, including MIBPs.

In a low-pressure plasma, the charged particle flux density, $\Gamma_{\mathbf{r}} = \langle \mathbf{n}_e \mathbf{v}_r \rangle = \mathbf{n}_{e0} \mathbf{v}_{r0} + \langle \tilde{\mathbf{n}}_e \tilde{\mathbf{v}}_r \rangle$, occurs due to convection ($\Gamma_{\mathbf{r}0} = \mathbf{n}_{e0} \mathbf{v}_{r0}$) and electrostatic fluctuations in the plasma density $\tilde{\mathbf{n}}_e$ and electric field $\tilde{\mathbf{E}} = -\nabla \tilde{V}_s$. This leads to fluctuations in the drift velocity $\mathbf{v}_r \approx \mathbf{E}_\theta / B$. The Fourier transform in time gives

$$\Gamma_{\mathbf{r}} - \Gamma_{\mathbf{r}0} = \sum_{\omega > 0} \Gamma(\omega) = \frac{2}{B} \sum_{\omega > 0} \sqrt{\langle |\mathbf{n}_e(\omega)|^2 \rangle \langle |\mathbf{E}_\theta(\omega)|^2 \rangle} \times \gamma_{n_e E}(\omega) \sin \alpha_{n_e E}(\omega). \quad (27)$$

where

$$\gamma_{n_e E}(\omega) = \langle \mathbf{n}_e(\omega) \mathbf{E}_\theta(\omega)^* \rangle / \sqrt{\langle |\mathbf{n}_e(\omega)|^2 \rangle \langle |\mathbf{E}_\theta(\omega)|^2 \rangle}$$

is the cross coherence and $\alpha_{n_e E}(\omega) = \arg \langle \mathbf{n}_e(\omega) \mathbf{E}_\theta(\omega)^* \rangle$ is the cross-phase between \mathbf{n}_e and \mathbf{E}_θ . Linear superposition of waves yields

$$\Gamma_{\mathbf{r}} - \Gamma_{\mathbf{r}0} = \sum_{\omega > 0} \Gamma(\omega) = \frac{2}{B} \sum_{\omega > 0} \sqrt{\langle |\mathbf{n}_e(\omega)|^2 \rangle \langle |\tilde{\mathbf{V}}_s(\omega)|^2 \rangle} \times \mathbf{k}_\theta(\omega) \gamma_{n_e V}(\omega) \sin \alpha_{n_e V}(\omega). \quad (28)$$

From these expressions it is seen that the flow is optimized if $\alpha_{n_e E} = 0$ and $\alpha_{n_e V} = 3\pi/2$. The flux is zero if $\alpha_{n_e E} = \pi/2$ or $3\pi/2$ and $\alpha_{n_e V} = 0$ or π .

From equation (27) it is clear, that we need to have instantaneous measurements of $\mathbf{n}_e(t)$ and $\mathbf{E}_\theta(t)$ to evaluate the flux density spectrum. The cross-field anomalous energy transport may be obtained from [10]

$$Q_r = \frac{3}{2} \Gamma_r T_e + \frac{3}{2} \mathbf{n}_e \frac{\langle \tilde{\mathbf{E}}_\theta \tilde{T}_e \rangle}{B}. \quad (29)$$

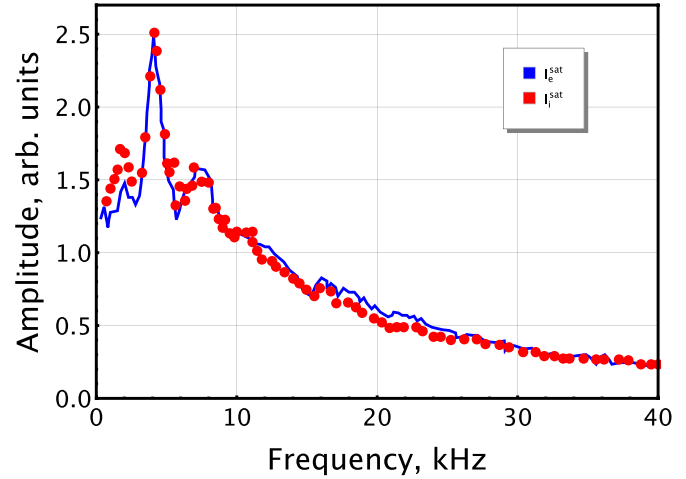


Figure 41. Amplitude spectra of I_e^{sat} (red dots) and I_i^{sat} (blue curve) fluctuations measured by a plug probe. Adapted from [42], with the permission of AIP Publishing.

It is seen from equation (29) that measurements of energy transport is possible if \tilde{T}_e is measured in addition to $\tilde{\mathbf{E}}_\theta$ and $\tilde{\mathbf{n}}_e$.

7.2. Measurements of plasma density oscillations

As we can see from section 2.3, plasma density or its fluctuations can be found from electron or ion saturation current. Electron density can be found, for example, for the case of $T_e \gg T_i$ from formula (3) as [44, 46]

$$n_e = \frac{B I_e^{\text{sat}}}{8 R T_e}. \quad (30)$$

Correspondingly, density oscillations can be found as

$$\tilde{n}_e = \frac{B \tilde{I}_e^{\text{sat}}}{8 R \tilde{T}_e}. \quad (31)$$

From equation (31) it is seen that to measure plasma density fluctuations, it is necessary to measure the electron or ion temperature oscillations as well as temperature oscillations. In order to demonstrate that the oscillations of the ion and electron currents give the same result, in figure 41 both oscillations of the electron and ion saturation currents are demonstrated and shown in one figure. They give with very good accuracy the same result for measurements.

7.3. Experimental measurements of anomalous particle and energy fluxes

As it is seen from section 7.1, to determine the fluxes of particles and energy, it is necessary to measure the instantaneous power spectra of oscillations of the electric field, space potential, density of charged particles and electron temperature. Examples of such measurements are shown in figure 42. Those measurements were carried out under conditions similar to those discussed in previous sections 4–6 for toroidal plasma in the Blaumann device in the outer plasma at the +6 cm position (see also figures 20, 26 and 32).

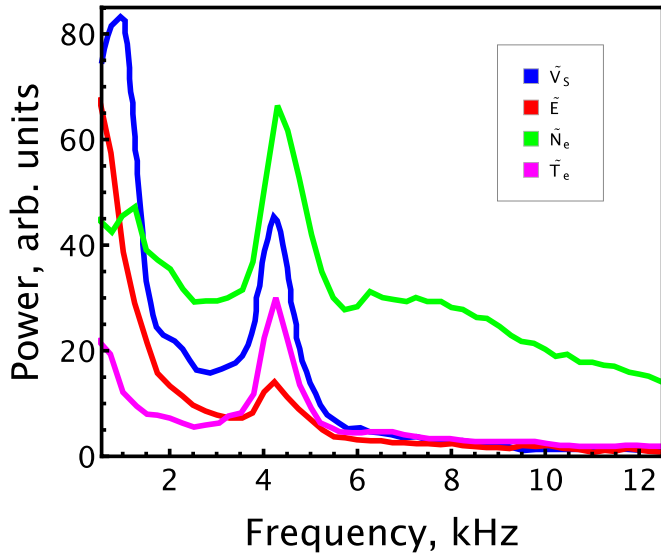


Figure 42. Power spectra of electric field, plasma potential, plasma density and electron temperature at position $r = +6$ cm. Arbitrary units for each curve. Adapted figure with permission from [44], Copyright (2002) by the American Physical Society.

It is seen, that the spectra of all these quantities have peaks at frequency of about 4.5 kHz, which belongs to the flute mode, as it was discussed in sections 5 and 6. Under studied conditions, this oscillation mode is mostly absent in the inner plasma and that suggests that those oscillations during propagation to the direction perpendicular to the magnetic lines, have a sufficiently strong damping. Figure 42 shows that the power of the plasma density oscillation appears instead at the high-frequency end of the spectrum (higher than 6 kHz).

Figure 43 shows cross-phases between density and electric field, temperature and electric field and density and electron temperature. In outer plasma, the first two cross-phases have values of about $\pi/2$ and the last one is about zero which is consistent with the flute mode dynamics. If the inner plasma had the same oscillations as the outer plasma, then in the configuration in which the experiment was carried out, the displacement of the probe cluster into the inner plasma would lead to a change in the measured cross-phase by π for the pairs of oscillations of the $T_e - E$ and $n_e - E$ and the preservation of the zero phase for $n_e - T_e$, as electric field vector is changing direction. However, in inner plasma cross-phase between density and electric field is about the same as in outer plasma, while temperature and electric field cross-phase is added $\pi/2$ with respect to outer plasma and cross-phase density and electron temperature is shifted by $3\pi/2$ compare to outer plasma. This is typical for the drift waves in the adiabatic regime and indicates that density and electric field fluctuations are dominated by drift waves in the inner plasma. The weak electron temperature oscillation in the inner plasma suggests that they survived from flute mode during convection from outer plasma. Thus, the oscillation properties obtained earlier in sections 5 and 6 receive additional confirmation.

Figure 44 shows particle fluxes calculated according to equations (27) and (29) for the inner (bottom green curve) and

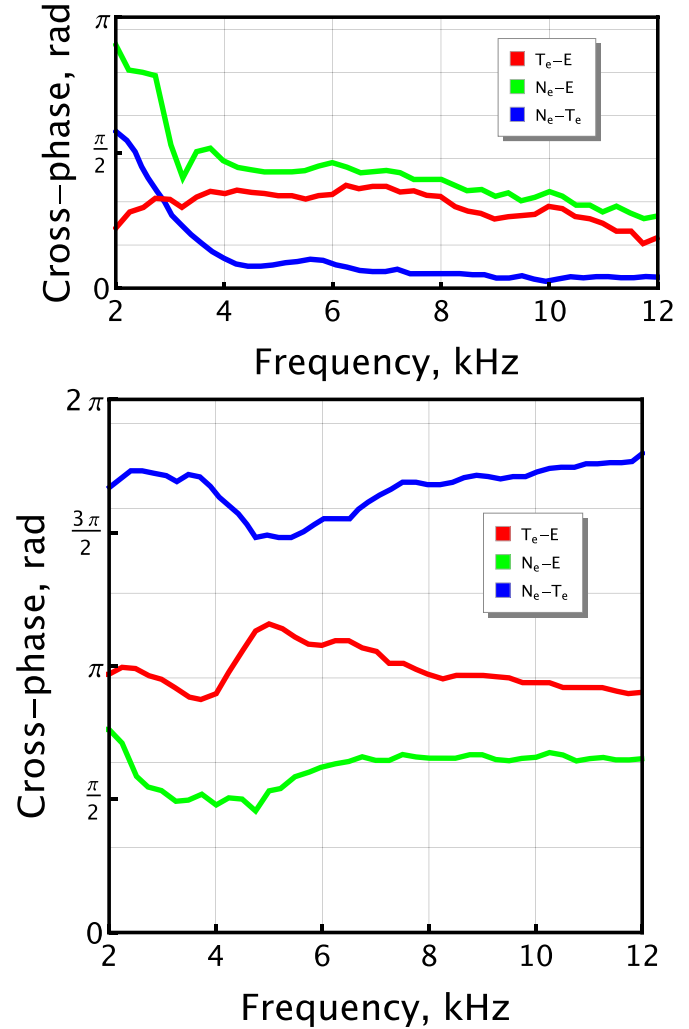


Figure 43. Cross-phase spectra between density and electric field, density and electron temperature and temperature and electric field measured at $r = +6$ cm (upper figure) and $r = -6$ cm (lower figure). Adapted figure with permission from [44], Copyright (2002) by the American Physical Society.

outer (top blue curve) plasmas. The particle flux is directed down the gradient towards the wall on the outer as well as the inner slopes. In outer plasma about a half of the particle flux is due to the large-scale coherent structures responsible for the spectral peak at 4.5 kHz and the rest is due to the turbulent spectrum on higher frequencies. In the inner plasma most of the flux is due to the high frequencies.

Figure 44 also shows energy fluxes calculated from equation (29). Since the cross-phase between temperature and electric field fluctuations is close to $\pi/2$ in the outer plasma, this is not favorable for energy transport. The situation is reversed in the inner plasma. There, the considered cross phase is close to π and this facilitates energy transfer. Therefore, the energy flux in the inner plasma is somewhat higher than in the outer plasma, despite the fact that the level of temperature fluctuations in the inner plasma is significantly lower than in the outer plasma. Flux measurements show that the large-scale structure at frequencies below 5 kHz plays an essential role in the transport of both particles and energy.

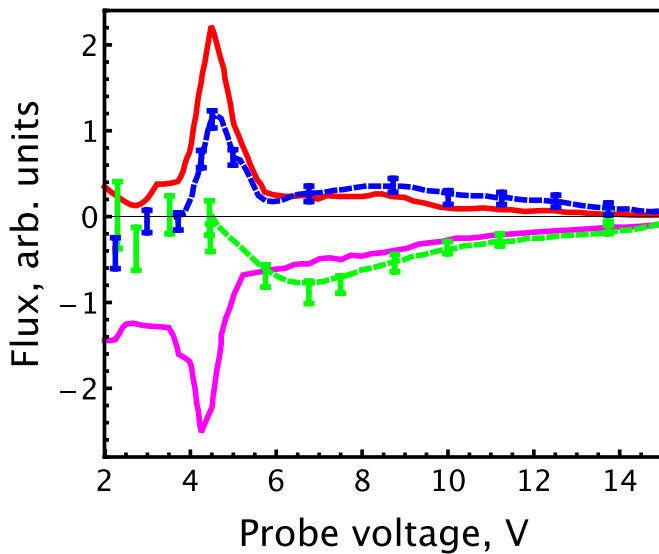


Figure 44. Particle flux spectra at $r = +6$ cm, top blue and $r = -6$ cm, bottom green solid curves, and heat flux spectra, top red and bottom magenta dashed curves, in the same positions, measured by method described in section 7 [44] in a simple magnetized torus. The plasma conditions are $B = 0.154$ T, helium pressure $p = 0.35$ Pa, $n_e = 3 \times 10^{11} \text{ cm}^{-3}$ and $T_e = 1$ eV. Adapted figure with permission from [44], Copyright (2002) by the American Physical Society.

In the inner plasma, the levels of the plasma potential and the electric field oscillations have comparable values (see figures 20, 26 and 27), while the level of temperature fluctuations in the outer plasma is about 3 times higher than in the inner plasma (compare figures 32 and 33). This suggests that the thermal conductivity parallel to the magnetic field plays an important role in the dynamics of modes in the inner plasma, which one more time corresponds to the case of drift waves in the inner plasma.

Thus, the flux measurements show that the large-scale flute mode structures play a substantial role in both particle and energy transport on the outside. In the inner plasma only drift waves contribute to particle transport, while the coupling between temperature fluctuations in flute modes and electric field fluctuations in drift waves yields the major contribution to the energy transport.

The time-averaged radial particle flux densities measured at $r = \pm 6$ cm are $5 \times 10^{18} \text{ m}^{-2} \text{ s}^{-1}$. If we assume that this value also corresponds to the spatially averaged radial flux density on a toroidal surface with minor radius of 6 cm, we should have a total particle flux of $7.5 \times 10^{18} \text{ s}^{-1}$. This may be compared to the total ionization rate due to the injected primary electrons.

The net time-averaged radial flux of energy density was measured as 2 Wm^{-2} and the corresponding net radial flux of energy was 3 W. The total injected power with discharge current of 1 A is 140 W, implying that only about 2% of this power is transported to the wall as radially lost plasma energy. The remainder is radiated in all directions as emitted light from excited helium, consumed for ionization and for heating of neutrals via inelastic ion-neutral collisions.

8. Measurements of electron and ion distribution functions

In this section, measurements of the charged particle energy distribution functions and/or temperatures are considered. The most interesting is the measurements of the IDF and/or ion temperatures by the MIB probes. So, the ion IDF/ion-temperature measurements are discussed in more detail in this section, since they are hardly possible with standard probes. To make them with the MIB probes, it is necessary to substantially suppress the electron current for the positive potentials of the probe [10, 118, 119]. Such measurements can also be carried out in a plasma without a magnetic field or with a weak magnetic field not sufficient for the required suppression of the electron current, as, to the best of our knowledge, proposed in [10] and experimentally carried out in [120].

To measure the EDF, a $I_e^{\text{sat}} \gg |I_i^{\text{sat}}|$ mode is needed, which can be achieved with an open probe. Of course, such measurements are also possible for a weak magnetic field or its absence. Measurements with the MIBPs make meaning when it is not possible to install the additional standard probes, for example, due to problems with spatial restrictions. For such measurements, one can use previously developed theories for various probe modes (see [10, 12, 13]). In this case, one may consider the possible influence of the baffles. In the simplest case, they can lead to unessential decrease in the electron current to the probe, which can be considered by introducing shading coefficients if necessary (neglect of the shading coefficient does not distort the EDF shape, but somewhat underestimates the measured electron density). In more complex cases, the influence can be more significant and even distort the measurement results. This should be verified experimentally on a case-by-case basis, for example by comparison with measurements with standard probes. Since the use of standard theories has already been well described in previous publications and their use is more straightforward, this is not covered in detail in this review.

We only note that, strictly speaking, it is possible to measure IDF and EDF only if the charged particles are in a collisionless mode (do not have collisions near the probe). In this case, Druyvesteyn formula (9) can be used for measurements (see section 2 and [10, 12]). For electrons, EDF measurements can also be carried out in the non-local regime, in which, for a weakly ionized plasma, collisions of electrons near the probe do not change their total energy using formulas (10), (14) and (16) (see section 2 and [10, 13]). If the conditions for the absence of near-probe collisions or nonlocality are not satisfied, only the temperature of electrons or ions can be measured using suitable formulas (for example, formulas (5)–(7)). For conditions in which there are no reliable theories (for example, for anomalous transport of charged particles to the probe), temperature measurement becomes problematic or impossible. Validation of ion temperature measurement using MIBP technique in finite boundary RF plasma has been conducted in [121].

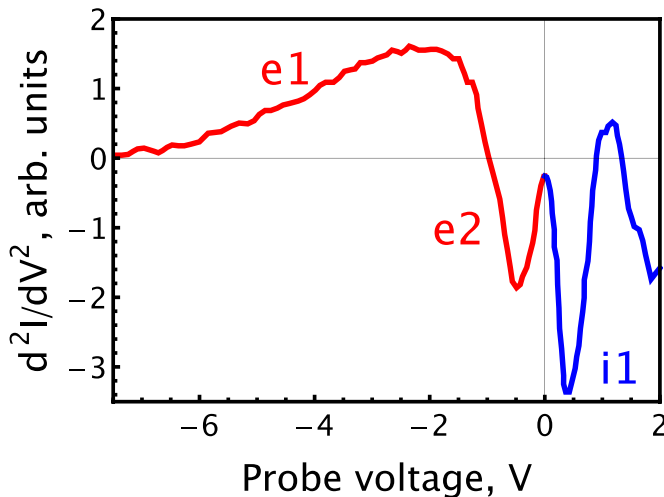


Figure 45. Typical result of measurements of d^2I/dV^2 in a magnetized helium plasma for gas pressure of 0.4 Pa and magnetic field $B = 0.01$ T [45]. Electron current features (e1, e2) and ion current feature (i1) are shown. $V = 0$ is the plasma potential. Electrons are in a nonlocal regime and ions are in a collisionless regime. Adapted from [45], with the permission of AIP Publishing.

8.1. Toroidal low-temperature plasma

Measurements of the second derivative of the MIB probe current with respect to the probe potential were carried out in the plasma of the simple magnetized torus Blaamann [45]. The measurements were carried out in helium at a gas pressure of 0.35 Pa in a magnetic field of 4–40 mT and a discharge current of 100–300 mA. Conditions associated with insignificant levels of fluctuations in the plasma potential and other parameters were investigated, a case for which better than 0.2 eV energy resolution of the probe bias is required. For measurements, a cylindrical molybdenum plug probe with a radius of 0.125 mm and a length of 3.5 mm was used. The radius of the ceramic plugs was 0.4 mm. For the measurements, conditions required by the collisionless theory are satisfied for both ions and electrons.

Figure 45 shows a typical measurement of the second derivative of the probe current with respect to the probe potential [45]. The structure of the measured second derivative is typically more complicated than the analogous structure for a plasma without a magnetic field, since there are maxima associated with the derivatives of not only the electron, but also the ion current (which are small and practically invisible compared to the electron maxima in a nonmagnetic plasma). Therefore, the curve has three maxima, two of which can be attributed to the electron current (red part of the curve), and one to the ion current (blue part of the curve).

Figure 46 demonstrates calculation of the second derivative of the probe current with respect to the probe potential. The model for the IV -trace derivatives, which is valid for magnetized electrons, allows us to obtain a curve containing the essential features of the experimental curve shown in figure 45. For repelled electrons ($V < 0$) with $\rho_L^e < R \ln(L/R)$, the nonlocal kinetic description (see section 2.3) is valid. Ions are unmagnetized and the ion current density second derivative for

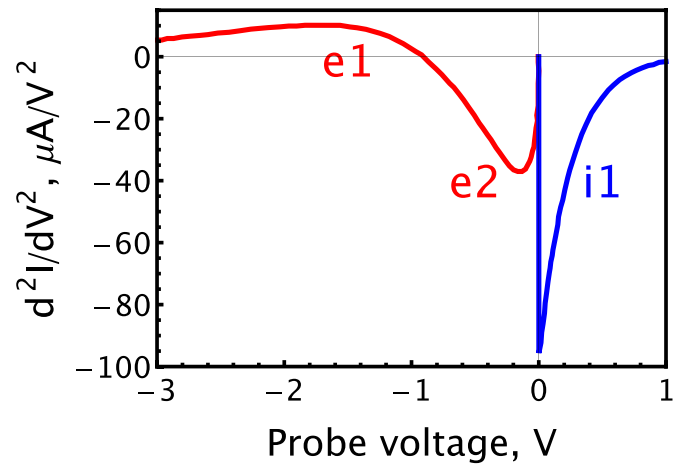


Figure 46. Result of modeling d^2I/dV^2 in a magnetized helium plasma [45] for plasma parameters: $n_i = n_e = 10^{10}$ cm $^{-3}$, $T_i = 0.2$ eV, $T_e = 0.85$ eV and $B = 0.013$ T. Electron current features (e1,e2) and ion current feature (i1) are shown. $V = 0$ is the plasma potential. For repelled electrons, the nonlocal kinetic description is valid (red line). Repelled ions follow to collisionless regime (blue line). Adapted from [45], with the permission of AIP Publishing.

repulsive probe voltage is given by the Druyvesteyn formula (9). IV -trace in figure 46 was calculated with temperatures of ions and electrons of 0.2 and 0.9 eV, respectively. A better correspondence to the experimental curve in figure 45 could have been obtained by hypothesizing a form for electron and ion saturation currents and by including the distortion effects of the differentiation method.

8.2. Strongly ionized cold low-temperature plasma

The Q-machine condition of equal electron and ion temperature is ideal for illustrating the capability of MIBP to characterize both ion and electron distribution functions [118]. In the plasma, it is possible to have electron saturation current, much higher than ion saturation current (as it is for an ordinary electric probe) for measurement of the EDF, T_e , or electron temperature oscillations, or to have vice versa, $I_e^{\text{sat}} \ll I_i^{\text{sat}}$, for measurements of the IDF, T_i , or ion temperature oscillations (note, that a possibility of such measurements may depend on the applicable probe theory [10]). It is also possible to adjust the ratio of electron to ion saturation current between both limiting cases.

The results of modeling the measured probe current–voltage characteristics are shown in figures 11 and 12. Clearly, the modeling yields reasonable results. For the particular case, the modeling yields $n_e = 8 \times 10^{10}$ cm $^{-3}$, $T_e = T_i = (0.16 \pm 0.01)$ eV and space potential $V_S = (7.30 \pm 0.15)$ V [46].

8.3. Hot fusion-boundary plasma

In the hot-fusion plasma the temperature of electrons and ions can be determined by modeling the IV -trace in the case of classic diffusion of charged particles onto the absorbing surface

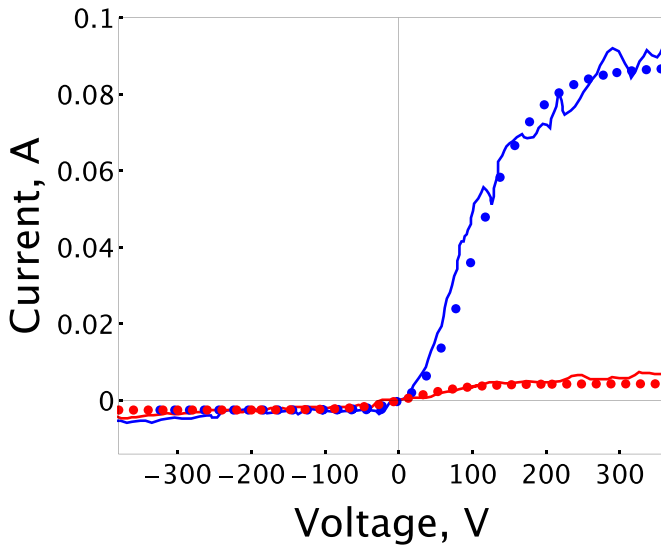


Figure 47. Smoothed experimental *IV*-traces for equalized baffled probe (red line) and open baffled probe (blue line). V_j is taken as zero [40]. Modelled *IV*-traces for equalized baffled probe (red dots) and open baffled probe (blue dots). For the calculations the following plasma parameters were taken: $T_e = 31$ eV, $T_i = 22$ eV and $n_e = 6 \times 10^{11}$ cm $^{-3}$. $B = 0.5$ T. Adapted from [40], with the permission of AIP Publishing.

of the probe, as was done in section 3 for the stellarator HSX. This simulation is shown in figure 47. There was found that the temperature of electrons is 31 eV, and the temperature of ions is 22 eV. Simulation of the same curve allows one to calculate the density of charged particles in the plasma. It is equal to 6×10^{11} cm $^{-3}$. For larger fusion devices with a high magnetic field, it may be necessary to use the theory of anomalous transport to the probe, however, we are not aware of such work performed by the MIBP.

9. Epilogue

MIBP determination of oscillations of fluid observables, such as electron and ion temperatures, electrostatic plasma potential, and electron and ion density reveal plasma instabilities and waves. For the regime wherein the relevant probe-tip dimension is logarithmically midway between the magnetized plasma's thermal electron and ion gyro radii, the Langmuir probe is capable of enhanced, compared to a bare wire, diagnostic utility for studying fluctuations in plasma parameters and abnormal flows of charged particles and energy. Especially feasible for the condition of equal electron and ion temperature within this regime, the MIBP allows a more detailed study of key parameters of the plasma's ion component's distribution function, while retaining the ability to measure the temperature and distribution function of electrons. It is shown that the MIBP diagnostic is compatible with research intent over a wide range of plasma energy density, inclusive of low (industrial applications) and high (fusion applications) plasma density and temperature. The presented examples of measurement results make it possible to assess the prospect of success and difficulty for a specific application.

Interpreting the MIBP floating potential signal, or the MIBP collected-current to applied-bias-voltage ratio, in determining plasma parameters, straightforwardly relies on the elementary principle of magnetized-orbit particle trajectories. The review demonstrates that, while the use of even a single MIBP allows us to obtain important additional information about the plasma, the application of a closed/open combination (i.e. a MIBP cluster), comprising one open and one closed MIBP, filters out (decontaminates) unwanted-parameter contributions from the signal of interest in a detailed study of oscillatory processes. Knowledge of the spectra of various plasma parameters, the cross-phases between various parameters, and the cross coherences between them allow us to study specific processes in detail, identify a process' most important properties, and distinguish one process from another.

Comparing and contrasting MIBP designs and applications that have been documented in plasma research, and listing the implementation convenience and diagnostic usefulness as well as the inconvenience and drawbacks, is a focus of this review. Correct MIB usage depends on choosing a suitable probe theory having applicability to the plasma conditions of interest and to the probe system at hand. Careless application of theoretical models outside their realm of validity can lead to systematic errors, partially or completely incorrect results, and unfounded conclusions. Sometimes application of different probe constructions makes it possible to make two or more independent probe measurements of the same ac or dc plasma observable, which can independently verify or refute a specific methodology.

Note also that, in some cases, MIBP can be used in plasma without a magnetic field or with a weak magnetic field that is incapable of magnetizing the orbit of thermal particles in a species population, i.e. not capable of a magnetic field strong enough for independent operation of the MIBP, suppression of the electron current. For this, a localized magnetic field can be applied, which does not distort the global properties of the plasma.

Data availability statement

All data that support the findings of this study are included within the article (and any supplementary files).

Acknowledgment

This work was partially supported by National Natural Science Foundation of China under Grant No. 11775062.

ORCID iDs

C Yuan  <https://orcid.org/0000-0002-2308-6703>

I P Kurylyandskaya  <https://orcid.org/0000-0002-4592-1730>

V I Demidov  <https://orcid.org/0000-0002-2672-7684>

M Gryaznevich  <https://orcid.org/0000-0002-4518-5593>

M E Koepke  <https://orcid.org/0000-0001-9631-356X>
 Y Raitsev  <https://orcid.org/0000-0002-9382-9963>

References

- [1] McCarrick M, Ellis R F, Koepke M and Majeski R P 1985 Perpendicular ion energy analyzer for hot-ion plasmas *Rev. Sci. Instrum.* **56** 1463
- [2] Stark J, Retschinsky T and Schaposchnikoff A 1905 Untersuchungen über den Lichtbogen *Ann. Phys., Lpz.* **323** 213
- [3] Mott-Smith H M and Langmuir I 1926 The theory of collectors in gaseous discharges *Phys. Rev.* **28** 727
- [4] Chen F F 1965 *Plasma Diagnostic Techniques* ed R H Huddleston and S L Leonard (New York: Academic) p 113
- [5] Swift J D and Schwar M J R 1970 *Electrical Probes for Plasma Diagnostics* (London: Iliffe Books)
- [6] Hutchinson I H 1987 *Principles of Plasma Diagnostics* (Cambridge: Cambridge University Press)
- [7] Stangeby P C 1989 *Plasma Diagnostics* vol 2 (New York: Academic) p 157
- [8] Godyak V A 1990 *Plasma–Surface Interaction and Processing of Materials* (Dordrecht: Kluwer) p 95
- [9] Matthews G F 1994 Tokamak plasma diagnosis by electrical probes *Plasma Phys. Control. Fusion* **36** 1595
- [10] Demidov V I, Ratynskaia S V and Rypdal K 2002 Electric probes for plasmas: the link between theory and instrument *Rev. Sci. Instrum.* **73** 3409
- [11] Chen F F 2003 *Mini-Course on Plasma Diagnostics (Lecture Notes on Langmuir Probe Diagnostics)* (IEEE-ICOPS Meeting, Jeju, Korea)
- [12] Godyak V A and Demidov V I 2011 Probe measurements of electron-energy distributions in plasmas: what can we measure and how can we achieve reliable results? *J. Phys. D: Appl. Phys.* **44** 233001
- [13] Demidov V I, Koepke M E, Kurlyandskaya I P and Malkov M A 2020 Basic factors for acquiring, correcting, and interpreting probe current-voltage characteristic in moderate-collisional plasma for determining electron energy distribution *Phys. Plasmas* **27** 020501
- [14] Demidov V I, Adams S F, Miles J A, Koepke M E and Kurlyandskaya I P 2016 Suprathermal electron energy spectrum and nonlocally affected plasma-wall interaction in helium/air micro-plasma at atmospheric pressure *Phys. Plasmas* **23** 103508
- [15] Adams S F, Demidov V I, Hensley A L, Koepke M E, Kurlyandskaya I P, Miles J A and Tolson B A 2018 Probe measurements of electron energy spectrum and plasma-wall interaction in Helium/air micro-plasma at atmospheric pressure *J. Phys.: Conf. Ser.* **982** 012013
- [16] Chiodini G, Riccardi C and Fontanesi M 1999 A 400 kHz, fast-sweep Langmuir probe for measuring plasma fluctuations *Rev. Sci. Instrum.* **70** 2681
- [17] Troll O, Conde L, Criado E, Donoso J M and Herdrich G 2005 Measurements of plasma properties using fast sweep Langmuir probes in unmagnetized weakly ionized plasmas *Contrib. Plasma Phys.* **50** 819
- [18] Skoutnev V, Dourbal P, Rodríguez E and Raitsev Y 2018 Fast sweeping probe system for characterization of spokes in E×B discharges *Rev. Sci. Instrum.* **89** 123501
- [19] Wang E Y, Hershkovitz N, Intrator T and Forest C 1986 Techniques for using emitting probes for potential measurement in rf plasmas *Rev. Sci. Instrum.* **57** 2425
- [20] Balan P *et al* 2003 Emissive probe measurements of plasma potential fluctuations in the edge plasma regions of tokamaks *Rev. Sci. Instrum.* **74** 1583
- [21] Sheehan J P, Raitsev Y, Hershkovitz N and McDonald M 2017 *J. Propuls. Power* **33** 614
- [22] Mahdizadeh N, Greiner F, Ramisch M, Stroth U, Guttenfelder W, Lechte C and Rahbarnia K 2005 Comparison of Langmuir and emissive probes as diagnostics for turbulence studies in the low-temperature plasma of the torsatron TJ-K *Plasma Phys. Control. Fusion* **47** 569
- [23] Kraus B F and Raitsev Y 2018 Floating potential of emitting surfaces in plasmas with respect to the space potential *Phys. Plasmas* **25** 030701
- [24] Demidov V I, Kolokolov N B, Mezantsev A P and Mustafaev A S 1986 Electron velocity distribution and potential drop near the wall in the cathode plasma of an electric discharge *Sov. J. Plasma Phys.* **12** 1496
- [25] Bohm D, Burhop E H S and Massey H S W 1949 *The Characteristics of Electrical Discharges in Magnetic Fields* ed A Guthrie and R K Wakerling (New York: McGraw-Hill) p 13
- [26] Pitts R A and Stangeby P C 1990 Experimental tests of Langmuir probe theory for strong magnetic fields *Plasma Phys. Control. Fusion* **32** 1237
- [27] Ratynskaia S V, Demidov V I and Rypdal K 2000 Probe measurements of electron temperature and density in strongly magnetized plasma *Rev. Sci. Instrum.* **71** 3382
- [28] Demidov V I, Ratynskaia S V and Rypdal K 2001 The analysis of probe IV-characteristics in a magnetized low-temperature plasma *Contrib. Plasma Phys.* **41** 443
- [29] Demidov V I, Finnegan S M, Koepke M E and Reynolds E W 2003 Baffled probe for real-time measurement of space potential in magnetized plasma *Rev. Sci. Instrum.* **74** 4558; Finnegan S M 2005 Real-time measurements of space potential in magnetized plasma using a baffled Langmuir probe Master's Thesis West Virginia University, Morgantown
- [30] Demidov V I, Koepke M E and Raitsev Y 2010 Magnetically insulated baffled probe for real-time monitoring of equilibrium and fluctuating values of space potentials, electron and ion temperatures, and densities *Rev. Sci. Instrum.* **81** 10E129
- [31] Katsumata I and Okazaki M 1967 Ion sensitive probe—a new diagnostic method for plasma in magnetic fields *Japan. J. Appl. Phys.* **6** 123
- [32] Katsumata I 1996 A review of ion sensitive probes *Contrib. Plasma Phys.* **36S** 73
- [33] Schrittwieser R *et al* 2005 Probe methods for direct measurements of the plasma potential *Rom. J. Phys.* **50** 723
- [34] Li S, Yuan C, Yao J, Kurlyandskaya I P, Koepke M E, Demidov V I, Kudryavtsev A A and Zhou Z 2020 Evidence of effective local control of a plasma's nonlocal electron distribution function *Plasma Sources Sci. Technol.* **29** 077001
- [35] Demidov V I, Ratynskaia S V and Rypdal K 1999 New designs for electrostatic probes in magnetized plasma *Int. Topical Conf. on Plasma Physics: New Frontiers of Nonlinear Science (Faro, Portugal, 6–10 September 1999)*
- [36] Ratynskaia S V, Demidov V I and Rypdal K 2000 A probe for measurements of electrostatic fluctuations in a low-temperature magnetized plasma *Rev. Sci. Instrum.* **71** 1367
- [37] Demidov V I 2001 Probe measurements of low-frequency E-field fluctuations *Second Workshop on Simulation of Plasma Turbulence and Comparison with Experiment (Kiel, Germany, March 2001)*
- [38] Greiner F, Block D, Piel A, Hellblom G, Ratynskaia S, Demidov V and Rypdal K 2002 Vergleich der plasma potential Messung von Emissiven Sonden und Plugged

- Probes in magnetisierten Plasmen *Deutsche Physikalische Gesellschaft (Bochum, Germany, 18–22 March 2002)*
- [39] Ionita C *et al* 2019 Plasma potential probes for hot plasmas *Eur. Phys. J. D* **73** 73
- [40] Guttenfelder W, Lechte C, Koepke M E and Demidov V I 2004 Utility of a baffled Langmuir probe for applications to edge plasma and turbulence characterization in stellarator plasma *15th Topical Conf. on High Temperature Plasma Diagnostics San Diego, CA, USA (Presented on 19 April 2004)*; *Rev. Sci. Instrum.* **75** 3622
- [41] Greiner F, Block D, Piel A and Ratynskaia S 2003 Plasma potential measurement in a magnetized plasma *Deutsche Physikalische Gesellschaft (Aachen, Germany, 10–13 March Spring Meeting) Poster P10.24* (available at: http://web.archive.org/web/20070513211449/http://old.dpg-tagungen.de/archive/2003/p_10.html) (Accessed 4 August 2021))
- [42] Ratynskaia S V, Demidov V I and Rypdal K 2002 Probe measurements of low-frequency plasma potential and electric field fluctuations in a magnetized plasma *Phys. Plasmas* **9** 4135
- [43] Demidov V I, Ratynskaia S V and Rypdal K 1999 An electrostatic probe with end plugs for measurements in a magnetized plasma *Rev. Sci. Instrum.* **70** 4266
- [44] Ratynskaia S V, Demidov V I and Rypdal K 2002 Measurements of anomalous particle and energy fluxes in a magnetized plasma *Phys. Rev. E* **65** 066403
- [45] Ratynskaia S V, Demidov V I and Rypdal K 2002 Probe measurements of ion energy distribution in magnetized plasmas *Rev. Sci. Instrum.* **73** 4232
- [46] Demidov V I, Finnegan S M, Koepke M E and Reynolds E W 2004 Utility of a baffled probe for measurements of oscillations in magnetized plasma *Contrib. Plasma Phys.* **44** 689
- [47] Gryaznevich M, Stöckel J, van Oost G, Del Bosco E, Svoboda V, Melnikov A, Kamendje R, Malaquias A, Mank G and Miklaszewski R 2020 Contribution of joint experiments on small tokamaks in the framework of IAEA coordinated research projects to mainstream fusion research *Plasma Sci. Technol.* **22** 055102
- [48] Gryaznevich M, Van Oost G, Stöckel J, Kamendje R, Kuteev B N, Melnikov A, Popov T and Svoboda V 2015 Contribution to fusion research from IAEA coordinated research projects and joint experiments *Nucl. Fusion* **55** 104019
- [49] Gryaznevich M P *et al* 2005 Joint research using small tokamaks *Nucl. Fusion* **45** S245
- [50] Gryaznevich M *et al* 2009 Results of joint experiments and other IAEA activities on research using small tokamaks *Nucl. Fusion* **49** 104026
- [51] Rozhanskii V A and Ushakov A A 1998 Analytic model of the current-voltage characteristic of a small probe in a magnetic field *Tech. Phys. Lett.* **24** 869
- [52] Rozhansky V, Ushakov A and Voskoboinikov S 1996 Transverse conductivity and theory of a probe in a magnetized plasma *Contrib. Plasma Phys.* **36** 391
- [53] Rozhansky V and Ushakov A 1998 Theory of a flush-mounted probe in a magnetized plasma *Contrib. Plasma Phys.* **38** 19–24
- [54] Rozhansky V, Ushakov A and Voskoboinikov S 1999 Electric fields and currents in front of a biased electrode (flush mounted probe) and the I–V characteristics of the electrode for various mechanisms of transverse conductivity *Nucl. Fusion* **39** 613
- [55] Rozhansky V A and Tsendin L D 2001 *Transport Phenomena in Partially Ionized Plasma* (London: Taylor & Francis)
- [56] Zhilinskii A P and Tsendin L D 1980 Collisional diffusion of a partially-ionized plasma in a magnetic field *Sov. Phys.—Usp.* **23** 331
- [57] Rozhansky V A 2012 *Theory of a Plasma* (St. Petersburg, Russia: Lan)
- [58] Koepke M E, Demidov V I, Finnegan S M and Reynolds E W 2006 Baffled-probe cluster for simultaneous, single-point monitoring of magnetized plasma fluctuations *Contrib. Plasma Phys.* **46** 385
- [59] Harris B J, Smith M, Murphy-Sugrue S, Harrison J, Bradley J W and Bryant P M 2019 Ball pen probe in strongly magnetised RF plasmas *Plasma Sources Sci. Technol.* **28** 055018
- [60] Murphy-Sugrue S, Harrison J, Walkden N R, Bryant P M and Bradley J W 2017 Improved understanding of the ball-pen probe through particle-in-cell simulations *Plasma Phys. Control. Fusion* **59** 055007
- [61] Raitsev Y, Demidov V, Pigarov A and West P 2008 Baffled-probe measurements of plasma properties at the divertor *The DIII-D Research Opportunities Forum for the Experimental Campaign (16–18 October)* (San Diego: General Atomics)
- [62] Raitsev Y and Demidov V 2009 A baffled-probe technique for real-time edge diagnostics and its possible applications on NSTX *Boundary Physics TSG Meeting, PPPL (19 June)*
- [63] Demidov V I, Koepke M E, Kurlyandskaya I P and Raitsev Y, 2014 MIB probes for measurements of particle and energy fluxes in plasma of Wendelstein 7-X 56th American Physical Society DPP Meeting (New Orleans, LA, 27–31 October) (Bulletin of the American Physical Society) **59** 15 (available at: <http://meeting.aps.org/Meeting/DPP14/Session/CP8.47>) (Accessed 4 August 2021)
- [64] Demidov V I, Adams S F, Kaganovich I D, Koepke M E and Kurlyandskaya I P 2015 Measurements of low-energy electron reflection at a plasma boundary *Phys. Plasmas* **22** 104501
- [65] Rozhanskii V A and Tsendin L D 1978 Effective boundary conditions for a plasma in contact with a nonemitting electrode in a magnetic field *Sov. J. Plasma Phys.* **4** 218
- [66] Cohen I M 1969 Saturation currents to Langmuir probes in a collision-dominated plasma with uniform magnetic field *Phys. Fluids* **12** 2356
- [67] Stangeby P C 2000 *The Plasma Boundary of Magnetic Fusion Devices* (Bristol: IOP Publishing Ltd)
- [68] Sanmartín J R 1970 Theory of a probe in a strong magnetic field *Phys. Fluids* **13** 103
- [69] Rozhanskii V A and Tsendin L D 1978 Electrostatic probe in a magnetic field *Sov. Phys. Tech. Phys.* **23** 932
- [70] Druyvesteyn M J 1930 Der niedervoltbogen *Z. Phys.* **64** 781
- [71] Sanmartín J R and Estes R D 1999 The orbital-motion-limited regime of cylindrical Langmuir probes *Phys. Plasmas* **6** 395
- [72] Estes R D and Sanmartín J R 2000 Cylindrical Langmuir probes beyond the orbital-motion-limited regime *Phys. Plasmas* **7** 4320
- [73] Kagan Y M and Perel' V I 1964 Probe methods in plasma research *Sov. Phys.—Usp.* **6** 767
- [74] Bernstein I B and Rabinowitz I N 1959 Theory of electrostatic probes in a low-density plasma *Phys. Fluids* **2** 112
- [75] Lam S H 1965 Unified theory for the Langmuir probe in a collisionless plasma *Phys. Fluids* **8** 73
- [76] Chen F F 1968 Measurement of low plasma densities in a magnetic field *Phys. Fluids* **11** 811
- [77] Vasileva I A 1975 Effect of the electron energy distribution on ion probe characteristics *High Temp.* **12** 405

- [78] Laframboise J G 1966 Theory of spherical and cylindrical Langmuir probes in a collisionless, Maxwellian plasma at rest *Univ. Toronto Inst. Aerospace Rept.* Report #100
- [79] Kiel R E 1968 Electrostatic probe theory for free molecular cylinders *AIAA J.* **6** 708
- [80] Steinbrüchel C 1990 A new method for analyzing Langmuir probe data and the determination of ion densities and etch yields in an etching plasma *J. Vac. Sci. Technol. A* **8** 1653
- [81] Karamcheti A and Steinbrüchel C 1999 Parametrization of Laframboise's results for spherical and cylindrical Langmuir probes *J. Vac. Sci. Technol. A* **17** 3051
- [82] Mausbach M 1997 Parametrization of the Laframboise theory for cylindrical Langmuir probe analysis *J. Vac. Sci. Technol. A* **15** 2923
- [83] Chen F F 2001 Langmuir probe analysis for high density plasmas *Phys. Plasmas* **8** 3029
- [84] Sudit I D and Woods R C 1994 A study of the accuracy of various Langmuir probe theories *J. Appl. Phys.* **76** 4488
- [85] Hopkins M B and Graham W G 1986 Langmuir probe technique for plasma parameter measurement in a medium density discharge *Rev. Sci. Instrum.* **57** 2210
- [86] Annaratone B M, Allen M W and Allen J E 1992 Ion currents to cylindrical Langmuir probes in RF plasmas *J. Phys. D: Appl. Phys.* **25** 417
- [87] Kaganovich I D, Demidov V I, Adams S F and Raitses Y 2009 Non-local collisionless and collisional electron transport in low-temperature plasma *Plasma Phys. Control. Fusion* **51** 124003
- [88] Malkov M A 1991 Electron sink to a probe in medium-pressure plasma and in a plasma in magnetic field *High Temp.* **29** 329
- [89] Demidov V I, Ratynskaia S V, Armstrong R J and Rypdal K 1999 Probe measurements of electron energy distributions in a strongly magnetized low-pressure helium plasma *Phys. Plasmas* **6** 350
- [90] Arslanbekov R R, Khromov N A and Kudryavtsev A A 1994 Probe measurements of electron energy distribution function at intermediate and high pressures and in a magnetic field *Plasma Sources Sci. Technol.* **3** 528
- [91] Gunther K and Carlson A 1994 Fluid theory of Langmuir probes in a magnetized plasma with open flux tubes *Contrib. Plasma Phys.* **34** 484
- [92] Gunther K 1995 A new approach to evaluation of *IV*-characteristics and application to highly collisional divertor plasmas abstr. *22nd EPS Conf., Contr. Fusion and Plasma Phys. (Bournemouth)* vol I p 433
- [93] Carlson A 2001 Linearized magnetohydrodynamic theory of Langmuir probes with resistivity, friction, and polarization *Phys. Plasmas* **8** 4732
- [94] Rozhansky V, Ushakov A and Voskoboinikov S 1998 Transverse plasma conductivity and the theory of a probe in a magnetic field *Plasma Phys. Rep.* **24** 777
- [95] Rozhansky V 2013 Perpendicular currents and electric fields in fully and partially ionized magnetized plasma *Phys. Plasmas* **20** 101614
- [96] Nogami S, Koepke M, Demidov V I and Gentle K W 2019 Interaction between velocity shear and turbulent fluctuations in Texas Helimak *APS Division of Plasma Physics Meeting Abstract* PP10.119
- [97] Koepke M E, Nogami S H, Demidov V I, Williams C B and Gentle K 2016 Magnetically insulated baffled probe measurement of unfiltered fluctuating space potential in the Texas Helimak *APS Division of Plasma Physics Meeting Abstract* TP10.038
- [98] Nogami S H, Koepke M E, Demidov V I, Gentle K W and Williams C B 2017 Baffled-probe compact-cluster measurement of microturbulence and electron temperature fluctuation in the Texas Helimak *APS Division of Plasma Physics Meeting Abstract* TP11.091
- [99] Koepke M, Demidov V, Nogami S, Hidalgo C and Melnikov A 2019 WVU contributions to the TJ-II physics program on mechanisms that decouple particle and energy transport *19th Coordinated Working Group Meeting, Helmholtz Headquarter, SpreePalais am Dom, Berlin, Max-Planck-Institut für Plasmaphysik (12–14 March, Germany)*
- [100] Killer C, Grulke O, Drews P, Gao Y, Jakubowski M, Knieps A, Nicolai D, Niemann H, Sitjes A P and Satheeswaran G 2019 Characterization of the W7-X scrape-off layer using reciprocating probes *Nucl. Fusion* **59** 086013
- [101] Rudischhauser L, Endler M, Hofel U, Hammond K C, Kallmeyer J P and Blackwell B D (Wendelstein 7-X Team) 2020 The Langmuir probe system in the Wendelstein 7-X test divertor *Rev. Sci. Instrum.* **91** 063505
- [102] Qin C M *et al* 2013 Experimental investigation of the potentials modified by radio frequency sheaths during ion cyclotron range of frequency on EAST *Plasma Phys. Control. Fusion* **55** 015004
- [103] Adamek J, Horacek J, Seidl J, Müller H W, Schrittwieser R, Mehlmann F, Vondracek P and Ptak S (COMPASS Team, ASDEX Upgrade Team) 2014 Direct plasma potential measurements by ball-pen probe and self-emitting Langmuir probe on COMPASS and ASDEX Upgrade *Contrib. Plasma Phys.* **54** 279
- [104] Adamek J *et al* 2016 Profile measurements of the electron temperature on the ASDEX Upgrade, COMPASS, and ISTTOK tokamak using Thomson scattering, triple, and ball-pen probes *Rev. Sci. Instrum.* **87** 043510
- [105] Ochoukov R, Whyte D G, Lipschultz B, LaBombard B and Wukitch S 2010 Interpretation and implementation of an ion sensitive probe as a plasma potential diagnostic *Rev. Sci. Instrum.* **81** 10E111
- [106] Brunner D, LaBombard B, Ochoukov R, Sullivan R and Whyte D 2013 Space-charge limits of ion sensitive probes *Plasma Phys. Control. Fusion* **55** 125004
- [107] Stöckel J *et al* 2004 Edge plasma physics and relevant diagnostics on the CASTOR tokamak (Germany) (available at: <https://www.osti.gov/etdeweb/servlets/purl/20622866>) (Accessed 4 August 2021)
- [108] Gryaznevich M (Tokamak Energy team) 2019 Faster fusion: ST40, engineering, commissioning, first results *AIP Conf. Proc.* **2179** 020008
- [109] Dimitrova M *et al* 2017 Plasma potential and electron temperature evaluated by ball-pen and Langmuir probes in the COMPASS tokamak *Plasma Phys. Control. Fusion* **59** 125001
- [110] Sykes A *et al* 1997 High- β performance of the START spherical tokamak *Plasma Phys. Control. Fusion* **39** B247
- [111] Rypdal K, Gronvoll E, Oynes F, Fredriksen A, Armstrong R J, Trulsen J and Pecseli H L 1994 Confinement and turbulent transport in a plasma torus with no rotational transform *Plasma Phys. Control. Fusion* **36** 1099
- [112] Almagri A F, Anderson D T, Anderson F S B, Probert P H, Shohet J L and Talmadge J N 1999 A helically symmetric stellarator (HSX) *IEEE Trans. Plasma Sci.* **27** 114
- [113] Ellis R F 1974 Current-driven collisional drift instability *Phys. Fluids* **17** 582
- [114] Carroll III J J, Koepke M E, Zintl M W and Gavrishchaka V 1993 Resonant-to-non-resonant transition in electrostatic ion-cyclotron wave phase velocity *Nonlinear Process. Geophys.* **10** 131
- [115] Mantica P, Vayakis G, Hugill J, Cirant S, Pitts R A and Matthews G F 1991 Broadband fluctuations and particle

- transport in the edge plasma during ECRH in DITE *Nucl. Fusion* **31** 1649
- [116] Hugill J 2000 Edge turbulence in tokamaks and the L-mode to H-mode transition *Plasma Phys. Control. Fusion* **42** R75
- [117] LaBombard B 2002 An interpretation of fluctuation induced transport derived from electrostatic probe measurements *Phys. Plasmas* **9** 1300
- [118] Finnegan S M, Koepke M E and Demidov V I 2021 Ion-temperature determination with a baffled Langmuir probe *Rev. Sci. Instrum.* **92** 033541
- [119] Okazaki K, Tanaka H, Ohno N, Ezumi N, Tsuji Y and Kajita S 2012 Measurement of ion and electron temperatures in plasma blobs by using an improved ion sensitive probe system and statistical analysis methods *Rev. Sci. Instrum.* **83** 023502
- [120] Čada M, Hubička Z, Adánek P, Olejníček J, Kment Š, Adánek J and Stöckel J 2015 A modified Katsumata probe—ion sensitive probe for measurement in non-magnetized plasmas *Rev. Sci. Instrum.* **86** 07351
- [121] Takahashi H, Ogasawara K, Boonyarittipong P, Saikyo T, Seino T, Kitajima S, Okamoto A and Tobita K 2019 Validation of ion temperature measurement using an ion sensitive probe technique in finite boundary RF plasma *Phys. Plasmas* **26** 022511